C9orf72 expansions disrupt ATM-mediated DNA repair

By Callum Walker

Submitted for the degree of Doctor of Philosophy (PhD)

Sheffield Institute for Translational Neuroscience

Sheffield Molecular Biology & Biotechnology department

University of Sheffield

Acknowledgments

I would like to thank my joint supervisors, Prof Mimoun Azzouz and Prof Sherif El-Khamisy, as well as my co-supervisor Dr Guillaume Hautbergue, for their continued support, guidance and interest in developing both my scientific research and myself as a scientist. In addition, I would like to thank the funding bodies, the European Research Council and the Wellcome Trust, for without their funding my research would not have been possible.

I would also like to thank all of the members of the El-Khamisy and Azzouz laboratories for their training, for their direct assistance with experiments, and for their advice and useful discussions. In particular, I would like to thank Dr Saul Herranz-Martin for assisting greatly with my scientific research – his contribution to the data in this thesis is significant: He was involved in producing viral vectors, generating animal models, processing mouse tissues and isolating primary neuronal cell cultures. I would also like to mention Dr Evangelia Karyka, who helped greatly with foci quantifications and primary neuronal cultures. I should thank Dr Jude Chiang for her help with DNA repair assays, and Dr Chunyan Liao for performing TOP1-cc assays. I would also like to thank Waheba Elsayed and Mohammed Hassan for their important contribution, which was performing the neutral comet assays presented in this thesis. I should also thank Mateusz Jurga for helping with S9.6 staining, and Drs Katherine Lewis and Vera Lukaschuck for their assistance with mouse work and tissue processing.

I give my thanks to Prof Pamela Shaw, Dr Adrian Higginbottom, and Dr Padraig Mulcachy for their research expertise and for generating the C9orf72 expansion plasmids. Finally, I would like to thank Dr Kurt De Vos and Prof Grant Stewart for kindly providing the poly-GA (34, 69) DPR and RNF68-GFP cDNA plasmids, respectively.

Contents

Abstract

Hexanucleotide repeat expansions, contained within the C9orf72 gene, represent the most common genetic cause of amyotrophic lateral sclerosis (ALS) and frontotemporal dementia (FTD), though the mechanisms by which such expansions cause neurodegeneration are poorly understood. Here, we report elevated levels of DNA-RNA hybrids (R-loops) and double strand breaks (DSBs) in human cells, rodent neurons, and C9orf72 ALS patient tissues. Accumulation of endogenous DNA damage is concomitant with defective ATM- and 53BP1-mediated DNA repair signalling, and the accumulation of protein-linked DNA breaks. We reveal that defective DNA repair is a consequence of p62 accumulation, which impairs H2A ubiquitylation, and perturbs ATM signalling. These findings identify R-loops, double strand breaks, and defective ATM-mediated repair as pathological consequences of C9orf72 expansions and suggest that C9orf72-linked neurodegeneration is driven, at least partly, by genomic instability.

Chapter 1: General Introduction

1.1. An Introduction to the DNA damage response (DDR)

The ability to maintain genomic integrity is fundamental to the Darwinian doctrine of genetic inheritance. Whilst the DNA double helix is generally a stable structure, a variety of agents are known to induce DNA damage (Ciccia & Elledge, 2010), and each cell is estimated to process ~10^{13} DNA lesions each day (Lindahl & Barnes, 2000). Physical DNA damaging agents, such as ionising and ultraviolet radiation, cause up to 10^5 DNA lesions per day (Hoeijmakers, 2009). Chemical genotoxic agents, such as camptothecin (CPT) and etoposide, also induce DNA damage by inhibiting the re-ligation activities of topoisomerase-1 (TOP1) and topoisomerase-2, respectively (Hsiang *et al.*, 1985).

In addition to exogenous sources, a number of endogenous cellular processes threaten the genome. Reactive oxygen species (ROS) form as a by-product of the electron transport chain, and cause oxidative damage to nucleic acids (Jackson & Bartek, 2009; Valko *et al.*, 2006). Endogenous damage can also arise due to the spontaneous deamination or depurination of DNA bases (Jackson & Bartek, 2009). Moreover, the fundamental cellular processes of transcription and replication are intrinsically linked to genomic instability since they render cells susceptible to DNA breakage (Jackson & Bartek, 2009).

Given their frequent occurrence and heterogeneity in nature, it is perhaps unsurprising that a number of different DNA break repair mechanisms have evolved to rectify DNA breaks (Figure 1). DNA breaks are usually limited to one strand of the DNA phosphodiester backbone, broadly termed single stranded DNA breaks (SSBs). The DNA damage response (DDR) is somewhat analogous to a Swiss army knife, since there are multiple repair pathways that take precedence in response to different forms of DNA damage – each pathway representing a specific tool for a specific type of DNA lesion. Mismatch repair (MMR), for example, is used to replace misincorporated nucleotides (Jiricny, 2006), and base excision repair (BER) is used to restore small chemical moderations to the DNA, by excising the damaged bases and replacing them (Lindahl & Barnes, 2000).

More complicated DNA lesions, like UV-induced thymidine dimers, are repaired by the nucleotide excision repair (NER) pathway, which first excises an oligonucleotide stretch of

DNA surrounding the damage base(s) before replacing them (Hoeijmakers, 2009). This type of repair occurs genome wide, using global-genome NER, but can also occur more rapidly in transcribed regions of the genome, using transcription-coupled NER. Unlike global-genome NER, transcription-coupled NER uses the stalling of RNA polymerase 2 (Pol 2) as a signal for the recruitment of repair factors (Hoeijmakers, 2009).

When two SSBs occur in close proximity, it can lead to DSB formation. Whilst less abundant than SSBs, DSBs are highly cytotoxic (Khanna & Jackson, 2001). To address this danger, intricate DSB repair pathways have evolved. The two most widely studied DSB repair pathways have been termed homologous recombination (HR) and non-homologous end-joining (NHEJ). HR represents a high fidelity mechanism for repairing DSBs, utilising sister chromatids as a template for polymerase rectification (Hartlerode & Scully, 2009). The second pathway, NHEJ, represents an error-prone repair pathway that uses little or no homology to guide repair (Ciccia & Elledge, 2010). During G2 and S phase of the cell cycle, repair of DSBs can occur via HR. However, post-mitotic neurons can only repair DSBs using NHEJ (Rulten & Caldecott, 2013). As such, despite being fundamentally error-prone, NHEJ is generally considered to be the predominating DSB repair pathway in mammalian cells.

DSB repair is primarily orchestrated by two members of the phosphatidylinositol 3-kinase-like protein kinases (PIKKs) family - Ataxia Telangiectasia Mutated (ATM) and DNA-dependant protein kinase (DNA-PK). ATM and DNA-PK are both activated in response to double-stranded DNA breaks (Harper & Elledge, 2007; Meek *et al.*, 2008). Whilst DNA-PK specifically controls the activity of a smaller number of substrates involved in NHEJ, ATM has hundreds of substrate proteins and plays a more general role in DSB repair signalling (Shiloh, 2003).

Figure 1: Differential DNA repair toolkits are available for different types of DNA lesion

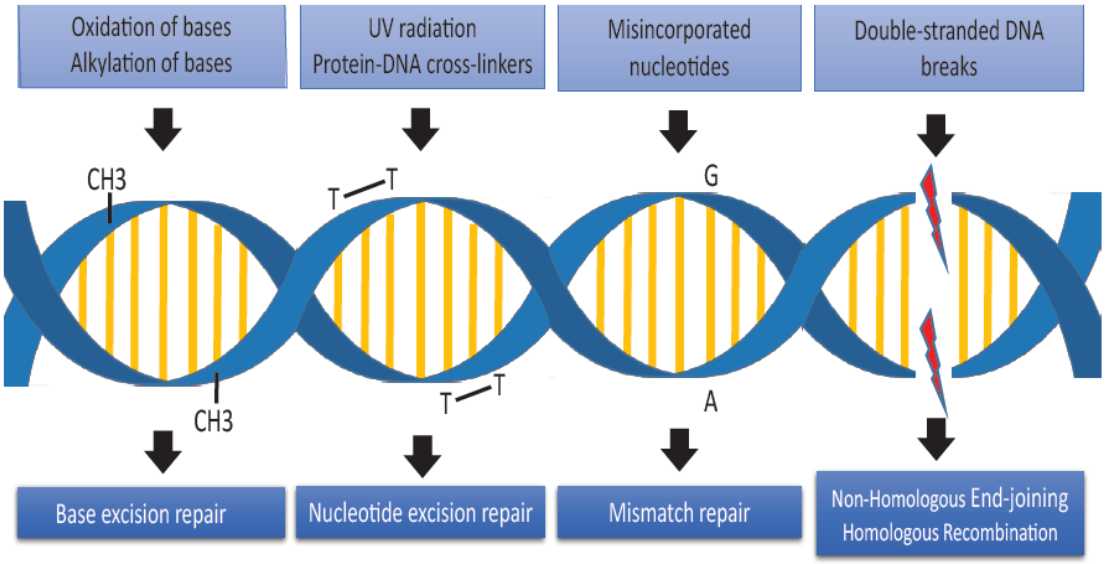

Figure 1. Different DNA repair toolkits are available for different types of DNA lesion. Chemical base modifications like oxidation or alkylation are repaired by base excision repair. Bulky adducts, such as UV-induced thymine dimers are repaired by nucleotide excision repair. Replication errors that lead to misincorporated nucleotides are repaired by mismatch repair. Double-stranded DNA breaks are repaired primarily by non-homologous end-joining, but can also utilise homologous recombination during S-phase and G2 stages of the cell-cycle. Adapted from (Genois *et al.*, 2014)**.**

1.2. DNA repair and neurodegeneration

Interestingly, whilst genomic instability is typically associated with cancer predisposition, mutations in a number of DDR genes drive neurological disease (Madabhushi et al, 2014). Such diseases clearly highlight how the central nervous system (CNS) relies on DNA repair processes for functionality. DNA repair defect likely drive neurological disease because of an intrinsic vulnerability bestowed upon neuronal cells: Firstly, a fifth of all oxygen is consumed by the brain (Madabhushi *et al.*, 2014; Magistretti & Pellerin, 1996), despite representing only ~2% of total body mass. High levels of oxidative respiration in the brain likely renders neuronal cells susceptible to oxidative DNA damage (Weissman et al, 2007). Secondly, neurons are also highly transcriptionally active, a potent source of endogenous DNA damage (Aguilera & Garcia-Muse, 2012). As well increased exposure to endogenous damage, neuronal cells are intrinsically deficient in HR-mediated DSB repair (Rulten & Caldecott, 2013), all of which likely leaves neurons particularly sensitive to defects in DNA repair processes.

In-line with the notion that oxidative and transcription-coupled DNA damage is a particular problem for the non-mitotic cells of the CNS, mutations in genes linked to the repair of these kinds of breaks are known to cause neurological diseases (Madabhushi *et al.*, 2014). Perhaps the most well characterised example of this phenomenon is the disease ataxia telangiectasia (A-T), a disease caused by mutations affecting DSB repair kinase, ATM (Biton *et al.*, 2008; Lavin & Shiloh, 1997). In addition to lymphoma and breast cancer predisposition, these patients develop an ataxic neurological phenotype. Similarly, A-T-like disorder (AT-LD) is caused by mutations in the gene encoding for the MRN complex member, Mre11 (Taylor *et al.*, 2004). The similarity between these disorders is particularly interesting given that Mre11 plays a similar role to ATM in the initiation DSB repair signalling (Williams & Tainer, 2007; Williams *et al.*, 2007). These examples demonstrate how DSB repair defects can lead to an ataxic phenotype in man.

Ataxia is also the clinical phenotype of patients with defects in SSB repair. For instance, spinocerebellar ataxia with axonal neuropathy (SCAN-1) is a rare disease caused by a H493R mutation in the gene encoding for tyrosyl-DNA phosphodiesterase 1 (TDP1) (El-Khamisy *et al.*, 2005). To better describe the molecular mechanisms of SCAN-1 pathology, it is necessary to describe the cellular functions of another protein, topoisomerase-1 (TOP1).

TOP1 functions to induce enzyme-bridged transient SSBs in the DNA backbone, releasing torsional stress and promoting the unwinding of supercoiled DNA, allowing efficient transcription by enabling access to elongating RNA polymerases (Wang, 2002; Yang *et al.*, 1996). TOP1 also has enzymatic activity that re-ligates the DNA backbone shortly after creating the nick, preventing genome instability (Champoux, 2001). Problematically, TOP1 can sometimes stall shortly after DNA cleavage (e.g. due to the presence of damaged DNA), leaving covalently linked TOP1 cleavage-complexes (TOP1ccs) (El-Khamisy *et al.*, 2005; Hsiang *et al.*, 1985; Staker *et al.*, 2002). Because TOP1ccs are covalently linked to the 3' end of DNA backbone (Pouliot *et al.*, 1999), TDP1-mediated hydrolysis of the phosphotyrosyl linkage is required for TOP11cc resolution (Katyal *et al.*, 2007). Crucially, the H493R mutation detected in SCAN1 patients impairs the enzymatic activity of TDP1 (El-Khamisy *et al.*, 2005), and SCAN1 cells accumulate more TOP1ccs, which leads to genomic instability (El-Khamisy & Caldecott, 2007; El-Khamisy *et al.*, 2005). Curiously, the CNS appears to be specifically affected in the disease SCAN-1, supporting the notion that the brain is particularly sensitive to defects in transcription-associated DNA repair processes.

In addition to SCAN-1, ataxia with oculomotor apraxia-1 (AOA1) is another neurological disease that appears to specifically affect the CNS, and shares many of the neurological symptoms of the disease A-T (Moreira *et al.*, 2001). Mutation in the gene aprataxin (APTX) underpins AOA1, and the function of the APTX protein is to process DNA ends generated by abortive ligase reactions (Ahel *et al.*, 2006). Interestingly, APTX has been shown to interact with XRCC1 (Clements *et al.*, 2004), a scaffold protein involved in the assembly of SSB repair protein complexes (including TDP-1, APTX, and PNKP – all of which are linked to neurological disease) (Caldecott, 2003). Recently, a patient exhibiting an ataxic clinical phenotype was found to have a heterozygous XRCC1 mutation, and XRCC1 deletion in mice similarly exhibits a neurological phenotype (Hoch *et al.*, 2017). Thus, alike DSB repair defects, SSB repair dysfunction can also lead to ataxia in man.

As well as the ataxic phenotype presented in the above diseases, DNA repair defects can also lead to other neurological diseases, such as Xeroderma Pigmentosum (XP) and Cockayne Syndrome (CS). XP is a particularly interesting disease spectrum, which leads to the predisposition to many different types of cancer, extreme photosensitivity, and neurological problems. XP can be caused by mutations in a number of different genes involved in NER. Mutations in those genes whom partake in transcription-coupled and global-genome NER

(such as XPA, XPB, XPD, XPF, and XPG) develop both cancer and neurological problems, whist mutations in XPC, which is dispensable for TC-NER, does not elicit a neurological phenotype (Kraemer *et al.*, 1987; Mimaki *et al.*, 1986). Cockayne syndrome patients, which bare a defect in transcription-coupled NER specifically, also do not appear to be predisposed to cancer - though it should be noted that they do not survive past their twenties (Iyama & Wilson, 2013). Such disease spectrums indicate that the CNS is particularly sensitive to transcription-associated genomic instability.

Taken together, these diseases demonstrate how DNA repair fidelity is critical to the CNS. It should be noted that these examples are not isolated cases, and there is an array of neurological conditions known to be linked to DNA repair defects (Madabhushi *et al.*, 2014) and are summarised in Table 1. More recently, a link between DNA repair processes and neurodegeneration has become an emerging theme within the field of motor neuron disease.

Table 1. Summary of mutated DNA repair genes and their links to neurodegeneration

Gene Mutated	Human Disease	Function of protein
CSA, CSB	Cockayne Syndrome (CS)	Transcription-coupled nucleotide excision repair
XPA-XPG	Xeroderma Pigmentosum (XP)	Nucleotide excision repair
XPD, ITDA	Trichothiodystrophy (TTD)	Nucleotide excision repair
APTX	Ataxia with oculomotor apraxia-1 (AOA1)	Single-strand break repair, resolving abortive ligation complexes
TDP1	Spinocerebellar ataxia with axonal neuropathy-1 (SCAN1)	Single-strand break repair, resolving abortive topoisomerase-1 cleavage complexes
XRCC1	Oculomotor apraxia	Single-strand and double-strand break repair pathways
ATM	Ataxia Telangiectasia (A-T)	Double-strand break repair signalling
MRE11	A-T Like Disease (ATLD)	Double-strand break repair
NBS1	Nijmegen Breakage Syndrome	Double-strand break repair
LIG4	Ligase 4 syndrome	Double-strand break repair
XLF	XLF syndrome	Non-homologous end-joining
FUS, TARDP	Amyotrophic Lateral Sclerosis (ALS)	Double-stranded break repair, R-loop resolution/prevention
SETX	Amyotrophic Lateral Sclerosis-4 (ALS4) and Ataxia with oculomotor apraxia-2 (AOA2)	Double-stranded break repair, R-loop resolution
SMN1	Spinal Muscular Atrophy (SMA)	R-loop resolution

Adapted from (Madabhushi et al., 2014)

1.3. Introduction to Amyotrophic Lateral Sclerosis (ALS)

ALS, the most common form of motor neuron disease, represents a devastating neurodegenerative disease in which motor neurons in the spinal cord and brain degenerate. ALS affects people in the midst of their life (average age of onset, 50 years), and has an extremely poor prognosis with death usually occurring within 2-4 years of diagnosis (Chio *et al.*, 2009).

Approximately 90% of ALS cases are sporadic (sALS), in that no familial history of the disease is known. Of the remaining 10%, driver mutations in a number of different genes have been identified (Valdmanis & Rouleau, 2008). Mutations in SOD1 were the first to be identified, and account for approximately 20% of familial ALS (fALS) cases (Rosen *et al.*, 1993). Recently identified ALS-causing mutations in NEK1 account for a similar percentage of fALS cases as SOD1 (Kenna *et al.*, 2016). Mutations in other genes collectively make up a further ~20% of fALS cases (Valdmanis & Rouleau, 2008). Most importantly, though, a hexanucleotide repeat expansion within the C9ORF72 gene has now been identified as being the most common familial cause of ALS, accounting for approximately 40% of fALS, but also accounting for between 5-10% of sALS cases (DeJesus-Hernandez *et al.*, 2011; Renton *et al.*, 2011).

Curiously, C9orf72 repeat expansions are also the most common genetic cause of frontotemporal dementia (FTD) (Couratier *et al.*, 2017; Ferrari *et al.*, 2011). FTD is the second most common form of dementia, and represents a neurodegenerative disease characterised by the degeneration of spindle neurons within the frontal and temporal lobes. Interestingly, ALS and FTD disease phenotypes are not mutually exclusive, and a disproportionate number of patients develop both ALS and FLD in unison, leading to the speculation that ALS and FTD exist on the same disease spectrum (Couratier *et al.*, 2017; Ferrari *et al.*, 2011).

The genetic and neuropathological aetiology of FTD can be loosely divided into 2 subtypes: The first type of FTD exhibits Alzheimer's like tau proteinopathy and can be driven by mutations in the MAPT gene (which encodes tau) (Ji *et al.*, 2017). Alternatively, FTD can be driven by mutations in ALS-linked genes, including TARDP, C9orf72, VCP and SQSTM1 (Ji *et al.*, 2017). Intuitively, FTD-causing mutations in these genes produces hallmark ALS

neuropathology, discussed below. The extraneous factors that dictate the disease phenotype of these patients are currently unknown.

As previously mentioned, mutations in the TARDP gene (encoding TDP-43) can drive ALS/FTD (Ji *et al.*, 2017). TDP-43 is a ubiquitous RNA/DNA binding protein, which plays a diverse role in several aspects of RNA processing (Ayala *et al.*, 2011; Gregory *et al.*, 2004; Polymenidou *et al.*, 2011). Though predominantly nuclear, ~30% of TDP-43 protein may reside in the cytoplasm (Barmada *et al.*, 2010). Importantly, TDP-43 is present in cellular aggregates found in cortical and motor cells from FTD and ALS patients (Neumann *et al.*, 2006). Its mislocalisation from the nucleus is also a common feature of the disease (Neumann *et al.*, 2006), and has collectively been termed TDP-43 proteinopathy (Kwong *et al.*, 2007). Peculiarly, TDP-43 depletion, or overexpression, can promote neurological phenotypes in mouse models, suggesting that both loss and gain of TDP-43 functions contributes to the disease in ALS/FTD (Diaper *et al.*, 2013; Yang *et al.*, 2014).

Driver mutations in the SQSM1 gene (encoding p62) also cause ALS/FTD (Fecto *et al.*, 2011). In addition to TDP-43 proteinopathy, ALS/FTD patient tissues show a second disease hallmark - the accumulation and aggregation of p62 (Blokhuis *et al.*, 2013). P62 is important for the autophagic degradation of misfolded proteins, protein aggregates, and depolarised mitochondria (Katsuragi *et al.*, 2015). Since p62 is itself degraded during the process of autophagic clearance, functional autophagy serves as a mechanism for regulating p62 protein homeostasis (Rusten & Stenmark, 2010). In turn, the over-accumulation of p62 protein is thought to represent a defect in the autophagy. Intuitively, defective autophagy is strongly implicated in the pathogenesis of ALS (Brady *et al.*, 2011; Lee *et al.*, 2015).

1.4. Introduction to C9orf72-ALS/FTD

As mentioned above, a hexanucleotide G4C2 repeat expansion, contained within the first intron of the C9ORF72 gene, represents the most common genetic cause of amyotrophic lateral sclerosis (ALS) and frontotemporal dementia (FTD) (DeJesus-Hernandez *et al.*, 2011; Renton *et al.*, 2011). The size of the expansion, using southern blot analysis, is estimated to be anywhere in the range of 30 and 4000 hexanucleotide repeats in disease genomes, with less than 30 repeats thought to be non-pathogenic (Dols-Icardo *et al.*, 2014).

Promisingly, C9orf72-ALS/FTD patient samples also display TDP-43 and P62 disease hallmarks, which are shared by ~97% of ALS patients and ~50% of FTD patients (Ling *et al.*, 2013; Neumann *et al.*, 2006). Thus, targeted therapeutic strategies for C9orf72-ALS/FTD may also be valid for other forms of the disease. In addition to hallmark ALS proteinopathies, C9orf72-ALS/FTD patient tissues display 3 additional disease hallmarks: Firstly, C9orf72-ALS/FTD patients show decreased C9orf72 mRNA and protein levels (Belzil *et al.*, 2013; Ciura *et al.*, 2013; Cooper-Knock *et al.*, 2012; DeJesus-Hernandez *et al.*, 2011; Gijselinck *et al.*, 2012; Gijselinck *et al.*, 2016; Waite *et al.*, 2014). Secondly, fluorescence in situ hybridisation experiments have identified sense and antisense RNA foci in patient sections (Cooper-Knock *et al.*, 2014; Zu *et al.*, 2013). Thirdly, repeat-associated non-ATG dependant (RAN)-translation of the sense and antisense repeat transcripts have been observed in patient tissue (Mori *et al.*, 2013; Zu *et al.*, 2013). How C9orf72-specific pathologies conspire with TDP-43 and P62 proteinopathies to drive disease is a poorly understood paradigm and is the subject of intense investigation.

1.4.1. What is toxic about the C9orf72 repeat expansion

1.4.1.1. Haploinsufficiency (loss of function)

The C9orf72 gene has three splice variants, two of which harbour the expansion within the first intron, whilst the third harbours the expansion in a promoter region (DeJesus-Hernandez *et al.*, 2011). Variant 1 encodes a long isoform of the C9orf72 protein, whilst variants 2 and 3 encode a shorter isoform (Xiao *et al.*, 2015). Haploinsufficiency of the C9ORF72 gene product was initially suggested to play a role in pathogenesis, since RNA and protein levels of the C9orf72 gene product are depleted in patient tissue. Silencing of the C9orf72 gene may be a consequence of epigenetic shut-down (Belzil *et al.*, 2013) and abortive transcription (Haeusler *et al.*, 2014).

C9orf72 belongs to the DENN (differentially expressed in normal and neoplastic cells) domain-containing family of proteins, which usually function as Rab-GTPase exchange factors (Levine *et al.*, 2013). Interestingly, recent reports have indicated that the C9orf72 protein plays a role in autophagy: The long C9orf72 isoform has been shown to form a complex with WD repeat-containing protein 41 (WDR41), where it functions to initiate autophagy (Sellier *et al.*, 2016; Webster *et al.*, 2016; Yang *et al.*, 2016). Less is currently

known about the short C9orf72 isoform. Promisingly, C9orf72 depletion in cell culture experiments leads to decreased autophagy clearance, and increased numbers of p62 puncta (Farg *et al.*, 2014; Webster *et al.*, 2016), suggesting that C9orf72 haploinsufficiency could be responsible for driving the hallmark accumulation of p62 in C9orf72-ALS/FTD.

Moreover, depletion of the C9orf72 orthologue in C. elegans leads to age-dependant paralysis (Therrien *et al.*, 2013) and a motor phenotype in zebrafish (Ciura *et al.*, 2013). These results may be explained by altered actin dynamics (Sivadasan *et al.*, 2016), and/or the result of dysregulated autophagy (Webster *et al.*, 2016).

Critically, however, C9orf72 ablation in mice does not induce a neurodegenerative phenotype (Koppers *et al.*, 2015; O'Rourke *et al.*, 2016; Sudria-Lopez *et al.*, 2016), nor is it inherently toxic in cell culture experiments (Sellier *et al.*, 2016). These data suggest that the depletion of C9orf72 transcripts is not sufficient to drive ALS/FTD disease progression. In line with a passive role in the disease progression, C9orf72 ablation in mice has been shown to impede macrophage and microglial function, leading to a neuroinflammatory response (O'Rourke *et al.*, 2016).

1.4.1.2. RNA- and DPR-mediated toxicity (gain of function)

The consensus, therefore, is that haploinsufficiency is not the driving force of the disease (Mizielinska & Isaacs, 2014). Thus, a toxic gain of function, mediated by GC-rich RNA and/or dipeptide species, appears to play a major role in C9orf72-related disease.

In-line with a toxic gain-of-function hypothesis, overexpression of C9orf72-related repeat expansions leads to neurodegeneration in mice (Chew *et al.*, 2015; Herranz-Martin *et al.*, 2017). Using adeno-associated viral vectors (AAV) to deliver 2 or 66 hexanucleotide repeat expansions, it was shown that longer GC expansions cause a neurodegenerative phenotype in mice (Chew *et al.*, 2015). Importantly, repeat expression also led to TDP-43 proteinopathy, RNA foci, and dipeptide repeat pathology. Our lab has also demonstrated similar findings with a construct expressing 10 or 102 hexanucleotide repeat expansions (Herranz-Martin *et al.*, 2017). Importantly, we also observed increased p62 proteinopathy in mice expressing longer hexanucleotide repeat expansions. These data favour a toxic-gain of function as being the predominating driver of neurodegeneration in C9orf72-ALS/FTD.

In addition, expression of ATG-driven poly-Glycine-Alanine (poly-GA) dipeptide repeats in the murine CNS leads to a neurodegenerative phenotype (Walker *et al.*, 2017; Zhang *et al.*, 2016). Similar findings have also been reported in cell culture models (May *et al.*, 2014; Zhang *et al.*, 2014). Interestingly, poly-GA DPRs interacts with or sequesters p62 (May *et al.*, 2014), and the expression of poly-GA causes massive p62 accumulation (May *et al.*, 2014; Walker *et al.*, 2017). Thus, poly-GA DPRs are linked to p62 accumulation, a hallmark of ALS/FTD, and are toxic in mammalian models. It is noteworthy that poly-GA DPRs do not cause toxicity in Drosophila melanogaster (Freibaum *et al.*, 2015; Mizielinska *et al.*, 2014), suggesting the mechanism by which they induce toxicity may be specific to mammalian cells.

These reports support the idea that C9orf72-ALS/FTD is driven by an RNA/DPR-mediated toxic gain of function. Problematically, these experiments relied upon overexpression and/or non-ATG driven expression systems to express DPR sproducts. Concerns about the physiological validity of these experiments can be raised, particularly because DPRs are seldom observed in human C9orf72-ALS/FTD tissue samples and poorly correlate with the disease/clinical phenotype (Davidson *et al.*, 2016; Davidson *et al.*, 2014; Mackenzie *et al.*, 2013; Mackenzie *et al.*, 2015). Thus, whilst RNA/DPR overexpression is neurotoxic, the importance of this toxicity to the disease progression is not yet fully clear.

In addition to the viral models of C9orf72 expansion toxicity, 4 bacterial artificial chromosome (BAC)-derived mouse models have been produced and characterised, but display profoundly different phenotypes. Initially, two separate laboratories developed BAC models expressing the whole C9orf72 gene derived from expansion-carrying ALS patients (O'Rourke *et al.*, 2015), or just a fraction of the gene loci (including the expansion) (Peters *et al.*, 2015). In both instances, the mice developed pathological features (RNA foci and DPRs), but the researchers were unable to detect any evidence of neurodegeneration or neuropathological behaviour. Follow-up attempts to obtain a valid model of C9orf72-related neurodegeneration were more successful, reporting hippocampus-associated cognitive neuropathy (Jiang *et al.*, 2016) and progressive motor and behavioural phenotypes as well as reduced survival (Liu *et al.*, 2016). The reasons for these discrepancies could be due to the mouse strain, which is known to influence the resulting phenotype (Ishimura *et al.*, 2014).

Despite the limitations and discrepancies in current mouse models, evidence that hexanucleotide expansions can drive neurodegeneration without any modulation of the endogenous C9orf72 gene, particularly in the BAC mice in which the expression of the expansions are controlled by the endogenous C9orf72 promoter, strongly suggests that a toxic gain of function is sufficient to drive disease.

1.4.1.3. Unravelling the toxicity associated to C9orf72 RNA and DPRs

Evidence therefore suggests that the expression of repeat expansions leads to neurotoxicity. It is not yet fully clear as to whether this is due to the ensuing production of DPR species, or whether the RNA molecules themselves are inherently toxic. Due to easier genetic manipulation, much of the work focused on answering this question comes from studies that use Drosophila melanogaster as a model organism.

Work in the Isaacs laboratory demonstrated that overexpressing GC repeats (36 or 103 repeats) is neurotoxic in Drosophila (Mizielinska *et al.*, 2014). Introduction of stop codons in each frame, however, fully prevented RAN-translation and abolished eye degeneration. Thus, in Drosophila, C9orf72-associated toxicity appears to be driven *specifically* by the effects of DPR species.

As mentioned previously, C9orf72 RNA foci sequester a number of RNA binding proteins, including RNA export factors. Such factors may serve to target these RNA transcripts to the ribosomes, leading to DPR production and toxicity. In-line with this notion, depletion of the RNA export factor, serine-rich splicing factor-1 (SRSF1), leads to reduced DPR production and is neuroprotective (Hautbergue *et al.*, 2017). These data imply that DPRs are the predominating toxic mechanism for the disease, whilst RNA and RNA focal accumulation may function as a gatekeeper to DPR production.

Elsewhere, a Drosophila model of C9orf72-associated disease suggests RNA-mediated toxicity. In this research, expression of 30 GC repeats, which did not produce any *detectable* DPRs, was shown to be neurotoxic (Xu *et al.*, 2013). Toxicity was alleviated in Drosophila and murine neuronal cultures by overexpressing the RNA binding protein, pur-alpha, which is sequestered by C9orf72 expansion RNA molecules. These data suggest that RNA foci-mediated sequestration of RNA binding proteins is toxic to neuronal cells. It was also

demonstrated that 42 GC repeats were toxic to mouse motor neurons, with no *detectable* DPRs being produced (Wen *et al.*, 2014). The same study also demonstrated much greater levels of neuronal toxicity were associated with poly-PR DPRs.

In addition to non-ATG driven expansion systems, several experiments have used recombinant DPRs or codon degeneracy to explore the toxicity associated to DPRs in the absence of pure-GC RNA. A general consensus has emerged: Arginine-rich DPRs (poly-PR and poly-GR) are the most toxic (Kwon *et al.*, 2014; Lee *et al.*, 2016; Wen *et al.*, 2014; Yang *et al.*, 2015), whilst poly-GA displays comparatively less, but still substantial, cellular toxicity (Chang *et al.*, 2016; May *et al.*, 2014; Mizielinska *et al.*, 2014; Walker *et al.*, 2017; Zhang *et al.*, 2014).

DPRs are seldom observed in patient tissues, although they are highly cytotoxic in modelling experiments (Davidson *et al*., 2014). Alternatively, RNA foci are abundant in patient tissues, but much less toxic in modelling experiments (Davidson *et al*., 2014). As such, a stalemate still exists, and it is difficult to pinpoint the extent to which each pathology contributes to the disease. Importantly, RNA repeat expansions are linked to TDP-43 and P62 proteinopathy (Chew *et al.*, 2015; Herranz-Martin *et al.*, 2017), whilst DPRs are only associated with P62 proteinopathy. It is possible that there are two distinct pathological pathways that conspire in C9orf72-related disease: (A) an RNA-mediated toxicity that disrupts RNA processing and drives TDP-43 proteinopathy, and (B) the production of toxic DPRs, which causes P62 accumulation.

Antisense oligonucleotide (ASO) therapy, which targets hexanucleotide RNA repeat expansions for degradation, have shown promise in cellular and mouse models of C9orf72-related disease (Donnelly *et al.*, 2013; Jiang *et al.*, 2016; Lagier-Tourenne *et al.*, 2013). ASOs have been shown to reduce RNA foci levels (Donnelly *et al.*, 2013; Jiang *et al.*, 2016; Sareen *et al.*, 2013) and prevent DPR production (Jiang *et al.*, 2016). The apparent success of ASOs in treating the disease strongly supports the notion that a toxic gain-of-function primarily drives the disease. It is not clear as to whether ASOs also reduce endogenous levels of the C9orf72 mRNA and protein, which could have clinical consequences, such as neuroinflammation (O'Rourke *et al.*, 2016).

1.4.2. Molecular mechanisms underpinning RNA- and DPR- associated toxicity

1.4.2.1. Aberrant RNA structures and the sequestration of RNA binding proteins

Since C9orf72 expansions are G-rich, they are likely to be highly prone to the formation of G-quadruplexes. These occur when 4 guanine bases associate via Hoogsten hydrogen bonds to form a structure known as a G-tetrad. Spectrophotometric studies suggest that C9orf72 RNA molecules form G-quadruplex and hairpin loop structures (Fratta *et al.*, 2012; Haeusler *et al.*, 2014; Reddy *et al.*, 2013; Su *et al.*, 2014), whilst the DNA of C9orf72 expansions can also form G-quadruplex structures (Haeusler *et al.*, 2014; Sket *et al.*, 2015). Since G-quadruplexes function in multiple cellular pathways, such as telomere maintenance and gene expression, their aberrant formation in C9orf72-ALS/FTD may have important disease consequences.

One consequence of G-quadruplex susceptibility may be the stabilization of RNA foci. It is well-documented that these RNA foci lead to the transient sequestration of multiple RNA binding proteins (Conlon *et al.*, 2016; Cooper-Knock *et al.*, 2014; Lee *et al.*, 2013; Mori *et al.*, 2013; Rossi *et al.*, 2015; Xu *et al.*, 2013; Zamiri *et al.*, 2014). Interestingly both sense and antisense RNA foci appear to have similar protein interactomes (Cooper-Knock *et al.*, 2015a). The sequestration of RNA binding proteins may cause toxicity due to partial loss of function of the sequestered proteins or due to the aberrant processing of RNA repeat expansions.

Pur-alpha is a sequence specific DNA- and RNA-binding protein that has been shown to play a role in DNA replication (Gallia *et al.*, 2000), gene transcription (Johnson, 2003) and in neuronal dendrite development (Johnson *et al.*, 2006). Loss of function of the pur-alpha/beta proteins may mediate RNA-driven toxicity in C9orf72-ALS/FTD. RNA pull-down assays identified pur-alpha and pur-beta to be the most abundant interactors with C9orf72 expanded RNA (Rossi *et al.*, 2015; Xu *et al.*, 2013). As mentioned earlier, Drosophila studies demonstrated that pur-alpha overexpression alleviates toxicity associated with C9orf72 expansions (Xu *et al.*, 2013), implying that the loss of pur-alpha functions as a toxic consequence of C9orf72 repeat RNA accumulation.

In other work, SRSF1 was shown to co-localise with RNA foci (Cooper-Knock *et al.*, 2014; Lee *et al.*, 2013). In this instance, it is thought that the sequestration of this RNA export

factor actively drives the export of the RNA into the cytoplasm, promoting RAN-translation. Hautbergue and colleagues provide compelling evidence for this phenomenon, and demonstrate that SRSF1 depletion leads to a reversal of eye degeneration in a Drosophila model of C9orf72 expansions (Hautbergue *et al.*, 2017). Importantly, the sequestration of RNA binding proteins appears to be transient (Cooper-Knock *et al.*, 2014). Thus, it may be the case that, although particular proteins are sequestered, they are still functional. Little is currently known as to whether the endogenous function of RNA binding proteins are altered by the presence of RNA foci.

1.4.2.2. Nucleolar Stress

Using RNA pull-down assays, Haeusler and colleagues initially identified that C9orf72 RNA G-quadruplexes interact with the key nucleolar protein, nucleolin (Haeusler *et al.*, 2014). In patient fibroblasts and IPSC-derived motor neurons, nucleolin and nucleophosmin staining patterns were more disperse and irregular, indicative of nucleolar stress. This pattern has also been seen in some, but not all, neurons in patient tissues (Cooper-Knock *et al.*, 2015b). It was therefore hypothesised that accumulated C9orf72 RNA transcripts may lead to nucleolar stress.

Interestingly, arginine-rich DPRs have also been shown to localise to the nucleolus in cell-lines and primary neuronal cultures, leading to diffuse and irregular nucleolin stainings (Kwon *et al.*, 2014; Tao *et al.*, 2015; Wen *et al.*, 2014). The localisation of poly-PR/GR to the nucleolus is pathological, since it impedes rRNA biogenesis and kills cells (Kwon *et al.*, 2014; Tao *et al.*, 2015).

Problematically, the nucleolar localisation of arginine-rich DPRs is disputed in patient tissues (Davidson *et al.*, 2016). Whilst one study did find evidence of this phenomenon (Wen *et al.*, 2014), other studies have not been able to repeat this (Mackenzie *et al.*, 2015; Schludi *et al.*, 2015), and found that arginine-rich DPRs were predominantly cytoplasmic. Taken together, data suggests that arginine-rich DPRs and C9orf72 RNA expansions can induce nucleolar stress in cell models, ultimately leading to impaired nucleolar stress.

1.4.2.3. Nucleocytoplasmic transport defects

Recently, a genome wide screen of disease modifiers in yeast models that express poly-PR DPRs, identified a number of factors involved in nucleocytoplasmic transport, such as the karyopherin import receptors (Jovicic *et al.*, 2015). Freibaum and colleagues performed a similar screen in Drosophila, in a disease model that expressed both RNA and DPRs, and similarly found an enrichment of proteins linked to nucleocytoplasmic trafficking (Freibaum *et al.*, 2015). In particular, they identified defects in the trafficking of mRNAs, which resulted in the nuclear accumulation of mRNA. This has also been reported in cultured cells (Rossi *et al.*, 2015), and may be explained by the sequestration and impairment of RNA export factors.

RanGAP (human orthologue, RanGAP1), a nucleocytoplasmic regulator, was also identified from genome-wide screens in Drosophila (Freibaum *et al.*, 2015). Zhang and colleagues demonstrated that C9orf72 RNA expansions physically interact with RanGAP1 and is mislocalized in C9orf72 Drosophila, C9orf72-ALS patient IPSC-derived motor neurons, and in C9orf72-ALS patient brain tissues (Zhang *et al.*, 2015a). Importantly, genetically altering the expression of nucleocytoplasmic proteins can modify C9orf72 expansion driven toxicity (Freibaum *et al.*, 2015; Zhang *et al.*, 2015a). As such, a dysregulation of nucleocytoplasmic shuttling appears to occur as a result of arginine-rich DPRs and RNA repeat expression. Whilst this is clearly important in driving neurodegeneration in Drosophila models, more work needs to be done to verify these findings in mouse models.

1.4.2.4. Transcriptional dysregulation

Since several RNA processing proteins are sequestered by RNA foci, it is plausible that there will be a defect in RNA processing in C9orf72-ALS/FTD. Indeed, C9orf72-ALS/FTD patient IPSC-derived neurons and motor cortex tissues display distinct gene expression profiles (Donnelly *et al.*, 2013), with a small percentage of genes being dysregulated in both models. Lagier-Tourenne and colleagues also found distinct RNA sequencing profiles in patient fibroblasts when compared to non-ALS controls, but also detected notable gene expression differences between C9orf72-ALS and non-C9orf72-ALS control cells (Lagier-Tourenne *et al.*, 2013). Cooper-Knock and colleagues demonstrated that RNA splicing factors were commonly mis-regulated in C9orf72-ALS patient samples, when compared to non-diseased controls (Cooper-Knock *et al.*, 2015c). Taken together, these data imply that gene expression profiles of C9orf72-ALS patient models are dysregulated.

More compelling evidence of transcriptional dysregulation was recently provided from the Petrucelli laboratory (Prudencio *et al.*, 2015). Using RNA sequencing, they show distinct brain transcriptomes in C9orf72-ALS patient motor cortex and cerebellum, when compared to sALS and non-ALS control subjects. Key hits were also validated with RT-qPCR, adding greater confidence in their findings. Importantly, in addition to genome wide transcriptome changes, they also identified a number of common splicing errors, which were detected in C9orf72-ALS and sALS cases. Interestingly, errors such as intronic retention were three-times more severe in C9orf72-ALS, when compared to sALS, suggesting that splicing dysfunction is an important aspect of C9orf72-ALS.

The dysregulation of splicing in C9orf72-ALS is hypothesised to be a consequence of RNA foci-mediated sequestration events (Cooper-Knock *et al.*, 2014). In addition, arginine-rich DPRs have also been shown to induce splicing errors in cultured cells (Kwon *et al.*, 2014). Interestingly, poly-PR dipeptides induced both intronic retention as well as exon exclusion, suggesting that arginine-rich DPRs cause a general dysregulation of pre-mRNA splicing activity. As such, nucleolar stress, nucleocytoplasmic transport, and dysfunctional splicing are strongly linked to the expression of C9orf72 RNA and/or arginine-rich DPRs.

1.4.2.5. Dysregulation of protein degradation pathways

The majority of molecular research has focused on the expression of RNA repeat expansions (non-ATG-driven) or on the expression of the highly toxic poly-PR and poly-GR DPRs. Poly-GA DPRs are the most abundant DPR species in human tissues (Davidson *et al.*, 2016; Davidson *et al.*, 2014; Mackenzie *et al.*, 2015), and are toxic in cell culture and mouse models (Walker *et al.*, 2017; Zhang *et al.*, 2016). Thus, whilst they are less toxic than arginine-rich DPRs, their relative abundance may actually make them a more important element of disease progression.

Poly-GA is biochemically distinct from the arginine-rich DPRs, since it is hydrophobic, and aggregates in the cytoplasm, nucleus and perinuclear space of cells (May *et al.*, 2014; Walker *et al.*, 2017; Wen *et al.*, 2014; Zhang *et al.*, 2016). These aggregates co-localise with p62- and profoundly increase p62 protein levels (Walker *et al.*, 2017), suggesting that poly-GA DPRs lead to impaired autophagy and/or proteasome degradation. Studies have demonstrated that poly-GA DPRs lead to an impairment of the ubiquitin proteasome system (UPS) (May *et*

al., 2014; Zhang *et al.*, 2014), suggesting that poly-GA DPRs may be toxic by impairing - or saturating - protein clearance pathways. Mutations in protein clearance genes, such as SQSTM1 (encoding p62) and UBQLN2 (encoding ubiquilin-2), can cause ALS (Fecto *et al.*, 2011; Kovacs *et al.*, 2016), demonstrating that defects in protein clearance pathways can cause ALS.

As such, since the discovery of the C9orf72 repeat expansion, several molecular pathways have been linked to the disease progression. Figure 2 summarises the most prominent molecular features, which have thus far been associated to C9orf72 expansion-specific disease pathologies.

1.4.2.6. Genomic Instability is an emerging paradigm in C9orf72-ALS/FTD

Recently, a number of seminal research papers have implicated a role for genomic instability in motor neuron disease. Mutations in SETX are found to cause juvenile ALS (ALS4) as well as ataxia with oculomotor apraxia type 2 (OAO2) (James & Talbot, 2006; Palau & Espinos, 2006). SETX is well-documented to play a role in the maintenance of genome stability (Groh *et al.*, 2014; Yuce & West, 2013). In cellular models of spinal muscular atrophy (SMA), a childhood form of motor neuron disease, increased levels of genomic instability are observed (Zhao *et al.*, 2016). Increased genome instability has also been demonstrated in FUS-ALS (Rulten *et al.*, 2014; Wang *et al.*, 2013) as well as in sALS cases (Murata *et al.*, 2008).

The link between genome instability and C9orf72 expansions has also been established recently. In a recent study, poly-GR was shown to increase DNA damage levels, as measured by γH2AX immunostaining and COMET tail moments (Lopez-Gonzalez *et al.*, 2016). Genome instability in these cells was thought to occur via reactive oxygen species, since treatment with antioxidants reduced the levels of DNA damage in poly-PR expressing cells. Moreover, poly-PR DPRs were shown to bind to a number of mitochondrial ribosomal proteins, suggesting a disruption of mitochondrial homeostasis underpins ROS production and elevated levels of DNA damage. Similar data was also obtained using C9orf72-ALS patient IPSC-derived neurons (Lopez-Gonzalez *et al.*, 2016). In other research, poly-GA DPRs were shown to sequester Rad23a and Rad23b, which lead to decreased levels of the global genome NER factor, XPC (Zhang *et al.*, 2016). Whether this translates into genomic instability, however, was not tested. As such, growing evidence suggests that genome

instability is a likely consequence of ALS mutations and, in particular, C9orf72 repeat expansions.

Given the growing evidence linking ALS and C9orf72 repeat expansions to genomic instability, we aimed to assess whether C9orf72 expansions lead to genome instability. In addition, we aim to investigate the molecular drivers of C9orf72-associated genomic instability, and to assess how these repeat expansions affect DNA repair pathways.

Figure 2. Summary of toxic mechanisms caused by C9orf72 repeat expansion pathology.

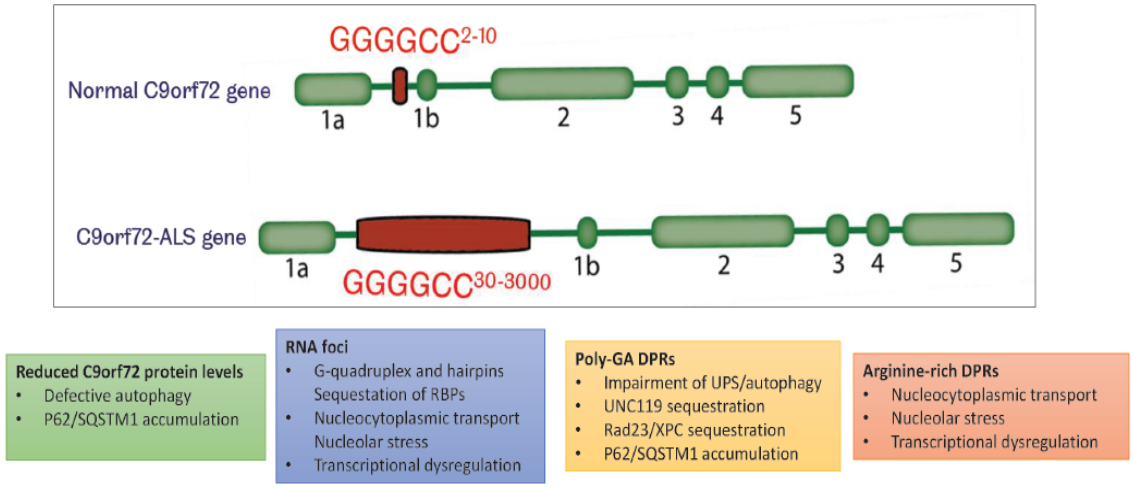

Figure 2. Summary of toxic mechanisms associated with C9orf72 repeat expansions. Haploinsufficiency of the C9orf72 protein leads to impaired autophagy and an increase in p62 puncta. The expanded RNA transcripts form stable secondary structures and focally accumulate in cells, leading to the sequestration of RNA binding proteins (RBPs). Poly-GA DPRs disrupt cellular clearance mechanisms, such as the UPS and autophagy, leading to p62 accumulation. They also sequester proteins, such as Unc119, Rad23a/Rad23b and XPC. Arginine-rich DPRs localise to the nucleolus, impair rRNA biogenesis, and lead to nucleolar stress. Alike arginine-rich DPRs, RNA foci bind nucleolin and cause nucleolar stress. Transcriptional dysregulation, including splicing malfunction, have also been reported in cells expressing C9orf72 RNA expansions and arginine-rich DPRs.

Chapter 2: Methods

2.1. Human cell culture, transfection, and transduction.

MRC5 cells were grown in Minimum Essential Media (MEM) (Sigma Aldrich) supplemented with 10% Foetal Bovine Serum (FBS) (Sigma Aldrich), 2mM L-Glutamine (Sigma Aldrich) and 1% Penicillin/Streptomycin (Sigma Aldrich). HEK 293T cells were grown in Dulbecco's Modified Essential Media (Sigma Aldrich) supplemented with 10% Foetal Bovine Serum (FBS), and 1% Penicillin/Streptomycin (Sigma Aldrich). MRC5 cells were seeded on coverslips into the wells of a 24-well plate at a density of 3×10^5 cells/cm^2. For other experiments, HEK 293T cells were seeded into the wells of a 12-well plate at a density of 3×10^5 cells/cm^2. The following day, cells were transfected with 250ng of DNA/cm^2 of each DNA plasmid, using polyethylenimine at a molar concentration of 3:1 (PEI: DNA). 6-hours post-transfection, the media was replaced and cells were incubated for a further 2 or 3 days, as indicated in the figure legends.

For p62 knockdown experiments, MRC5 cells were co-transfected with cDNA plasmids using PEI (as described above) alongside control siRNA particles or p62 targeting particles (Santa Cruz, sc-29679) at a molarity of 25nm. Dharmafect was used as the transfection reagent for all siRNA experiments at a molar ratio of 1:1 (siRNA:Dharmafect). Recombinant adenovirus (Adenovirus-type 5 dE1/E3) encoding for SETX or RFP were purchased from Vector Biolabs. Viral stocks (10^9 viral genomes/mL) were diluted 1:5000 for MRC5 and 1:20000 for HEK293T cells to give an approximate multiplicity of interest (MOI) of 10 and 2.5 for MRC5 and HEK 293T cells, respectively. Virus containing media was added 2-3 hours prior to transfection, and then replaced with fresh. For Western blotting, cell death assays, and COMET assay experiments, MRC5 cells and HEK 293T cells were grown for 72 hours post-transfection. For DNA repair immunocytochemistry assays, cells were grown for 48 hours post-transfection.

2.2. Generation of Repeat Expansion Constructs (performed by Adrian Higginbottom, Padraig Mulcachy, and Kurt De Vos)

Synthesised TCGAC(G4C2)^{10} sense and ACGT(G2C4)^{10} antisense ssDNA oligonucleotides (Sigma-Aldrich) were designed with SalI/XhoI overhangs. The dsDNA oligos were generated by denaturing oligos at 99ºC for 30 min and then annealing by stepwise cooling (0.5ºC/min).

The $(G4C2)^{10}$ expansions were ligated into SalI and XhoI digested pcDNA6.2-GW/EmGFP-miR (Invitrogen), to generate pcDNA6.2-GW/EmGFP-$(G4C2)^{10}$. Further $(G4C2)^{102}$ repeats were subcloned using the 3' XhoI site. pCMV-EmGFP-$(G4C2)^{n}$ vectors containing 10 and 102 repeats were then generated via this method. EmGFP was subsequently excised using the flanking DraI restriction site. The $(G4C2)^{10}$ and $(G4C2)^{102}$ constructs were sub-cloned into pcDNA5/FRT/TO HIS (Addgene) using DraI and XhoI restriction sites. Transformations of plasmids containing the $(G4C2)^{n}$ repeat constructs were performed using recombination-deficient β-10 E.coli (NEB) to minimise $(G4C2)^{n}$ repeat shrinkage.

To model gain-of-function via RAN translation of C9orf72 repeat expansions. we produced two expression constructs coding for uninterrupted V5-tagged poly-GA DPRs, using an expandable cloning strategy with Age1 and Mre1 as compatible enzymes. We first constructed a 'start acceptor' pCi-Neo vector (Promega) by cloning a V5-3xGA insert into the Xho1/Not1 sites (ctc gag gcc acc atg ggc aaa ccg att ccg aac ccg ctg ctg ggc ctg gat agc acc ggt gca ggt gct ggc gcc ggc gga tcc gaa ttc tag ccg cgg ccg c) and a 'start donor' vector with a 14xGA insert (ctc gag acc ggt gca ggt gct gga gct ggt gca ggt gct gga gca ggt gca ggt gct gga gct ggt gca ggt gct gga gca ggt gct ggc gcc ggc gga tcc gaa ttc ccg cgg ccg c) in the Xho1/Not1 sites. These sites were then used to propagate the repeats to construct 34 and 69 GA repeats. A V5 construct that lacked DPRs was created by AgeI and NGOMIV digestion, which excised the DPR coding region.

2.3. Primary Cortical Neuron Cultures (performed by Saul Herranz-Martin)

The cortex from the brains of E17.5 rat pups were harvested and stored in Hank's Balanced Salt Solution (without calcium, without magnesium) (HBSS -/-) (Sigma Aldrich). The tissue was washed with HBSS (-/-) and then incubated with 0.0035% Trypsin (Sigma Aldrich) for 15 minutes. DNAse (10µg/mL)(Sigma Aldrich) was then added at a ratio of 1:1 (v/v), and the tissue was re-suspended in 1mL triturating solution (1% Albumax, 25mg Trypsin Inhibitor, 10µg/mL DNAse) (Sigma Aldrich). Neurobasal media (ThermoFisher), supplemented with 2 mM L-Glutamine (Sigma Aldrich), 1% Penicillin/Streptomycin (Sigma Aldrich) and 1 x B-27 (Sigma Aldrich) was then added at a ratio of 1:5 (Triturating solution:Neurobasal media). Cells were then plated onto Poly-D-Lysine coated coverslips, in the wells of a 24 well-plate at a density of 9.365×10^4 cells/cm^2. 1.5×10^5 viral genomes (vg) per cell of AAV9 was added to cultures after 5 days *in vitro* (DIV). Half of the culture media was replaced with

fresh media every 3 days. 7-days post-transduction (13 DIV), cells were treated with CPT (10μM) where indicated, and fixed using 4% paraformaldehyde or methanol:acetone (50:50).

2.4. Production of viral vectors (performed mainly by Saul Herranz-Martin)

Sixty 15cm^2 plates containing HEK 293T cells (~80% confluent) were transfected using polyethylenimine with a mixture of three plasmids (at a molar ratio of 2:1:1 in order as listed) required to generate an infectious AAV9 viral particle: (1) a plasmid providing helper genes isolated from adenovirus that enhance viral infectivity (pHelper); (2) an ITR-containing plasmid containing the 10, 102 RRE or 34, 69 DPR driven by the CMV promoter; (3) a plasmid that carries the AAV Rep-Cap proteins (pAAV2/9). A total of 52μg of DNA was transfected per plate. For all experiments, we used the pAV2-CMV-GFP consisting of two ITRs in a truncated genome that resulted in a self-complementary AAV9 (scAAV9). Four days after transfection, the AAV enriched media was collected, incubated at 37°C for 2 hours with 3,750 units of benzonase (Sigma, USA), filtered through a 0.22 μm filter, and concentrated to a volume of 1 mL using Amicon spin filter units (Millipore, USA). The virus was then washed with 50 mL of phosphate buffered saline (PBS, pH 7.3) in the same Amicon spin filter units, and concentrated to a final volume of 0.5 ml. The viral sample volume was expanded to 14ml with PBS, separated through a discontinous iodixanol (D1556, Sigma, USA) gradient (4ml of 54%, 9 ml of 40%, 9 ml of 25%, 5 ml of 15%), and centrifuged at 69,000 rpm for 1.5 hours at 18°C. The purified virus, which was found as a white layer between the 54% and 40% iodixanol gradient, was subsequently removed in 0.5ml fractions using a syringe. 10μl of each fraction was mixed at an equal ratio with 2X SDS-PAGE loading buffer, heated to 75°C for 20 minutes, separated on a 4-20% precast TGX mini-gel (Biorad, USA), and stained with Sypro-Ruby according to the manufacturer's protocol (Life Technologies, USA). Fractions that showed a pure virus composed solely of the VP1, VP2 and VP3 bands were combined, and washed against 5 full volumes (15ml each) of PBS with an Amicon spin filter, before collecting in a final volume of between 300-500μl. Concentrated viral stocks were stored at -80°C until usage.

Viral titres were determined with the Quantifast SyBR Green PCR Kit (Qiagen, Cat 204054) on a BioRad CFX96 thermal cycler, following the manufacturer's instructions. The number of viral copies in three dilutions of a purified AAV9 virus (100x, 1000x, 10,000x) was compared to a standard curve generated by serial dilutions of a linearized vector. Primers

used to quantify viral genomes were (Poly A, Forward: 5'-ATT TTA TGT TTC AGG TTC AGG GGG AGG TG-3'), (PolyA, Reverse: 5'-GCG CAG AGA GGG AGT GGA CTA GT-3'), (GFP, Forward: 5'- GAC GGC AAC ATC CTG GGG CAC AAG-3'), and (GFP, Reverse: 5': CGG CGG CGG TCA CGA ACT C-3').

2.5. RNA Fluorescent-In-Situ-Hybridisation (FISH)

FISH was performed following a modification of the method described previously (Cooper-Knock *et al.*, 2014). MRC5 cells or rat cortical neurons were fixed with 4% PFA for 10 minutes at room temperature. For S9.6 staining however, fixation was performed using ice-cold methanol:acetone (50:50) for 10 minutes at -20°C. Cells were then incubated with pre-hybridisation buffer (50% formamide, 2X saline sodium citrate (SSC), 100 mg/ml dextran sulphate, 50 mM sodium phosphate pH 7.0) for 1 hour at 66°C. Subsequently, cells were incubated with hybridisation buffer containing a 5' TYE-563-labelled locked nucleic acid (16-mer fluorescent)-incorporated DNA probe against the GGGGCC RNA hexanucleotide repeat (Exiqon, Inc., batch number 607323), at a concentration of 400 ng/mL for 1 hour or overnight at 66°C. A 1 hour incubation period was preferred for phospho-ATM staining, due to the loss of antigen signal after overnight treatment in hybridisation buffer. After hybridization, slides were washed once in 2 X SSC with 0.1% Tween-20 at room temperature and three times in 0.1 X SSC at 66°C. All washes were performed for 10 minutes. All solutions were made with DEPC-treated water. Following the completion of this FISH protocol, ICC was then performed as described below, though using DEPC-treated PBS solutions.

2.6. Immunocytochemistry (ICC)

MRC5 cells or rat cortical neurons were fixed with 4% PFA for 10 minutes at room temperature, or with ice-cold methanol:acetone (50:50) for 10 minutes at -20°C. Cells were then washed 3 times with Phosphate Buffered Saline (PBS), incubated with 0.5% Triton-X (in PBS) for 5 minutes, and washed a further 3 times with PBS. In order to confirm the specificity of the S9.6 antibody, MRC5 cells, fixed with methanol:acetone, were incubated with RNASE H enzyme (100units/mL) in 3% BSA in PBS overnight at 4°C before ICC/FISH-ICC. For ub-H2A staining, cells were incubated with PBS containing 0.5% Triton-X for 2 minutes at room temperature before fixation with 4% PFA. Subsequently, cells were

incubated with 3% BSA for 30 minutes, before being incubated with primary antibodies (in 3% BSA) for 1 hour (with the exception of Ub-H2A, which was incubated overnight at 4°C). For DPR experiments, a V5 antibody was always used to detect DPR-positive cells. Cells were washed 3x with PBS and incubated with fluorescent secondary antibodies (in 3% BSA) for 1 hour, before being washed another 3x with PBS. Coverslips were mounted onto glass slides using Fluoromount™ Aqueous mounting medium (Sigma Aldrich).

Anti-V5 antibodies: mouse (Abcam, ab27671), and rabbit (Bethyl, A190-120A) were used at 1:1000. A mouse anti-RNA:DNA hybrid (S9.6) antibody (Kerafast, ENH001) and a mouse anti-ub-H2a antibody (Merck Millipore, E6C5) were used at a concentration of 1:500 for immunocytochemistry, and at 1:5000 for FISH-ICC double staining. A mouse anti- γH2AX (Ser 139) antibody (Merck Millipore, JBW301), a rabbit anti-53BP1 antibody (Bethyl, A300-272A), a rabbit anti-phospho-ATM antibody (Abcam, EP1890Y), a mouse anti-phospho-P53 antibody (Cell Signalling, 9286s), a mouse anti-cleaved PARP (Cell Signalling, 9548), and a rabbit anti-Nbs1 antibody (Sigma, N3162) were all used at a concentration of 1:1000. A rabbit anti-HDAC4 antibody (Abcam, ab1437) was used at a concentration of 1:250. A rabbit H3K9me3 antibody (Abcam, ab8898) was used at a concentration of 1:2000. Subsequently, cells were washed 3 times with PBS and incubated with the corresponding Alexafluor secondary antibodies (all purchased from Life Technologies and used at a concentration of 1:500) as well as DAPI for 1 hour. For FISH-IF double staining, an Alexafluor 488 was used in conjunction with the Cy3 fluorescent probe. Cells were washed a further 3 times with PBS and coverslips were mounted onto glass slides using Fluoromount™ Aqueous mounting medium (Sigma Aldrich).

2.7. Immunohistochemistry

Mouse brain and spinal cord sections were incubated with 0.5% Triton-X for 30 minutes, followed by a 1 hour incubation with 3% BSA (with 0.2% Triton-X) for 1 hour. Subsequently, sections were incubated with primary antibodies (in 3% BSA with 0.2% Triton-X) overnight at 4°C. The following day, sections were washed 3 times with PBS, and were incubated with fluorescent secondary antibodies alongside DAPI for 1 hour at room temperature. For γH2AX and HDAC4 staining in DPR mice sections, a biotinylated secondary antibody was used in conjunction with a tertiary anti-streptavidin Alexa Fluor 488 antibody, in order to enhance the signal. Sections were washed a further 3 times, before

mounting with Fluoromount™ Aqueous mounting medium (Sigma Aldrich). For human spinal cord staining, 5µm paraffin embedded spinal cord sections from C9orf72-ALS and non-ALS controls (Table-1, Supplementary Information) were incubated with primary antibodies specific for HDAC4 (Abcam, ab1437), γH2AX (R&D systems, AF2288), S9.6 (Kerafast, ENH001), or H3K9me3 (Abcam, ab8898) at concentrations of 1:250, 1:500, 1:1000 and 1:1000; respectively. Before primary antibody incubation, antigen retrieval was performed in 10 mM Sodium citrate (pH6) or 10 mM Tris Base for HDAC4, S9.6 and H3K9me3, or 1 mM EDTA (pH9) for γH2AX. Antigen retrieval was performed for 30 minutes in a pressure cooker. Immunohistochemistry was performed using the intelliPATH FLX™ Detection Kit, according to the manufacturer's protocol. Work on human tissue was reviewed by the Sheffield Brain Tissue Bank (SBTB) Management Board and approval to release tissue under REC 08/MRE00/103 was granted. All post-mortem tissue stored at Sheffield Brain Tissue Bank was obtained with informed consent.

2.8. Cell Lysis, SDS-PAGE and Western Blotting

In order to collect whole-cell lysates, MRC5 cells, HEK 293T cells, or mice brainstem sections were lysed in RIPA buffer (150 mM NaCl, 0.5% sodium deoxycholate, 0.1% SDS, and 50 mM Tris, pH 8.0, supplemented with protease inhibitor cocktail, Sigma Aldrich) on ice for 30 minutes, before being sonicated in order to shear the DNA. For the isolation of chromatin fractions, the cytoplasmic and nuclear soluble proteins were first removed by hypotonic and hypertonic buffers. The remaining pellet was lysed with nuclear insoluble buffer (20mM Tris ph8, 150mM NaCl, 1% SDS, and 1% NP-40) for 30 minutes on ice before being sonicated. The protein concentration of each whole-cell lysate was estimated using a BCA assay (Pierce™), and equal quantities of protein were mixed with a 2X reducing sample SDS-PAGE buffer, heated to 95°C for 5 minutes, separated on a 4-20% precast TGX mini-gel (Biorad, USA), and transferred onto a PVDF membrane (Millipore, USA). Membranes were blocked with 3% BSA in TBS with 0.05% Tween (TBST) for 30 minutes, before incubating at either room temperature for 2 hours or 4°C overnight with agitation with primary antibody in 3% BSA in TBST. For Western Blotting, a mouse a rabbit ATM antibody (Abcam, ab82512) was used at 1:2000, a rabbit H3K9me3 antibody (Abcam, ab8898) was used at 1:5000, mouse anti-α Tubulin (Abcam, T9026) and mouse anti-GAPDH (Calbiochem, CB1001) were used at 1:5000. Rabbit anti-H2A antibodies (Abcam, ab18255) were used at 1:1000. Membranes were then washed 3 times for 5 minutes with TBST and

incubated with either a HRP-linked secondary anti-mouse antibody (Bio-Rad, 1721011) or an anti-rabbit antibody (Dako, D048701-2). Enhanced ChemiLuminescence (ECL) substrate was then added to the membrane to enable detection, and non-saturated images were acquired using a G:BOX EF machine (Syngene) and Snapgene software (Syngene).

2.9. Trypan Blue Cell Death Assay

3 days after transfection, HEK 293T cells were washed once with PBS and treated with trypsin until detached. Subsequently, 10% FBS-containing DMEM was added and cells were resuspended gently by pipetting up and down 3 times. Cell suspensions were then mixed with Trypan Blue (0.04%) at a ratio of 1:1. Immediately after, the percentage of cells that were permeable to Trypan Blue was calculated using a haemocytometer and a brightfield microscope. Scoring was performed under single-blinded conditions.

2.10. Measurement of topoisomerase I cleavage complexes (TOP1cc) (performed by Chunyan Liao)

TOP1 protein–DNA complexes were purified using caesium chloride density gradients: Approximately $2x10^6$ cells were lysed in 1% sarcosyl, 8 M guanidine HCl, 30 mM Tris pH 7.5 and 10mM EDTA. Cell lysates were then incubated at 70°C for 15 minute to remove all non-covalently bound proteins from DNA. Cell lysates were then loaded on a caesium chloride density step gradient (5 ml total volume) and centrifuged at 75,600g at 25°C for 24 hour to separate free proteins from DNA. Ten consecutive 0.5 ml fractions were collected and slot blotted onto Hybond-C membrane (Amersham). To ensure equal DNA loading, the DNA concentration in each extract was determined fluorimetrically using PicoGreen (Molecular Probes/Invitrogen). Covalent TOP1–DNA complexes were then detected by immunoblotting with anti-TOP1 polyclonal anti- bodies (sc-32736, Santa Cruz.) and visualised by ECL.

2.11. Neutral single-cell agarose gel electrophoresis (Comet) assays (performed by Waheba Elsayed and Mohammed Hassan)

HEK293T cells at density of 3×10^5 were seeded at 37°C overnight. The next day, cells were transfected using PEI (1µg/µl) transfection reagent with plasmid DNA 500 ng/well. Transfected cells were incubated at 37°C for 24h then the complete media replaced with 1% FBS media and incubated for an additional 48h. Transfection efficiency was assessed at

~75%. Cells were suspended in pre-chilled phosphate buffered saline (PBS) and mixed with equal volume of low-gelling-temperature agarose 1.3% (Sigma, Type VII) preserved at 42°C. Cell mixture was immediately spread onto pre-chilled frosted glass slides (Fisher), pre-coated with 0.6% agarose. The slides were incubated at 4°C in the dark until set, and for all further steps. Slides were incubated in pre-chilled lysis buffer (2.5 M NaCl, 10 mMTris-base, 100mM EDTA (pH 8.0), 0.5% Triton X-100, 1% N-laurylsarcosine sodium salt and 3% DMSO; pH9.5) for 2 h. After incubation, slides washed with pre-chilled distilled warer (2-10 min), and immersed for 1h in pre-chilled electrophoresis buffer (300mM sodium acetate, 100mM Tris-HCl, 1% DMSO, pH8.3). Electrophoresis was then conducted for 60 min at 1 V/cm, accompanied by washing 3 times with neutralization in 400 mM Tris- HCl (pH 7.5) for 15min. Finally, slides was stained with DNA Sybr Green I nucleic (1:10000, in PBS) (Sigma) for 30 min. Average tail moments were quantified from 100 cells per sample using Comet Assay IV software (Perceptive Instruments, UK).

2.12. Generation of AAV9-mediated mice (performed by Saul Herranz-Martin)

3 x 10^{10} vg of purified scAAV9 was injected into the cisterna magna of C57BL/6J P1 wild-type mice under general anaesthesia. Pups were placed over a red light torch in prone position to enable visualisation of the injection site. scAAV9 was loaded into a 5 µL syringe and the virus were injected under a flow rate of 1µL/min. Animals were housed in groups of up to 5 per cage. Six or 12 months after injection, mice were sacrificed under terminal anaesthesia and transcardially perfused using a solution of PBS-Heparin. Brain sections were then isolated and fixed using 4% PFA overnight at 4°C. After fixation, tissue was washed with PBS, cryoprotected in 30% of sucrose at 4°C and embedded in OCT (Cell Path®). 20 or 40µm brain coronal sections were derived using a cryostat, and then analysed using immunohistochemistry. All animal *in vivo* experiments were approved by the University of Sheffield Ethical Review Committee and performed according to the Animal (Scientific Procedures) Act 1986, under the Project License 40/3739.

2.13. Image Acquisition and Analysis

All representative images presented are Z stack projections acquired on a Leica SP5 confocal microscope, using the 63x 1.20 lens. For imaging cell monolayers, each stack was performed at 0.5µm intervals, scanning the entire nucleus. In tissue sections, images were acquired using

1µm Z stacks. Fluorescence intensity quantification was performed using Image J according to a protocol described previously (McCloy *et al.*, 2014): the corrected nuclear fluorescence value of the relevant channel was calculated using the formula: Corrected Nuclear Fluorescence (CNF) = Integrated Nuclear Density (IND) – Nuclear Area (NA) x Mean Fluorescence of Background (MFB). For *in vitro* foci counting, quantification was performed under the 100x lens of a Nikon Eclipse Ni microscope, with 20-100 cells/condition assessed (as indicated in the respective figure legend). For quantification of mice brain sections, brainstem or cerebellar sections were imaged on a confocal microscope, as described above, and analysed manually (with one exception). For γH2AX analysis in mice expressing 0, 69 poly-GA DPRs, foci quantification was automated, using image j. For human spinal cord sections, images were acquired using a Nikon Eclipse Ni microscope under the 100x and 20x objective lenses. Large motor neurons located in the ventral horn of spinal cord sections were considered for analysis, ~50 motor neurons (minimum 25) were analysed from 6 C9orf72-ALS samples and 6 non-ALS samples. Motor neurons were considered R-Loop or γH2AX positive when the whole nucleus was stained positive. We employed a double-blind randomization process in which experimental groups and the protein being analysed were blinded to the person analysing the data (e.g. counting nuclear foci or taking micrographs). For H3K9me3 analysis, 4 control and 4 C9orf72-ALS were imaged using a Leica LP5 confocal microscope and the mean fluorescence intensity (minus background signal) was calculated from 20 motor neurons per case.

2.14. Experimental repeats and Statistical analysis

All data are presented as the means ± standard errors of the mean (SEM) of 3 biological replicates, unless otherwise stated. Statistical differences were analysed using Student's t-tests for pair-wise comparisons or one-way ANOVA (with Tukey's correction) for comparing groups more than 2 but less than 9. A p-value less than 0.05 was considered to be statistically significant. Asterisks denote p values <0.05, double-asterisks denote p values <0.01, and triple asterisks denote p values <0.001, NS denotes p values >0.05. Table 3 summarises the statistical test used and p values obtained for each Figure.

Chapter 3: C9orf72 expansions cause R-loop-mediated genome instability

3.1. Introduction

3.1.1. Introduction to R-loop biology

RNA/DNA hybrids are formed in cells during replication, where short RNA oligonucleotides serve as primers for DNA synthesis (Santos-Pereira & Aguilera, 2015). They also occur during transcription, as the RNA polymerase incorporates each ribonucleotide triphosphate onto the RNA transcript (Santos-Pereira & Aguilera, 2015). In addition, much longer RNA/DNA hybrids can form during transcription, if the nascent RNA transcript anneals to its template DNA strand. Such hybrids cause the displacement of the complementary DNA strand, yielding a three-stranded nucleic structure known as an R-loop (Santos-Periera & Aguilera, 2015). R-loops are a transcriptional by-product that likely form when the nascent RNA transcript exits the RNA polymerase (termed the thread-back model). R-loop formation is known to be favoured at GC-rich sites of the genome (Ginno *et al.*, 2013, which may occur because guanine-rich RNA: cytosine-rich DNA duplexes are thermodynamically more stable than the respective DNA: DNA duplex (Roy & Lieber, 2009). R-loops are also increased by the presence of G-quadruplex structures and by negatively supercoiled DNA (Aguilera & Garcia-Muse, 2012; Duquette et al, 2004). Once formed, R-loops can be very stable structures as they are bound together by Watson-Crick base-pairing.

R-loops have been described as a double-edged sword (Skourti-Stathaki & Proudfoot, 2014): This is because R-loops have a number of critical functions, including the initiation of replication at prokaryotic and mitochondrial origins of replication (Masukata *et al.*, 1996) and for class-switch recombination of mammalian B lymphocytes (Yu *et al.*, 2003). In addition to these important functions, R-loop accumulation can lead to negative cellular consequences (summarised in Figure 3), including genomic instability (Huertas & Aguilera, 2003; Li & Manley, 2005; Sollier *et al.*, 2014; Tuduri *et al.*, 2009; Wahba *et al.*, 2011). This phenomenon was first observed when yeast mutant strains lacking the RNA processing factors of the THO complex (Huertas & Aguilera, 2003) displayed elevated levels of R-loops and genome instability. Similar results were seen after SRSF1 depletion in vertebrates (Li & Manley, 2005), suggesting that RNA processing factors are important in the maintenance of

R-loop homeostasis (Santos-Pereira *et al.*, 2013), presumably by binding to the nascent RNA transcript and actively preventing R-loop formation.

3.1.2. Mechanisms of genomic instability linked to R-loops

Whilst the link between R-loops and genomic instability is compelling, the mechanisms by which R-loops generate DNA damage are not well understood. One reason as to why R-loops drive DNA damage may be due to the displacement of the ssDNA strand, which is left vulnerable to chemical damage (Aguilera, 2002). The ssDNA may also be targeted by ssDNA-specific nucleases. For example, activation-induced cytidine deaminase (AID) is a nuclease that converts Cytosine to Uracil at ssDNA residues. This deamination event makes the DNA base attackable by the BER enzyme, uracil DNA glycosylase, whom excises the base and induces a DNA lesion (Gomez-Gonzalez & Aguilera, 2007). This process occurs during class-switch recombination (Basu *et al.*, 2011), but it has also been shown to induce DSBs in non-immunoglobulin genes (Chiarle *et al.*, 2011), suggesting that nuclease activity at sites of R-loops could represent a pathway to genomic instability.

NER-linked structure-specific endonucleases have also been linked to the processing of R-loops, by targeting the flaps that are produced at either end of the R-loop (Sollier *et al.*, 2014). R-loops formed due to the inhibition of TOP1, or due to the absence of RNA processing factors, can be processed into DSBs by the NER flap-endonucleases, XPF and XPG (Sollier *et al.*, 2014). The processing of the R-loop into DSBs required transcription-coupled NER factors, and not those involved with global-genome NER (Sollier *et al.*, 2014). It is not yet clear whether this process represents a healthy R-loop processing pathway, or whether the NER factors are mistaking the R-loop for their canonical substrates.

In addition to the processing of R-loops into DNA breaks by nucleases, R-loops can cause DSBs in dividing cells due to physical collisions with the replication machinery (Alzu *et al.*, 2012; Hamperl *et al.*, 2017; Tuduri *et al.*, 2009). Each of these events may contribute to R-loop-driven genomic instability.

Figure 3. Cellular effects of R-loop accumulation.

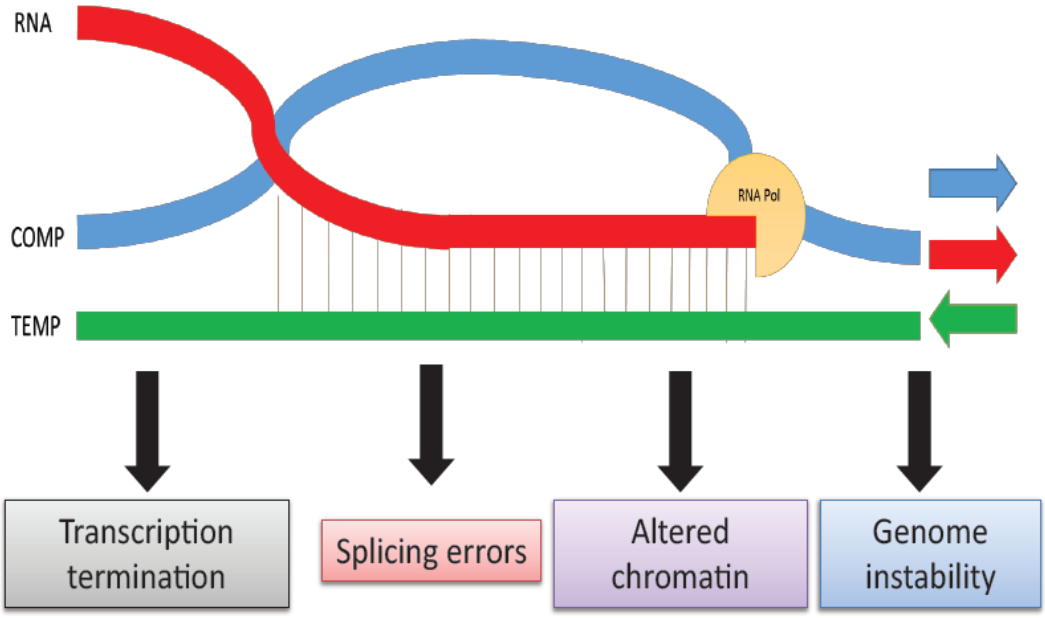

Figure 3. Cellular effects of R-loop accumulation. The pathological accumulation of R-loops has been shown to lead to premature transcriptional termination. In addition, splicing errors – namely intronic retention – are induced by the presence of excess R-loops. The accumulation of R-loops also results in the formation of repressive, compacted, or heterochromatic histone marks.Unresolved R-loops are processed into DNA breaks, leading to genome instability.

3.1.3. Mechanisms of R-loop resolution

Given their potentially catastrophic effects on the genome, it is perhaps unsurprising that cells have acquired a number of different mechanisms for repairing R-loops. RNASE H1 is a single polypeptide with ribonuclease activity towards the RNA strand of RNA/DNA hybrids (Cerritelli & Crouch, 2009). RNASE H1 is present in the nucleus and mitochondria, and has been shown to be essential for mitochondrial replication (Cerritelli *et al.*, 2003). RNASE H2 is a trimeric complex, with RNASE 2A being the catalytically active subunit (Cerritelli & Crouch, 2009). Unlike H1, which requires an R-loop at least 4 base-pairs in length, H2 can cleave even a single RNA molecule that is incorporated into the DNA duplex (Eder *et al.*, 1993), and is also important for removing Okazaki fragment RNA primers (Murante *et al.*, 1998). Whilst some crossover between the substrates of H1 and H2 exists, it has been shown

that RNASE H1 is primarily responsible for the resolution of transcription associated R-loops (Chon *et al.*, 2013).

In addition to RNASE H1/H2, senataxin (SETX), a DNA/RNA helicase, has been implicated in R-loop processing. Mutations in SETX are found to cause juvenile ALS (ALS4) as well as ataxia with oculomotor apraxia type 2 (OAO2) (James & Talbot, 2006; Palau & Espinos, 2006). Curiously, AOA2 mutations in SETX are recessive, suggesting loss of function, whilst ALS4 mutations in SETX are autosomal dominant, perhaps implying a toxic gain of function mutation (Arning *et al.*, 2013; Chen *et al.*, 2004). Disease mutations in either case appear to occur within the helicase domain or within its N-terminal protein-protein interaction domain. The mechanisms behind how these mutations cause either disease are not yet clear.

More recently, evidence has linked two DEAD (Asp-Glu-Ala-Asp)-box RNA helicases to the resolution of R-loops. Song and colleagues demonstrated that Ddx21 depletion leads to increased R-loop levels, and that its activity was controlled by its deacetylation (Song *et al.*, 2017). In addition, Ddx19 has been linked to the resolution of R-loops in proliferating cells (Hodroj *et al.*, 2017). Whilst primarily cytoplasmic, Ddx19 becomes nuclear during cellular replication, and nuclear Ddx19 was shown to be competent in R-loop helicase activity. Thus, mammalian cells likely comprise a number of distinct R-loop resolution pathways, which are currently being elucidated to.

3.1.4. R-loops regulate gene expression and promote chromatin condensation

R-loops are well documented to regulate the initiation and termination of transcription, and are enriched at the transcription start sites (TSS) and transcription termination sites (TTS) of genes (Ginno *et al.*, 2013; Ginno *et al.*, 2012; Skourti-Stathaki *et al.*, 2014; Skourti-Stathaki, *et al.*, 2011). CpG islands that display a strong GC skew are particularly enriched for R-loops and are also highly enriched for H3K4me3, H4K20me1 and H3K79me2 histone marks, which are linked to transcription initiation and/or elongation (Ginno *et al.*, 2013; Ginno *et al.*, 2012).

Paradoxically, the formation of R-loops at transcriptional termination sites of RNA polymerase 2 (Pol2) encoded genes has also been shown to induce and terminate Pol2 elongation. In yeast, Sen1 (SETX orthologue) and Rat1 (Exoribonuclease 2, XRN2,

orthologue) degrade mRNA transcripts to promote transcriptional termination (Kawauchi *et al.*, 2008), and Sen1 mutant strains display high levels of R-loops (Mischo *et al.*, 2011). Similarly, mammalian SETX and XRN2 are required for transcriptional termination and function to suppress R-loops in human cells (Skourti-Stathaki *et al.*, 2011). Interestingly, recent evidence has implicated a regulatory role for BRCA1 (breast cancer associated 1) and SMN (survival motor neuron) in the recruitment of SETX to R-loops at TTS (Hatchi *et al.*, 2015; Zhao *et al.*, 2016). Whether SMN- and BRCA1-mediated R-loop resolution are distinct or combining pathways is not yet clear.

In addition to controlling the transcription initiation and termination, R-loops alter the chromatin landscape by increasing levels of heterochromatic and condensed chromatin marks. Of note, THO mutant yeast strains display increased H3S10P (Castellano-Pozo *et al.*, 2013), a histone mark associated with condensed chromatin during mitosis (Hsu *et al.*, 2000). Depletion of SETX or THO complex members similarly increases in H3S10P (Castellano-Pozo *et al.*, 2013). More recently, it was demonstrated that R-loop-driven H3S10P formation is a requisite for subsequent genomic instability in Sen1 or THO mutants (García-Pichardo *et al.*, 2017), whilst non-pathological R-loops are not associated with this mark.

These studies also demonstrated that the heterochromatin mark H3K9me2 was enriched in thoc-2 mutant Caenorhabditis elegans (Castellano-Pozo *et al.*, 2013). Interestingly, this mark has also been associated with Friedreich's ataxia and fragile X syndrome, whereby trinucleotide repeat expansions lead to R-loop formation and H3K9me2 deposition (Groh *et al.*, 2014). The H3K9me2 mark is enriched, alongside R-loops, at GC-rich transcriptional pause sites (Skourti-Stathaki *et al.*, 2014). H3K9 methylation may protect cells from R-loop accumulation, since this histone mark was shown to supress R-loop accumulation in Caenorhabditis elegans (Zeller *et al.*, 2016). Taken together, these data couple R-loop accumulation to the formation of condensed chromatin. An attractive model for this association may be that the formation of repressive histones is induced by high levels of R-loop deposition, thereby decreasing transcriptional activity and protecting cells from R-loop-mediated genomic instability.

3.1.5. R-loop accumulation leads to intronic retention

Curiously, recent reports have demonstrated that R-loop accumulation, caused by RNASE H1/H2 depletion or by TOP-1 inhibition, leads to an increase in the number of transcripts with retained introns (Tresini *et al.*, 2015). It was subsequently discovered that R-loops promote the mobility of the late spliceosome, which leads to a loss of its canonical splicing activity (presumably in order to fulfil an undefined role in R-loop resolution). The spliceosome displacement in response to R-loops was later found to be amplified by the DDR master kinase, ATM, since ATM inhibitors were able to restore proper splicing and avoid intronic retention (Tresini *et al.*, 2015). These data implicate, for the first time, a role for ATM signalling in R-loop regulation.

3.1.6. The link between R-loops and ALS

In addition to SETX, several other motor neuron disease-linked proteins have recently been linked to R-loops. Nonsense mutations in the SMN1 gene lead to severe depletion of SMN protein, and are responsible for a juvenile form of motor neuron disease called spinal muscular atrophy (SMA) (Kolb & Kissel, 2011). Whilst the most documented function of SMN is with regards to its function in the spliceosome (Burghes & Beattie, 2009), recent evidence suggests that SMN functions in the resolution of R-loops by recruiting SETX to R-loop loci (Zhao *et al.*, 2016). Indeed, SMA patient fibroblasts display increased R-loop and DSB levels (Zhao *et al.*, 2016). In addition, a mouse model of SMA recapitulated these two findings, suggesting that SMN is an important factor in the prevention of R-loop-driven genomic instability (Jangi *et al.*, 2017). SMA cells also display increased levels of intronic retention by RNA sequencing technologies, which is in line with recent reports suggesting that R-loop accumulation leads to increased numbers of mRNA transcripts with retained introns (Tresini *et al.*, 2015).

FUS and TDP-43, two familial ALS-linked proteins with RNA binding properties, have recently been implicated in the prevention (or resolution) of R-loops (Hill *et al.*, 2016). In this study, both proteins were shown to co-localise with Pol2 and DNA damage markers after DNA damage. Interestingly, depletion of either protein increased levels of DNA damage, a phenotype that could be reduced by the overexpression of RNASE H1. These data imply that FUS and TDP-43 are involved in the process of preventing R-loop-mediated genome instability, and provide an additional link between motor neuron disease and R-loops. It

remains unclear as to the molecular mechanisms by which these two proteins function in regulating R-loop homeostasis.

R-loops preferentially occur are sites of the genome with high GC content (Ginno *et al.*, 2013). Moreover, defects in RNA processing pathways and the presence of G-quadruplex DNA structures, both promote R-loop accumulation. The C9orf72 repeat expansion has a GC content of 100%, forms G-quadruplex structures (Brcic & Plavec, 2017), and causes RNA processing defects (Barker *et al.*, 2017). Based on these observations, it is speculated that C9orf72 repeat expansions might promote R-loop accumulation.

3.2. Aims and Hypothesis

C9orf72 repeat expansions have been shown to form R-loops *in vitro* (Haeusler *et al.*, 2014), and so we speculated that the expression of C9orf72 repeat expansions in cellular systems will also lead to R-loop accumulation. Given that R-loops drive genomic instability, we further hypothesise that the presence of excess R-loops in C9orf72 disease models might lead to an increase in DNA damage. As such, the aims of the chapter are to:

- Investigate if the expression of C9orf72 expansions leads to R-loop accumulation
- Investigate if the expression of C9orf72 expansions leads to DSB accumulation
- Assess whether R-loop resolution can reduce DSBs
- Assess whether C9orf72-ALS patient spinal cord motor neurons also recapitulate these two key findings: increased R-loops and DSBs

3.3. Results

3.3.1. Expression of C9orf72 repeat expansions and poly-GA dipeptides leads to increased R-loop formation

Given the pure GC nature of the C9orf72 repeat expansion, we hypothesised that expression of C9orf72 expansions will lead to increased R-loop levels. To test this, we transfected MRC5 cells with 10 or 102 RNA repeat expansions (RREs), which are not ATG-driven, and visualised R-loops using R-loop-specific S9.6 antibodies. We concomitantly visualised RNA foci using fluorescence in situ hybridization (FISH). Expression of 102 RREs led to prominent RNA foci and triggered a length dependant increase in R-loop levels compared to cells transfected with a shorter expansion containing 10 RREs, which also displayed fewer

RNA foci (Figure 4a, p=0.009). Interestingly, R-loops and RNA foci co-localised in cells expressing 102 RREs, suggesting a physical relationship between R-loops and C9orf72 RNA foci. The R-loop signal was specific since it disappeared following addition of RNAse H1, an R-loop specific resolvase (Figure 4a).

Next, since poly-GA DPRs have been shown to induce neurodegeneration in the absence of pure-GC repeats (Walker *et al.*, 2017; Zhang *et al.*, 2016), we evaluated whether poly-GA DPRs also promote R-loop formation, which could explain their neurotoxicity. Transfection of MRC5 cells with either 34 or 69 poly-GA DPRs (ATG-driven and V5-epitope tagged) revealed a length-dependent predisposition to dipeptide aggregates, in which DPRs were more abundant in cells transfected with 69 poly-GA DPRs (Figure 4b). Expression of 34 DPRs led to ~4 R-loop foci per cell and expression of 69 poly-GA DPRs led to ~8 R-loop foci per cell, both of which were considered statistically higher than in control cells (Figure 4b, p=0.046 and p=0.003, respectively), but they were not statistically distinct from each other (Figure 4b, p=0.1). These observations suggest that C9orf72 RNA repeat expansions and poly-GA DPRs cause an increase in R-loop formation in human cells.

Since MRC5 cells are proliferating, and to test if this was cell cycle-independent, we repeated this experiment in post-mitotic neurons. Rat cortical neurons were transduced with adeno-associated serotype 9 (AAV9) viral particles expressing 10, 102 RREs (Figure 4c) or 34, 69 poly-GA DPRs (Figure 4d). Similar to human cells, expression of 102 RREs led to increased R-loop foci when compared to cells transduced with 10 RREs (Figure 4c, p=0.018). Likewise, 34 or 69 DPR expression increased the number of R-loop foci (Figure 4d; p=0.001; p=0.0002, respectively), though the difference between 34 and 69 was again not statistically significant (Figure 4d, p=0.07). Together, these data show that C9orf72 repeat expansions and poly-GA DPRs cause R-loop formation in neuronal cells.

Figure 4. Expression of C9orf72 expansions and poly-GA DPRs leads to increased R-loops and DSBs.

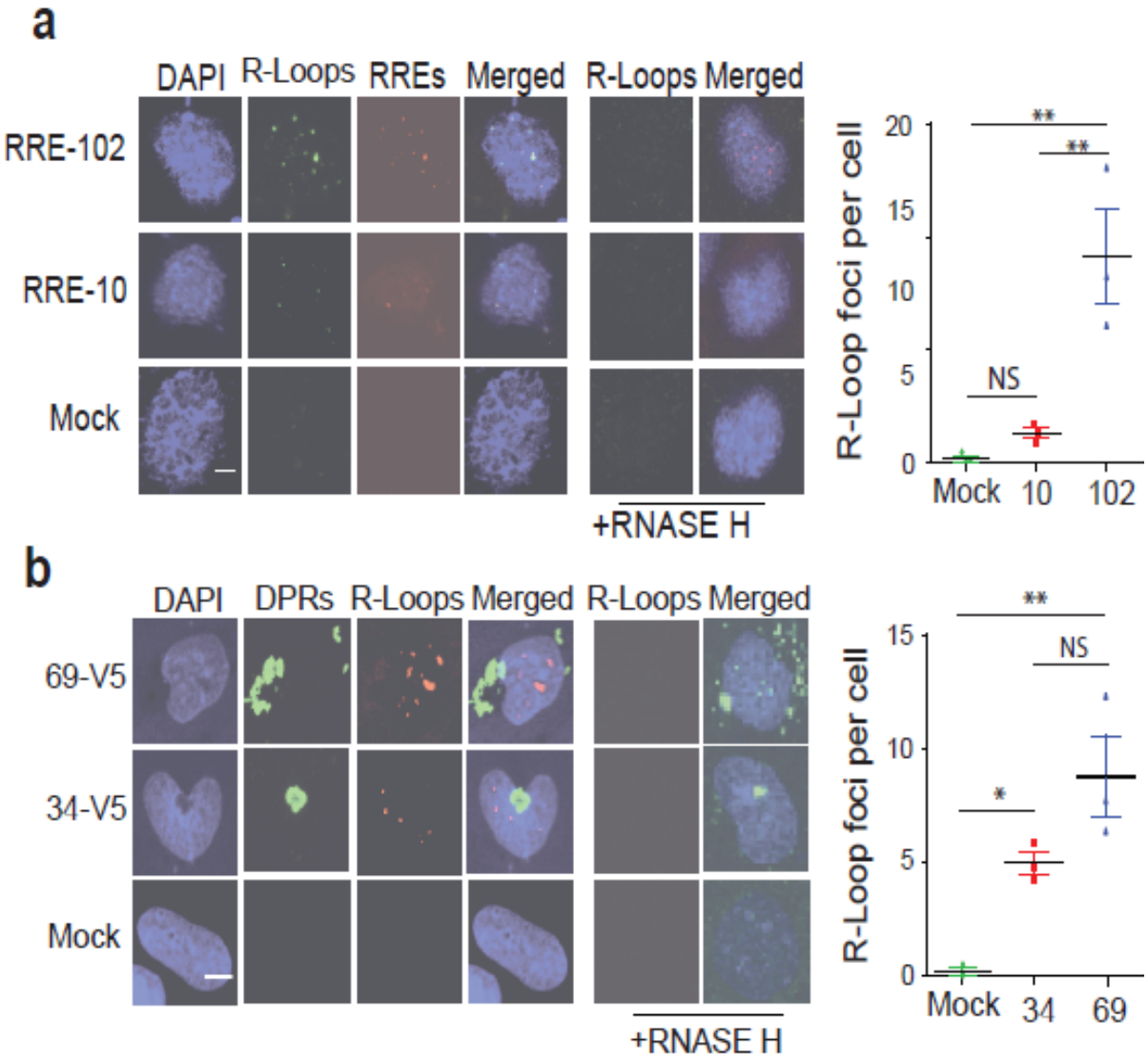

Figure 4. Expression of C9orf72 expansions leads to R-loop-driven DSBs and cellular toxicity. (a) MRC5 cells mock transfected or transfected with 10 or 102 RREs. FISH-IF was performed using a G4C2 fluorescent probe 'RNA' and S9.6 antibodies 'R-Loops'. Cells were treated with RNase H1 '+RNASE H'. *Left*, Representative images shown, scale bar 5µm. *Right*, the average (± SEM) number of nuclear S9.6 foci per cell was quantified from 3 cell culture replicates, 50 cells each. Significance assessed using a one-way ANOVA. **(b)** MRC5 cells mock transfected or transfected with 34 or 69 poly-GA DPRs. Cells examined by immunocytochemistry using anti-V5 'DPRs' and S9.6 antibodies 'R-Loops'. *Left*, Representative images are shown, scale bar 5µm. *Right*, S9.6 foci were quantified, presented, and analysed as described for (a).

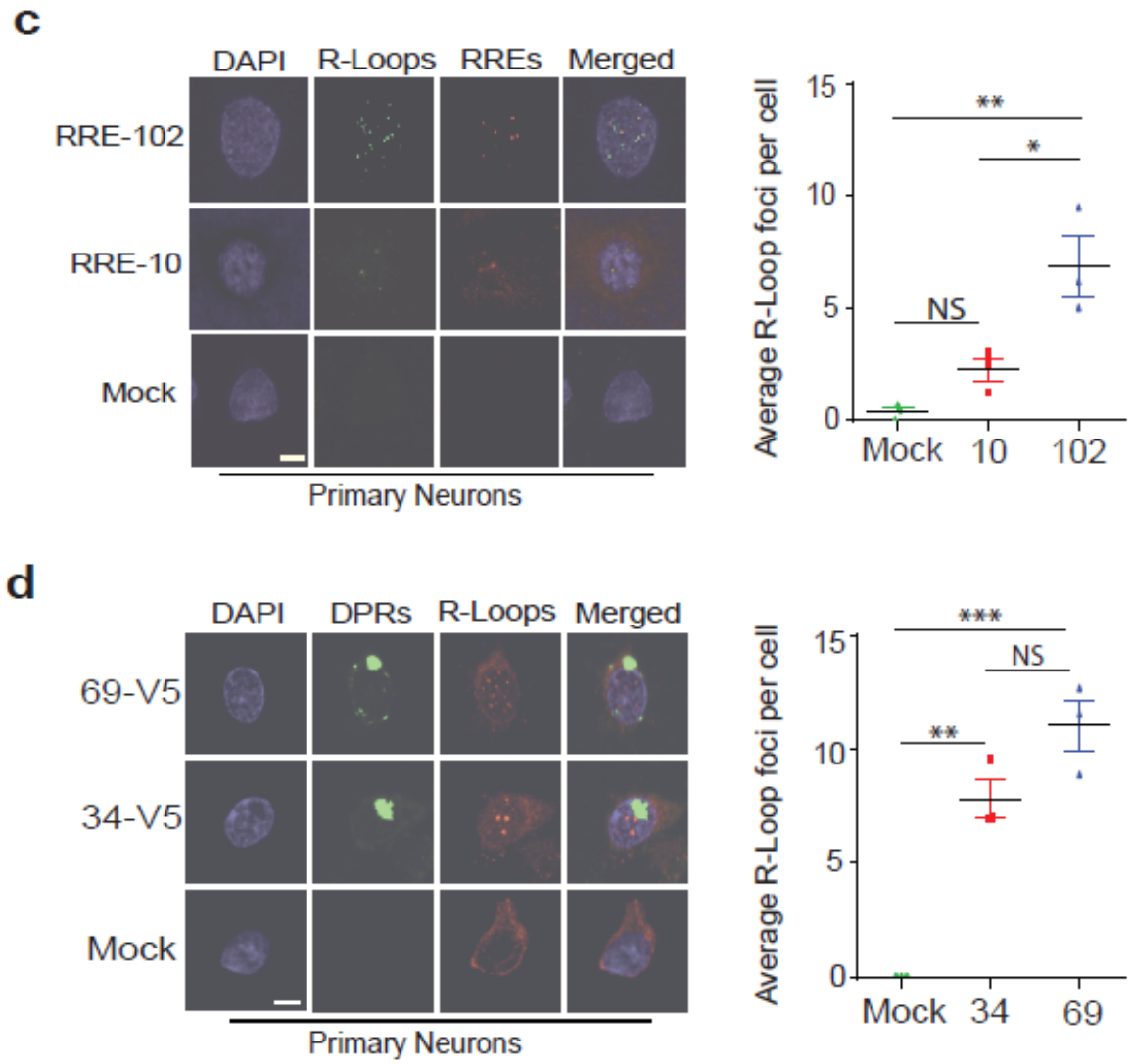

Figure 4. Expression of C9orf72 expansions leads to R-loop-driven DSBs and cellular toxicity. (c,d) Rat cortical neurons transduced with AAV9 viral-vectors encoding 10,102 RREs (c) or 34, 69 DPRs (d) were processed with FISH-IF double staining (c) or with immunocytochemistry (d), as described for (a,b). *Left*, Representative images shown, scale bar 5µm. *Right*, S9.6 foci quantified from 3 separate neuronal preparations, 20 neurons each, and data presented and analysed as described for (a).

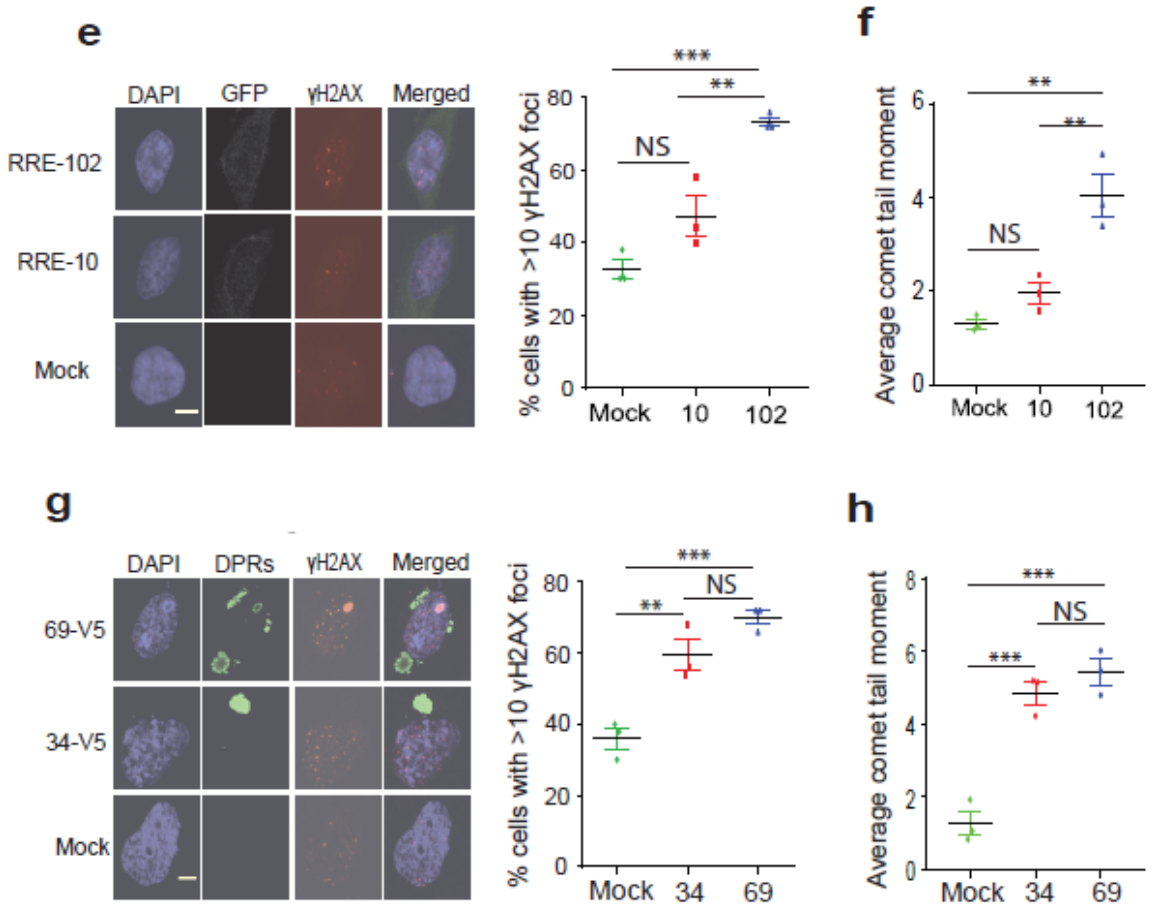

Figure 4. Expression of C9orf72 expansions leads to R-loop-driven DSBs and cellular toxicity. (e,g) MRC5 cells mock transfected or were transfected with 10,102 RREs (with GFP) (e) or 34, 69 DPRs (g). Cells were immunostained with anti-γH2AX antibodies 'γH2AX', with GFP (e) or anti-V5 antibodies 'DPRs' (g). *Left*, Representative images are shown, scale bar 5μm. *Right*, the percentage of cells with 10 or more foci was quantified, presented and analysed as described for (a). **(f,h)** HEK 293T cells mock transfected, transfected with 10,102 RREs (f), or 34, 69 DPRs (h). Neutral comet tail moments were quantified, 100 cells each, presented, and analysed as described for (a).

3.3.2. Expression of C9orf72 repeat expansions and poly-GA dipeptides leads to increased genome instability

Since the persistent accumulation of R-loops causes DSBs, we tested whether the expression of C9orf72 expansions would also lead to DSBs. We co-transfected MRC5 cells with 10, 102 RREs alongside GFP and examined DSBs using immunostaining with antibodies specific for γH2AX (Ser-139 phosphorylated histone H2AX), an established marker for DSBs. We considered each cell to be γH2AX-positive if it bared more than 10 distinct nuclear γH2AX foci. As anticipated, expression of 102 RREs led to a significant increase in the number of cells γH2AX-positive, when compared to mock transfected control cells and cells expressing 10 RREs (Figure 4e, p=0.005). Moreover, direct quantification of DSBs using the neutral comet assays (conducted by Waheba Elsayed and Mohammed Hassan) revealed a strikingly similar increase in DSBs in 102 RRE transfected cells compared to controls (Figure 4f, p=0.006).

Similarly to what we observed with our RNA repeat model, 34 and 69 poly-GA DPR expression caused a significant increase in DSBs compared to controls, as measured by γH2AX immunostaining (using the same criteria) and the neutral comet assay (performed by Waheba Elsayed and Mohammed Hassan) (Figure 4g, p=0.001; Figure 4h, p=0.0003, respectively). These data are in-line with our hypothesis that R-loop accumulation drives DNA damage in C9orf72 expansion expressing cells.

3.3.3. Senataxin overexpression leads to reduced R-loops, DSBs and cellular toxicity in cells expressing C9orf72 repeat expansions and poly-GA dipeptides

To directly test our hypothesis that R-Loops drive the formation of DSBs in cells expressing C9orf72 expansions, we assessed whether the elevated levels of R-Loops observed in C9orf72 cells could be reduced by overexpressing the R-Loop resolution helicase, senataxin (SETX). Whilst control adenovirus expression of RFP had no detectable impact on R-loops, expression of SETX from the same viral backbone led to a marked reduction of R-Loop foci (Figure 5a). Overexpression of SETX, but not RFP, also reduced the number of γH2AX-positive cells (Figure 5b, p=0.01; p=0.022), indicating that R-Loops are a major source of C9orf72 expansion-driven DSBs. Furthermore, SETX expression was able to reduce RRE- and DPR-driven cellular toxicity, as shown by a reduction in the % of cleaved-PARP1-positive cells (Figure 5c,e; p=0.009 and p=0.038, respectively) and by a similar reduction in

the % of Trypan Blue-positive cells (Figure 5d,f, p=0.037 and p=0.025, respectively). The effect of SETX was specific to RRE-102- and 69-V5-positive cells since it did not impact cell viability in control cells expressing RRE-10 or 0-V5 constructs (Figure 5c-f; p>0.05). Taken together, our data demonstrate that C9orf72 expansions promote R-Loop-driven DSB formation, which contributes to cellular toxicity.

Figure 5. SETX overexpression leads to reduced R-loops, DSBs, and cellular toxicity in cells expressing C9orf72 expansions.

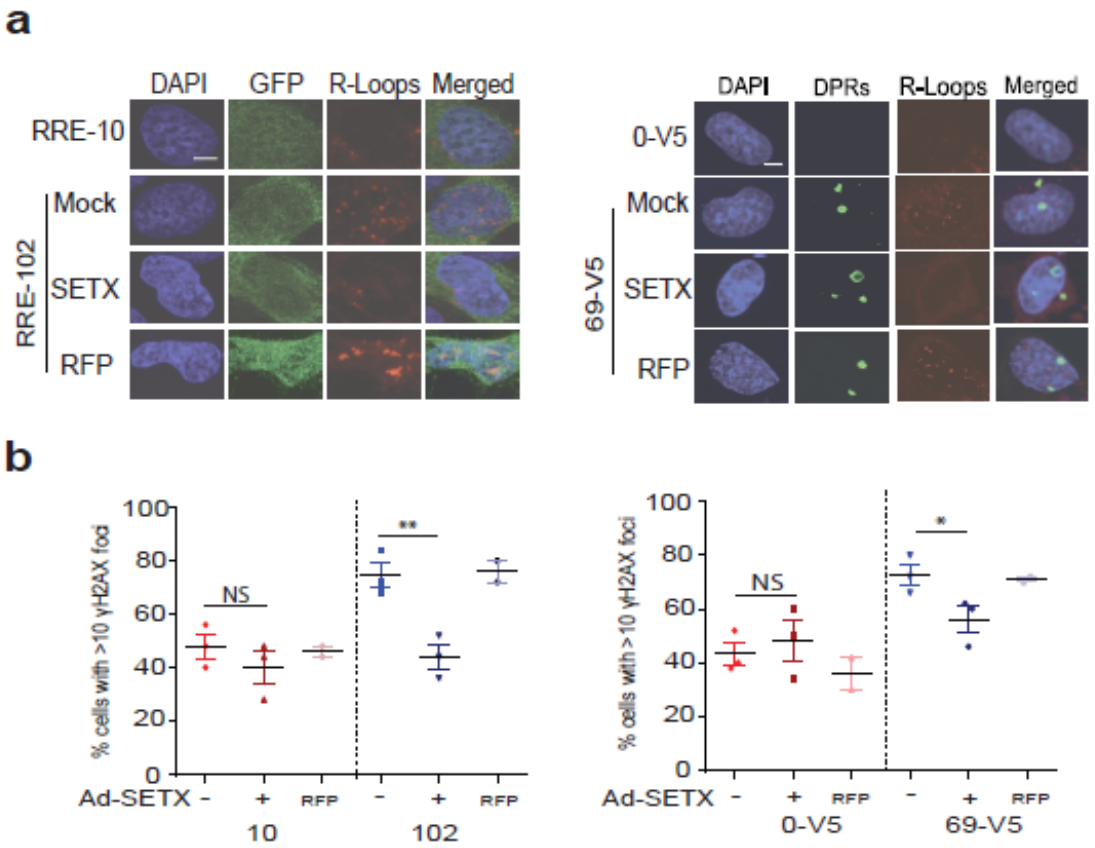

Figure 5. Senataxin overexpression leads to reduced R-loops, DSBs, and cellular toxicity in cells expressing C9orf72 expansions. (a) MRC5 cells mock transduced or transduced with adenoviral vectors encoding for SETX or RFP and then transfected with 10 or 102 RREs (with GFP) (*left*) or with 0, 69 DPRs (*right*). Cells were immunostained with S9.6 antibodies 'R-Loops' alongside GFP (*left*) or alongside anti-V5 'DPRs' antibodies (*right*). Representative images are shown, scale bar 5µm. **(b)** MRC5 cells mock transduced or transduced with adenoviral vectors encoding for SETX or RFP and then transfected with 10 or 102 RREs (with GFP) (*left*) or with 0, 69 DPRs (*right*). Cells were immunostained with anti-γH2AX antibodies and the average (± SEM) percentage of cells exhibiting 10 or more γH2AX foci was quantified, 25 cells each, and analysed using Student's t-test.

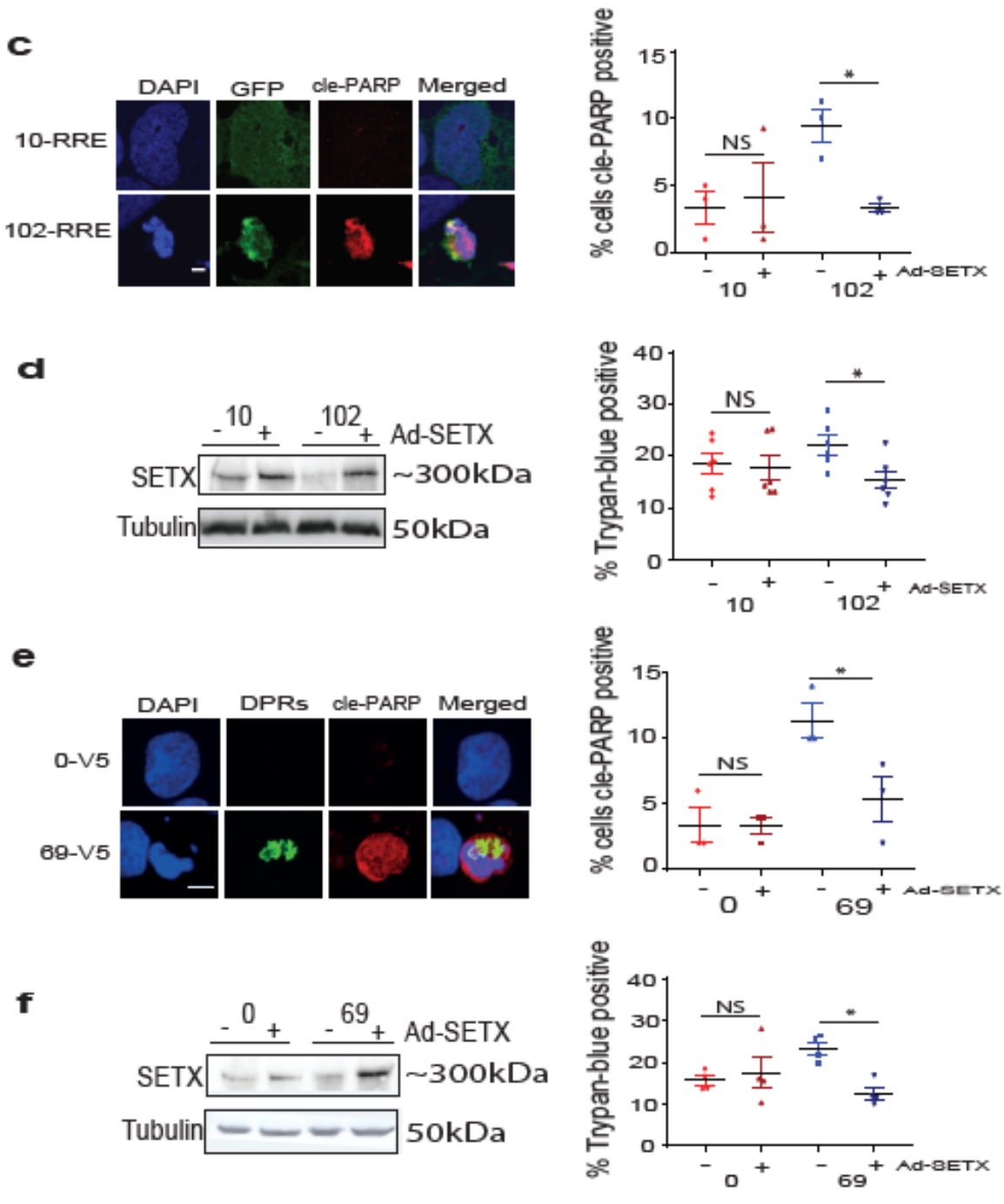

Figure 5. Senataxin overexpression leads to reduced R-loops, DSBs, and cellular toxicity in cells expressing C9orf72 expansions. (c,e) MRC5 cells transduced with adenoviral vector particles encoding for SETX or mock transduced and transfected with constructs encoding 10, 102 RREs (c) or 0 or 69 DPRs (e). Cells examined by immunocytochemistry using cleaved-PARP 'cle-PARP' antibodies alongside GFP (c) or anti-V5 'DPRs' antibodies (e). *Left*, Representative images of cle-PARP-positive and -negative cells shown, scale bar 5µm. *Right*, the percentage of cells cleaved-PARP-positive was quantified, 50-100 cells each, presented and analysed as described for (a). **(d,f)** HEK 293T cells were mock transduced or transduced with adenoviral vector particles encoding for SETX and transfected with 10,102 RREs (d) or 0 or 69 DPRs (f). *Left*, Whole cell lysates from samples used in (d) and (f) were analysed by western blotting, using anti-senataxin and anti-α-tubulin antibodies. *Right*, Cells were analysed using Trypan blue exclusion assays, and the % of cells Trypan-permeable was quantified from 6 (d) and 4 (f) cell culture replicates, ~200 cells each, and was presented and analysed as described for (a).

3.3.4. Post-mortem spinal cord motor neurons from C9orf72-ALS patients also display an increase in R-loop and DSB levels

Critically, our previous data in this chapter was limited to the overexpression of C9orf72-related constructs. As such, it is not fully clear as to whether these results are physiologically and clinically relevant, or whether they are an artefact of the overexpression systems. In order to address this issue, we obtained spinal cord sections from 6 C9orf72-ALS and 6 non-ALS control subjects. We used immunohistochemical analyses using S9.6 or γH2AX antibodies, and calculated the % of spinal cord motor neuron cells that were R-loop/γH2AX-positive (positive nuclei were defined as those in which the whole nucleus was stained). In line with our cellular data, C9orf72-ALS patient motor neurons displayed significantly higher levels of R-loop and γH2AX signal, in comparison to non-ALS age- and gender-matched controls (Figure 6a,b; $p<0.05$). Information related to the age and gender of patients is summarised in Table 2. Importantly, these data demonstrate that our key observations, increased R-loops and DSBs, are disease relevant.

Figure 6. Motor Neurons from C9orf72-ALS patients show elevated levels of R-Loops and DSBs.

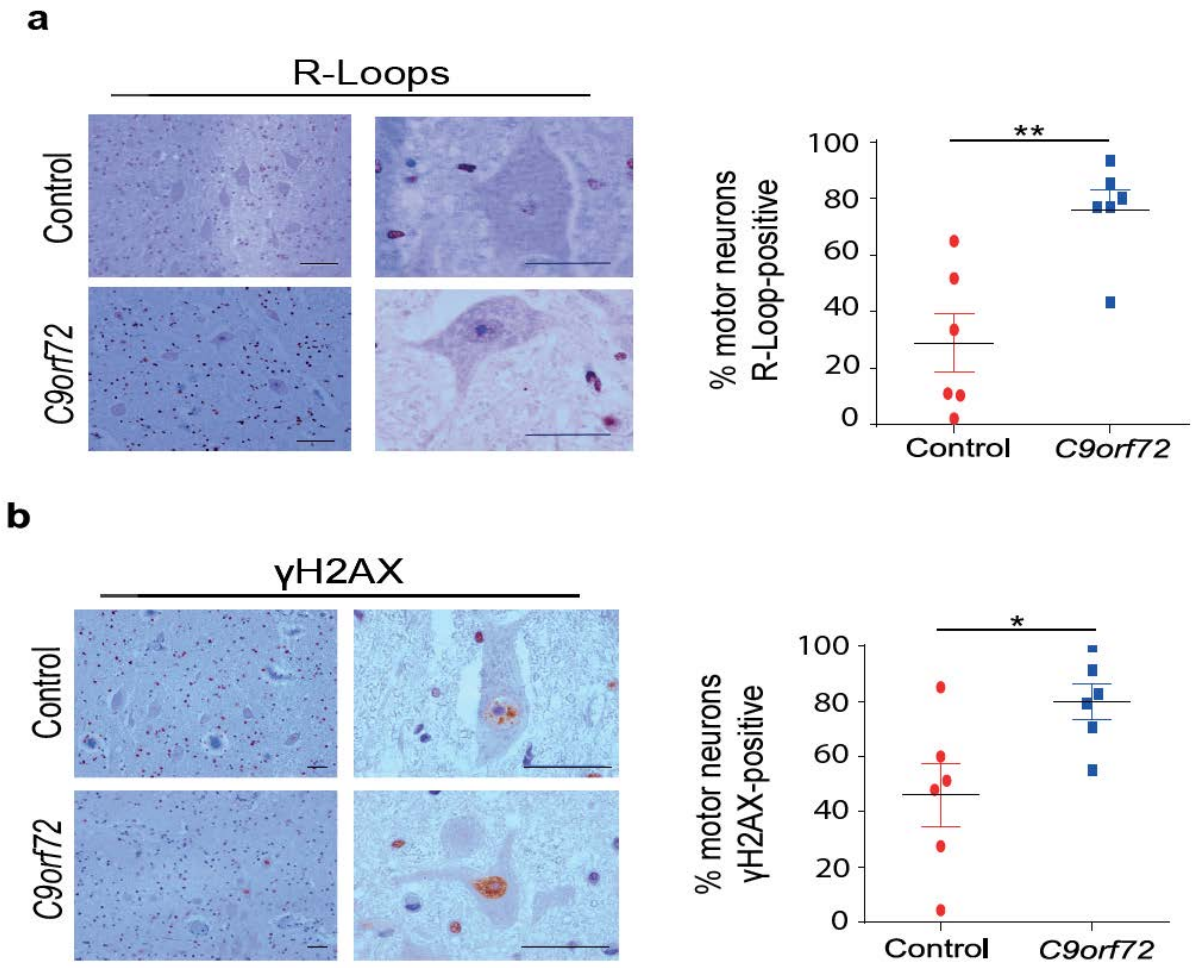

Figure 6. Spinal Cord Motor Neurons from C9orf72-ALS post-mortem show elevated levels of R-Loops and DSBs (a) *Left*, Human spinal cord sections (thickness 5µm) were analysed by immunohistochemistry using S9.6 antibodies. Representative images from 6 C9orf72 patient and 6 control sections are presented, scale bar 5µm. *Right*, The % of R-Loop-positive motor neurons was quantified from 6 C9orf72 patient and 6 control sections, each individual represented by a single point on the scatter plot, and presented as average ± SEM, with ~50 cells each. Significance assessed with Student's t-test. **(b)** *Left*, Human spinal cord sections were analysed by immunohistochemistry using anti-γH2AX antibodies. Representative images from 6 C9orf72 patient and 6 control sections are presented, scale bar 5 µm. *Right*, The % of γH2AX-postive motor neurons was quantified from 6 C9orf72 patient and 6 control sections and is presented as average ± SEM, with ~50 motor neurons each. Significance assessed using a Student's t-test.

Table 2. Age and gender distribution of C9orf72-ALS and non-ALS cases used in this study

Subject code	Type	Age	Sex
NA144/91	Non-ALS subject	65	F
LP0 85/07	Non-ALS subject	59	F
NA309/90	Non-ALS subject	82	M
R808/90	Non-ALS subject	51	M
LP098/07	Non-ALS subject	67	M
LP005/07	Non-ALS subject	63	M
LP066/08	C9 patient	59	F
LP063/08	C9 patient	69	F
LP069/09	C9 patient	48	M
LP039/11	C9 patient	72	M
LP081/09	C9 patient	59	M
NA273/99	C9 patient	68	M

3.4. Discussion

In summary, in human cells and rodent neurons, C9orf72 repeat expansions and poly-GA DPRs lead to an increase in R-loops and DSBs (Figure 4). Importantly, SETX overexpression decreased R-loop foci, reduced DSB levels, but also relieved C9orf72-associated cellular toxicity (Figure 5). Taken together, these data demonstrate that C9orf72 expansions lead to R-loop-driven genomic instability, which in turn leads cellular toxicity. Finally, we demonstrated that C9orf72-ALS patients are also enriched with R-loops and DSBs (Figure 6), confirming that these findings are indeed relevant to the disease.

3.4.1. Expression of C9orf72 repeat expansions leads to increased R-loops

Since R-loop formation occurs more frequently at GC-rich regions of the genome (Ginno *et al.*, 2013), we unsurprisingly identified that human cells and rodent neurons expressing 102 G4C2 repeat expansions displayed an increase in R-loop levels (Figure 4a,c). Interestingly, R-loops co-localised with RNA foci. Critically, R-loop foci, but not RNA foci, were ablated by RNASE-H1 pre-treatment, demonstrating the specificity of this signal (Figure 4a). This observation is particularly interesting because C9orf72 expansions are known to form G-quadruplex structures, which have been linked to R-loop predisposition (Duquette *et al.*, 2004). Indeed, it has been shown that G-quadruplex and RNA/DNA hybrids can be co-transcriptionally formed during the transcription of G-rich DNA, so-called G-loops (Duquette *et al.*, 2004), and it is feasible that this co-localisation is linked to this phenomenon.

Similarly to what we observed when expressing non-ATG driven expansions, expression of ATG-driven poly-GA DPRs led to increased R-loops in human cells and rodent neurons, but it was not length dependant (Figure 4b,d). Since these constructs purposely have reduced GC purity (though they are still 66% GC-rich), it is more difficult, but still feasible, to explain the increase in R-loop foci by the presence of GC-rich RNA transcripts. Indeed, in trinucleotide expansion disease contexts with less GC-rich expansions, R-loop accumulation has been observed (Groh *et al.*, 2014).

An important limitation of our data is that we were not able to pinpoint the genomic locations that show increased R-loop levels. In order to assess which gene loci display elevated R-loop levels, future work should utilise the DNA:RNA Immunoprecipitation (DRIP) technique to assess different genomic loci for R-loop enrichment. This is particularly important given the

growing concerns related to the specificity of the S9.6 antibody, when used with immunocytochemistry. This process can also determine whether it is only the C9orf72 expansion loci that accumulates R-loops, or, as we predict based on the distribution of S9.6 signal across the nucleus, whether it is a genome wide dysregulation of R-loop homeostasis. Moreover, RNA sequencing analysis of DRIP samples could be used to uncover genes that are dysregulated in C9orf72-ALS (due to the accumulation of R-loops) and, potentially, identify novel dysregulated gene networks.

Genome wide sequencing of R-loop immunoprecipitated samples represents an exciting avenue for future research, allowing the identification of R-loop-rich gene loci in ALS. These genes can then be correlated with genes that are enriched with DSBs (using γH2AX ChIP-sequencing), identifying genes that are vulnerable to R-loop-mediated genome instability in C9orf72-ALS. Mapping R-loop and DNA break gene loci within the context of a neurodegenerative disease is unprecedented at this stage, but it would function as a useful bioinformatics tool for understanding genome dysregulation in diseases associated with genomic instability.

In addition to driving DNA damage, R-loops have been shown to generate splicing errors, namely intron retention (Tresini *et al.*, 2015). Given the link between ALS and splicing dysfunction (Cooper-Knock *et al.*, 2015c; Kwon *et al.*, 2014; Prudencio *et al.*, 2015), it is feasible that R-loop accumulation plays an active role in this disease hallmark. This is particularly likely given it was recently demonstrated that SMN deficient cells generate more R-loops and DNA breaks, which was associated with an increase in intronic retention (Jangi *et al.*, 2017). An interesting question for future research is to assess whether the splicing dysfunction observed in C9orf72-ALS samples can be relieved by the overexpression R-loop resolvases, such as RNASE H1 and SETX.

3.4.2. Expression of C9orf72 repeat expansions leads to increased DSBs

In-line with the notion that R-loop accumulation causes genome instability (Skourti-Stathaki & Proudfoot, 2014), we similarly found that C9orf72 expansions and poly-GA DPRs cause increased DSBs in human cells (Figure 4e,g), as measured by γH2AX foci. We validated γH2AX as a readout for DSBs, by directly measuring DSB levels with the neutral COMET assay (Figure 4f,h). Whilst this increase in DSBs could potentially be explained by the

presence of excess R-loops, these data could also be explained by other molecular pathologies identified in C9orf72 expansion-expressing models. For instance, recent reports have demonstrated that C9orf72-related poly-GR and poly-PR lead to mitochondrial dysfunction, resulting in elevated levels of ROS, and in turn, DNA damage (Lopez-Gonzalez *et al.*, 2016). Since antioxidant species were able to reduce DNA damage in poly-PR/GR expressing cells, it is likely that mitochondrial dysfunction and ROS accumulation, also contributes to C9orf72 expansion-driven DNA damage.

Paradoxically, this previous report did not identify any increase in genomic instability (Lopez-Gonzalez *et al.*, 2016), when measuring DSBs (using γH2AX) in poly-GA expressing neurons. These data are firmly at odds with our γH2AX findings. Unfortunately, this paper failed to quantify γH2AX foci from these neurons, and relied solely on representative images and so it is currently difficult to explain the disparity between our data and theirs. Similarly, these reports did not identify any increase in DSBs in poly-GA DPR expressing cells using the alkaline COMET assay. These data could be explained by the fact that the alkaline COMET assay detects both SSBs and DSBs, whilst the neutral COMET assay used in our study directly measures DSBs. An alternative explanation for these differences could be the cell-types used and the length of the repeat constructs. Whilst the previous study used IPSC-derived neurons and transduced those cells with viral vectors containing 50 poly-GA repeats, we used a transfection based system and HEK 293T cells. Importantly, though, we validated our findings in mouse CNS tissues from mice transduced with 10, 102 RRE and 0, 69 poly-GA constructs (discussed in the following chapter).

Moreover, it has been shown that poly-GA dipeptides bind the UPS chaperone proteins, Rad23a and Rad23b (Zhang *et al.*, 2016). These proteins are known to regulate XPC, a protein involved in repairing UV radiation-mediated DNA repair. It was shown that poly-GA DPRs sequester XPC, thereby depleting the cellular pool of XPC (Zhang *et al.*, 2016). Thus, it is possible that the sequestration of DNA repair proteins might explain the co-localisation between γH2AX and poly-GA DPRs.

Since a number of nucleases, such as XPF, are known to process R-loops into DSBs (Sollier *et al.*, 2014), it would also be interesting to determine whether the depletion of such factors can reduce DSB levels in C9orf72 expansion-expressing cells. This would add more weight to our conclusion that R-loops drive DSBs in C9orf72-ALS/FTD. This may be problematic,

particularly in poly-GA expressing cells, since poly-GA DPRs sequester XPC, a protein involved in global-genome NER. Disrupting NER further with XPF depletion may cause genome instability and thereby mask any potential reduction in DSBs mediated by blocking the processing of R-loops by XPF (Figure 4g).

3.4.3. Senataxin attenuates R-loops, DSBs and toxicity that is driven by C9orf72 expansions

In order to test our hypothesis that the elevated levels of DSBs in C9orf72 cells is caused by the accumulation of R-loops, we overexpressed the RNA/DNA helicase senataxin (SETX) and assessed R-loop and γH2AX foci with immunocytochemistry. SETX overexpression, mediated by an adenoviral vector, relieved RRE- and DPR-expressing cells of R-loop foci (Figure 5a). More interestingly, SETX overexpression was able to attenuate DSBs levels as measured by γH2AX foci (Figure 5b). Finally, and most importantly, SETX overexpression was able to reduce cellular toxicity in expansion expressing cells, as measured by the percentage of cleaved-PARP-positive cells and Trypan-blue permeable cells (Figure 5c-f). These data suggest that R-loop-driven genomic instability plays an active role in the cellular toxicity driven by C9orf72 expansions.

The observation that R-loop foci were decreased by SETX overexpression is in line with reports linking SETX helicase activity to R-loop resolution (Yuce & West, 2013). Moreover, over-expressing SETX via adenoviral vectors represents a considerable breakthrough in the field - since, too our knowledge - researchers have been unable to over-express SETX by conventional DNA transfection methods. Thus, viral delivery of SETX represents a potential therapeutic tool, as indicated by our data, but also as a useful research tool to further understand the biology of SETX.

Therapeutically, our data demonstrates that R-loop resolution may protect C9orf72 expansion expressing cells from DNA breaks and cell death. Another R-loop resolvase, RNASE H1, has been frequently used to reduce R-loop accumulation in other studies. We preferred SETX, however, because RNASE H1 overexpression leads to other concerns, such as the binding and elimination of Okazaki fragments. We did not observe any toxicity in control cells over-expressing SETX, suggesting that SETX may be a better therapeutic candidate than RNASE H1. Further research is necessary, however, in order to directly compare the efficacy of SETX vectors versus those encoding for RNASE H1.

Whilst our data using senataxin overexpression is promising, it is important to note that R-loops have important functions in cellular health, as well as in disease (Santos-Pereira & Aguilera, 2015). Namely, R-loops are known to form at the promoters (Ginno *et al.*, 2012) and terminators of genes (Ginno *et al.*, 2013), and have been strongly implicated in the important process of transcription initiation and transcriptional termination. Moreover, R-loops are known to initiate immunoglobin class-switching in human B cells (Aguilera & Garcia-Muse, 2012). These studies have important implications with regards to the therapeutic overexpression of SETX or other R-loop resolvases.

3.4.4. R-loops and DSBs in patient IPSC-derived neuronal cultures and C9orf72-BAC mouse models

Although we have validated our key findings of R-loops and DSBs in patient post-mortem samples of the diseased cells (Figure 6), it would be useful to further validate these data in C9orf72-ALS patient IPSC-derived neuronal cells. These cells would be particularly useful for assessing the therapeutic potential of R-loop resolvases in a physiological model that does not use overexpression or artificial C9orf72 constructs.

In addition to validating these findings in IPSC-derived neurons, further research should assess R-loops and DSBs in C9orf72-BAC mouse models (Jiang *et al.*, 2016; Liu *et al.*, 2016). In particular, these models would be useful for assessing when R-loops and DSBs accumulate with respect to the disease progression (i.e. does genome instability precede or follow neurological or neurodegenerative changes). This would help determine whether R-loops and DSBs are a requisite for the disease progression or whether they are a consequence of the degenerative process. As with IPSC-derived neurons, BAC mouse models would be a useful *in vivo* tool for assessing the therapeutic potential of R-loops resolvases.

3.4.5. Concluding Remarks

In this chapter, we have demonstrated that C9orf72 expansions drive the formation of R-loops, leading to DSBs and cell death - all of which was relieved by SETX overexpression. Promisingly, C9orf72-ALS is not the only ALS subtype that has been linked to R-loops and/or DNA damage. Firstly, SETX mutations directly lead to autosomal-dominant ALS4 (or AOA2) (Yuce & West, 2013). In addition, TDP-43 and FUS have been shown to play a role in R-loop regulation (Hill *et al.*, 2016). FUS has also been shown to play a role in the DSB

repair pathway, NHEJ (Rulten *et al.*, 2014; Wang *et al.*, 2013). Moreover, SMN is known to play an important role in recruiting SETX to R-loop resolution sites, and SMA-linked mutations have been shown to lead to defective SETX recruitment, R-loop accumulation, and excessive DNA breaks (Zhao *et al.*, 2016). Indeed, data in our lab has indicated that SETX viral vectors can improve motor neuron survival in an SMN mouse model (unpublished data). Taken together, these studies, alongside our own data, indicate that R-loops and DNA breaks represent a common disease mechanism in ALS/MND, and suggest that SETX gene transfer (or other R-loop resolution strategies), could confer therapeutic potential to a number of ALS patients.

Chapter 4: C9orf72 repeat expansions disrupt ATM-mediated DSB signalling

4.1. Introduction

4.1.1. Double-strand break repair pathways

The genome is constantly under threat by a number of endogenous and exogenous agents. Reactive oxygen species generated during cellular metabolism (Chiang *et al.*, 2017), aldehydes (Tan *et al.*, 2017), abortive topoisomerases (El-Khamisy *et al.*, 2005), transcription/replication fork collisions (Hamperl *et al.*, 2017), as well as R-loops (discussed in chapter 1), all represent dangerous endogenous sources of DNA damage that can drive the formation of DSBs. In addition to endogenous sources, exogenous radiation and chemical substances, such as camptothecin (CPT), also promote DSBs (Katyal *et al.*, 2014). In mammalian cells, DSBs are repaired predominantly by two pathways: non-homologous end-joining (NHEJ) or homologous recombination (HR). Though these are, by far, the most well-studied DSB repair pathways, DSBs can also be repaired in two other ways - alternative-end-joining (a-EJ) or by single-strand annealing (SSA) (Chang *et al.*, 2017).

4.1.2. Homologous recombination (HR)

Homologous recombination is an error-free DSB repair pathway, that uses the sister chromatid as a template for DNA break repair. DSBs are principally identified by the MRN complex (Mre11, Rad50 and Nbs1) (Williams & Tainer, 2007; Williams *et al.*, 2007). Rad50 is involved in DNA binding (Williams *et al.*, 2007), whilst Mre11 contains endonuclease and exonuclease activity that is required for end resection and the initiation of HR (Williams & Tainer, 2007). In addition, Nbs1 functions to recruit and activate the ATM kinase, which plays an important role in DSB repair by both HR and NHEJ (Williams & Tainer, 2007).

Since HR is only possible at particular stages of the cell cycle, it is highly regulated by the process of end resection. Resection involves the nucleolytic degradation of the 5’ to 3’ DNA strand, resulting in a 3’ ssDNA that can be recognised by HR factors (Longhese *et al.*, 2010). The initial processing of DSBs involves C-terminal binding protein-interacting protein (CtIP). CtIP interacts with BRCA1, and its activity is controlled by ATM-mediated phosphorylation as well as by interactions with the MRN complex (Huen *et al.*, 2010).

DSB resection leads to ssDNA overhangs that are coated with replication protein A (RPA) (West, 2003). During G2 and S phase, BRCA2 associates with RPA in a CDK dependant manner (Esashi *et al.*, 2005), which is thought to promote HR by recruiting Rad51 to sites of DNA damage. Following Rad51 loading at sites of strand invasion, Rad51 catalyses strand exchange (Holliday junctions), which is enhanced *in vitro* by its association with Rad52 and RPA (Benson *et al.*, 1998; New *et al.*, 1998). DNA polymerase can then utilise the exchanged strand as a template for correct nucleotide replacement. Holliday junctions are then resolved without cross-overs by the topoisomerase II / Bloom helicase complex, or with crossovers by a set of different nucleases, including GEN1, SLX1, and MUS81 (West, 2003).

4.1.3. Non-homologous end-joining (NHEJ)

Whilst HR is only available to cells in S-phase and G2, when the sister chromatid is present, NHEJ is active during all stages of the cell cycle, and is the most predominant DSB repair pathway in mammalian cells. NHEJ is also essential for V(D)J recombination (Helmink & Sleckman, 2012), and mutations in core NHEJ factors (Ku70, Ku80, DNA-PKcs, XRCC4, Artemis) leads to radiosensitivity but also severe immunodeficiency disease (Woodbine *et al.*, 2014). Simplistically, NHEJ can be described in three stages: Detection by the Ku heterodimer, the processing of DNA termini by several enzymes including PNKP, and the rejoining of DNA ends by the XRCC4-DNA Ligase IV complex (Davis & Chen, 2013).

The first stage of classical NHEJ is the binding of the Ku heterodimer (Ku70 and Ku80) to the tethered DNA ends (Downs & Jackson, 2004). Whilst they do not have sequence homology, both consist of an amino-terminal von Willebrand domain (vWA) and a central Ku core domain, which function to promote heterodimerization (Downs & Jackson, 2004). A third domain, contained in the carboxyl terminal is thought to be responsible for DNA binding (Downs & Jackson, 2004). Remarkably, Ku70/80 can localise to laser-induced breaks within seconds (Britton *et al.*, 2013), which is probably due to its cellular abundance and extraordinary affinity for DNA ends (Downs & Jackson, 2004). The crystal structure of Ku demonstrates a ring-like structure, likely allowing it to slide onto the free DNA end (Walker *et al.*, 2001). It also demonstrated that Ku binds to the sugar moiety of DNA, explaining why its affinity for DNA is sequence independent (Walker *et al.*, 2001). Ku is a part of the DNA-PK complex, and binds to DNA-PKcs via the Ku80 carboxyl terminal (Falck *et al.*, 2005; Hammel *et al.*, 2010). DNA binding by Ku is required for DNA-PKcs recruitment and

activation (Gottlieb & Jackson, 1993; Uematsu *et al.*, 2007). DNA-PK (Ku + DNA-PKcs) is then able to recruit Artemis (Ma *et al.*, 2002), and XRCC4 (Mari *et al.*, 2006). Thus the binding of Ku to DNA breaks, functions as an important docking station for NHEJ factors, and recruits them to the break site.

DSBs are usually complex and contain DNA overhangs and/or non-ligatable termini (Cadet *et al.*, 2012; Georgakilas *et al.*, 2013). As such, DNA ends needs to be processed before they can be re-joined. Recently, Ku itself has been shown to possess 5' RP/AP lyase activity (Roberts *et al.*, 2010). Polynucleotide Kinase 3'-Phosphatase (PNKP) is an enzyme that is recruited by DNA-PK to DSBs, and possess 3' DNA phosphatase activity and 5' DNA kinase activity, making it an ideal enzyme for tidying up aberrant DNA ends (Weinfeld *et al.*, 2011). Another nuclease, Aprataxin-and-PNK-Like Factor (APLF), bears striking similarities to PNKP, in that it interacts with Ku80 and XRCC4 and it enhances NHEJ and the ligation activity of DNA ligase IV (Grundy *et al.*, 2013; Kanno *et al.*, 2007; Rulten *et al.*, 2011). The endonuclease, artemis, is also shown to interact with DNA-PK and plays a critical role in V(D)J (Ma *et al.*, 2002). Interestingly, artemis knock-out cells are only slightly radiosensitive, suggesting it is only required for a small subset of DNA overhangs induced by ionising radiation (Moshous *et al.*, 2003). Thus, the processing of DNA overhangs is a heterogeneous process, which likely requires different processing enzymes to process biochemically different overhangs.

DNA-PKcs phosphorylation is known to be integral to NHEJ (Kienker *et al.*, 2000; Kurimasa *et al.*, 1999). DNA-PK can auto-phosphorylate *in vitro*, and is highly phosphorylated *in vivo* (Dobbs *et al.*, 2010; Douglas *et al.*, 2007). Phosphorylated DNA-PK thereby functions to phosphorylate multiple NHEJ factors, which regulates the access of these enzymes to DNA ends (Meek *et al.*, 2008). Once DNA ends have been processed by the NHEJ enzymes in a DNA-PK-dependant manner, the broken DNA can be rejoined. This process is completed by DNA ligase IV, which forms a complex with XRCC4. XRCC4 binding acts to stabilize DNA ligase IV, and increases its activity (Grawunder *et al.*, 1997).

The cellular decision to repair DSBs with HR or NHEJ is an important question. HR is primarily induced by DSB resection by CtIP, a process that is inhibited by 53BP1 (Bunting *et al.*, 2010). Moreover, loss of 53BP1 can partly rescue HR defects caused by loss of BRCA1, suggesting that, in G2 and S phase, BRCA1 recruitment may outcompete 53BP1 to induce

HR (Bouwman *et al.*, 2010). Indeed BRCA1 mutant cells undergo translocations due to overactive NHEJ, and these events can be reduced by 53BP1 depletion (Bouwman *et al.*, 2010). As such, BRCA1 and 53BP1 may dictate DSB repair pathway choice via direct competition with each other.

4.1.4. Double-strand break repair signalling

In the event of a DSB, the MRN (Mre11, Rad50, Nbs1) complex form foci at the DSB site. ATM is then rapidly activated by a process that involves its autophosphorylation and a transition from dimer (or higher order polymer) to monomer (Bakkenist & Kastan, 2003), and this process is initiated by interactions with Nbs1 (Williams & Tainer, 2007). This interaction is mandatory, and sufficient to initiate the initial activation of ATM, leading to serine 1981 phosphorylation and lysine 3016 acetylation (Kaidi & Jackson, 2013).

After activation by Nbs1, ATM sets into motion the DNA Damage Response (DDR). Following ATM activation, histone H2AX becomes phosphorylated on serine 139 (Rogakou *et al.*, 1998). This process can occur by ATM kinase activity, but also by the kinase activity of ATR and DNA-PK (Blackford & Jackson, 2017). The phosphorylation of H2AX serves as a signal for the recruitment of the DNA repair factor, mediator of DNA damage checkpoint 1 (MDC1), which facilitates DSB repair via HR and NHEJ (Hartlerode & Scully, 2009). MDC1 binds to Nbs1 and ATM via its BRCT motifs, which enables the propagation of γH2AX signalling (Chapman & Jackson, 2008; Lou *et al.*, 2006). H2AX phosphorylation is important, not for the initial recruitment of DNA repair factors (53BP1, BRCA1, Nbs1), but for their sustained maintenance at the break site (Celeste *et al.*, 2003).

The recruitment of MDC1 to sites of DNA damage enables the subsequent recruitment of the E3 ubiquitin ligase, RNF8 (Kolas *et al.*, 2007). RNF8 associates with phosphorylated TQ sites of MDC1, and attaches K63-linked ubiquitin chains to H2A and γH2AX (Huen *et al.*, 2007; Kolas *et al.*, 2007; Mailand *et al.*, 2007). Another E3 ligase, RNF168 then associated with these chains, and further catalyses the mono- and poly-ubiquitylation of histones H2A and H2AX (Stewart *et al.*, 2009). The ubiquitylation of H2A(X) by RNF168 is mandatory for the recruitment of 53BP1 to sites of DSBs, but also serves to recruit RAP80, which in turn recruits BRCA1 to sites of DSBs (Wang & Elledge, 2007). This DSB repair signalling pathway is summarised in Figure 7.

Interestingly, 53BP1 recruitment to DSBs is mediated by RNF168, but 53BP1 does not contain any ubiquitin-binding activity. It is therefore proposed that the H2A(X) ubiquitylation may serve to alter the chromatin to a more decondensed state, which unmasks dimethyl H4K20 and/or H3K79 marks that can then be recognised by the tutor domain of 53BP1 (FitzGerald *et al.*, 2009). These methyl marks are not altered in response to DNA damage, suggesting that *de novo* methylation does not facilitate 53BP1 recruitment, which is fully in-line with the proposed model.

In addition to ubiquitylation signals, the accumulation of BRCA1 to sites of DSBs has been shown to depend upon sumoylation (Morris *et al.*, 2009). The sumo ligase, PIAS4, has been shown to localise to DSBs, and has also been shown to enhance RNF8 ligase activity (Galanty *et al.*, 2009). 53BP1 recruitment was also shown to depend upon PIAS4. Another sumo ligase, PIAS1, functions to sumoylate BRCA1, which in turn increases the ubiquitin ligase activity of BRCA1 (Galanty *et al.*, 2009). Thus, PIAS1 and PIAS4 appear to regulate HR and NHEJ, respectively, via sumoylation signalling.

Figure 7. An overview of DSB repair signalling

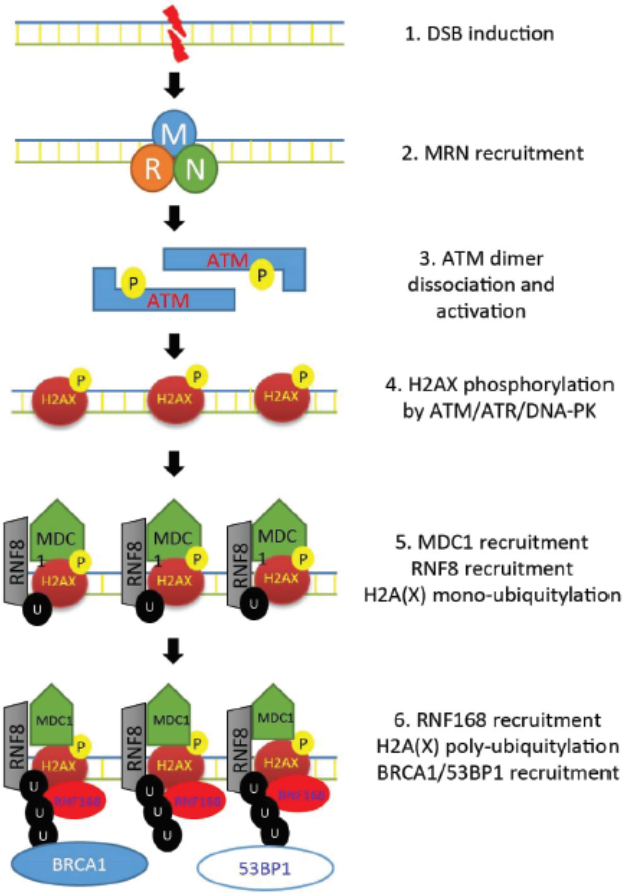

Figure 7: An overview of DSB repair signalling. 1. DSB formation can occur in cells due to a variety of exogenous and endogenous phenomena. 2. Initial DSB detection occurs via the MRN complex, which attaches to the DNA ends. 3. MRN focal accumulation at DSBs recruits and activates the ATM kinase. 4. ATM, along with ATR and DNA-PK, phosphorylate H2AX which serves as a beacon for the DNA repair factor, MDC1. 5. MDC1 is recruited to DSBs via interactions with H2AX, which leads to RNF8 recruitment and H2A(X) mono-ubiquitylation. 6. RNF168, another E3 ubiquitin ligase, binds to mono-ubiquitylated H2A(X) and serves to amplify mono- and poly-ubiquitylated H2A(X) signals. H2A(X) ubiquitiylation signals enable the recruitment of BRCA1 or 53BP1, whose binding promotes DSB repair via HR or NHEJ, respectively. Adapted from (Watts, 2016).

4.1.5. Canonical ATM signalling

ATM is a phosphatidylinositol 3-kinase-like family of serine-threonine kinase (PIKK), which phosphorylates substrates on serine or threonine residues that are followed by glutamine, so-called SQ or TQ motifs (Kim *et al.*, 1999; O'Neill *et al.*, 2000). Alike other PIKK members, ATM contains a FAT domain, a PI3K kinase domain, and a FAT carboxyl terminal domain (FAT-C). The FAT domain may function to interact with the kinase domain and stabilize the FAT-C domain (Bakkenist & Kastan, 2003). The ATM kinase also contains HEAT repeats in its amino terminal, which may act as a surface for protein interactions (Perry & Kleckner, 2003).

ATM is predominantly a nuclear protein, though it can also be found in the cytoplasm (Yang *et al.*, 2011). The levels of ATM protein are not affected by DNA damage induction (Banin *et al.*, 1998; Lakin *et al.*, 1996). Instead, ATM kinase activity dramatically increases after exposure to radiation (Canman *et al.*, 1998). This is believed to be the result of autophosphorylation, since kinase dead ATM does not undergo damage-induced phosphate incorporation (Kozlov *et al.*, 2006). Ionising radiation also increases the phosphorylation of ATM itself (Bakkenist & Kastan, 2003; Kozlov *et al.*, 2006).

The autophosphorylation of ATM at serine 1981 is thought to be crucial to ATM function, since ATM becomes phosphorylated at this site after ionising radiation, and serine to alanine mutation in this site leads to defective ATM-mediated phosphorylation of its substrate, p53 (Bakkenist & Kastan, 2003). Importantly, whilst serine 1981 is well-characterised, other sites on the ATM kinase are also phosphorylated and may be important in DNA repair (Kozlov *et al.*, 2006).

Whilst ATM is clearly responsive to the presence of DSBs, it was not clear initially as to whether ATM binds DSBs directly and whether it was a primary sensor of DSBs. Purified ATM can bind to dsDNA ends *in vitro*, is recruited to the chromatin fraction of cellular lysates after DNA damage, and serine 1981 specific antibodies form nuclear foci in response to DNA damage (Andegeko *et al.*, 2001; Bakkenist & Kastan, 2003; Smith *et al.*, 1999; Suzuki *et al.*, 1999). These studies indicate that ATM interacts with damaged DNA, though it is not clear whether these interactions were direct, or mediated by other factors.

As previously alluded to, ATM activation in response to DNA damage is not direct, and is mediated by the MRN complex (van den Bosch *et al.*, 2003). Cells null for Mre11 or Nbs1 display many characteristics of ATM null cells, including radiosensitivity and cell-cycle dysregulation (Taylor *et al.*, 2004). Several studies have demonstrated the MRN complex is upstream of ATM activation, and cells deficient in Nbs1 or Mre11 are defective in ATM phosphorylation (Carson *et al.*, 2003; Uziel *et al.*, 2003). Peculiarly, ATM activation appears to be dependent upon the nuclease activity of Mre11 (Uziel *et al.*, 2003), suggesting DNA end processing is required before ATM can become activated. More recently, it has been demonstrated that Nbs1 functions to recruit ATM to sites of DNA damage, which is also required for the autophosphorylation of ATM in response to DNA breaks (Difilippantonio *et al.*, 2005). ATM also phosphorylates Nbs1 at sites of DSBs (Lukas *et al.*, 2003). Taken together, these experiments imply that MRN binding to DSBs occurs first, leading to Mre11-dependant processing of the DNA ends, followed by Nbs1-mediated recruitment and activation of ATM, and then ATM-mediated phosphorylation of its substrates, which includes Nbs1 itself.

Activation of ATM by the MRN complex in response to DSBs results in the subsequent phosphorylation of a plethora of ATM substrate proteins, including serine 15 of p53 and serine 139 of H2AX (Kastan & Lim, 2000; Mu *et al.*, 2007; Shiloh & Ziv, 2013). In addition, ATM can activate other substrates indirectly, which occurs during ATM-mediated cell cycle control, via the activation of the cell cycle kinases, Chk1 and Chk2 (Goodarzi *et al.*, 2003). Given the importance of ATM in such pathways, it may appear surprising that ATM is not an essential protein. This likely reflects the fact that PIKK family kinases, such as ATR and DNA-PKcs have considerable crossover with ATM, when it comes to substrate phosphorylation (Blackford & Jackson, 2017).

4.1.6. Non-canonical ATM signalling

As well as mediating signal transduction during canonical DNA damage signalling, ATM signalling has also been linked to the repair of other types of DNA lesion. Of particular interest, ATM signalling has been shown to facilitate the repair of TOP1ccs, by phosphorylation of TDP1 at serine 81 (Das *et al.*, 2009). Evidently, A-T and SCAN1 mouse models accumulate more TOP1ccs (Alagoz *et al.*, 2013; Katyal *et al.*, 2014), which drives a neurodegenerative phenotype that can be phenocopied using the TOP1 inhibitor, CPT. Thus,

defective ATM-mediated repair of TOP1cc may play a role in driving the neurodegenerative aspect of the disease A-T.

ATM activity is also crucial to the efficient repair of heterochromatic DNA breaks. This was first discovered in the Jeggo laboratory, who demonstrated that heterochromatic DNA breaks have slower repair kinetics than euchromatic breaks (Goodarzi *et al.*, 2008). Moreover, ATM inhibition further impaired the resolution of heterochromatic, but not euchromatic, DNA breaks. Mechanistically, ATM-mediated phosphorylation of KRAB-Associated Protein 1 (KAP1), a bonafide heterochromatic protein, was shown to release KAP1 from heterochromatin, in turn helping to dissolve heterochromatic DNA (Goodarzi *et al.*, 2008). It is conceptualised that this process enables the access of DNA repair factors, therein promoting repair. In this study, the genetic inhibition of KAP1 or HDAC1 was able to restore heterochromatic DSB repair kinetics in ATM inhibited cells, which is in-line with the idea that ATM mediated local chromatin de-condensation is required to permit the repair of heterochromatic DSBs.

In addition to its role in DNA repair, other reports have demonstrated that ATM signalling is also important in the regulation of histone deacetylase 4 (HDAC4) (Li *et al.*, 2012). In this work, A-T patient cerebellar Purkinje cells were shown to display robust nuclear HDAC4 enrichment, whilst in control samples HDAC4 was predominantly cytoplasmic. This observation was also true in an A-T mouse model. Mechanistically, this was found to be a consequence of enhanced PP2A activity, whose activity is usually tamed by the presence of ATM signalling, resulting in HDAC4 hypo-phosphorylation and its nuclear translocation. The nuclear translocation of HDAC4 was shown to repress key neuronal survival genes (Li *et al.*, 2012). Crucially, blocking HDAC4 activity using Trichostatin A (TSA), or by lentiviral-mediated HDAC4 miRNA led to improved motor function and reduced cell death signalling in A-T mice (Li *et al.*, 2012). These data demonstrate the diverse nature of ATM signalling, and imply that the neurodegenerative aspect of A-T may not be completely dependent on DNA repair defects. In addition, these data imply that the nuclear enrichment of HDAC4 could be used as a biological marker of ATM signalling dysfunction.

In other work from the Herrup laboratory, it was shown that A-T patient and mouse models display an increase in H3K27 trimethylation (Li *et al.*, 2013). This was deduced to be the result of increased activity of the polycomb repressive complex (PRC2), since the core

catalytic domain of PRC2, enhancer of zeste homolog 2 (EZH2), was found to be a novel ATM substrate. EZH2-mediated increases in H3K27me3 were associated with cell-cycle re-entry in neuronal cells, ultimately leading neuronal cell death.

Moreover, other work from the Walker and Paull laboratory provides a link between ATM signalling and the regulation of reactive oxygen species (Guo *et al.*, 2010; Zhang *et al.*, 2015b), by regulating the selective autophagy of peroxisomes (pexophagy). Peroxisomes produce ROS via the process of fatty acid metabolism (Schrader & Fahimi, 2006). Since peroxisomes autonomously replicate, regulating their numbers is crucial for cellular homeostasis and their imbalance can drive disease (Spescha *et al.*, 2013). For instance, too many peroxisomes can lead to ROS accumulation (Schrader & Fahimi, 2006). ATM can be activated directly by ROS, by the formation of di-sulphide cross-linked cysteine residues (Guo *et al.*, 2010), which leads to the formation of an active ATM dimer. The activation of ATM by ROS leads to peroxisomal biogenesis factor 5 (PEX5)-mediated ATM recruitment to the peroxisome (Zhang *et al.*, 2015b). In turn, ATM induces Ulk1 activation and PEX5 phosphorylation, directing the autophagosome to the peroxisome, and driving the process of pexophagy (Zhang *et al.*, 2015b). Thus, defective ATM signalling may lead to increased ROS production by perturbing the degradation of peroxisomes and impairing ROS homeostasis. These data further demonstrates the diverse role of the ATM kinase (summarised in figure 8).

4.1.7. C9orf72 expansions are linked to heterochromatin formation

In other C9orf72 literature, it was demonstrated that C9orf72-ALS patient blood samples display increased levels of the heterochromatin marker, H3K9me3 (Belzil *et al.*, 2013). Given that heterochromatic DNA breaks display slower repair kinetics (Goodarzi *et al.*, 2008), the presence of excess heterochromatin may impede DNA repair in C9orf72-ALS, contributing to genome instability. Interestingly, the same study also demonstrated that H3K27me3 levels were higher in C9orf72 samples (Belzil *et al.*, 2013). This is intriguing because, as mentioned above, this could be a consequence of defective ATM signalling (Li *et al.*, 2013).

Figure 8. ATM signalling pathways

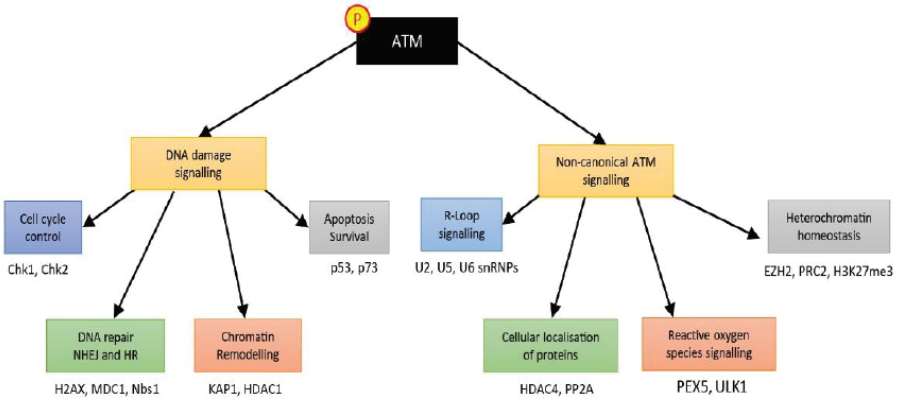

Figure 8: Cellular roles of ATM signalling in response to DNA damage and other stimuli. In response to DNA damage, ATM signalling regulates cell cycle progression via the phosphorylation of Chk1 and Chk2. Similarly, ATM signalling enhances the repair of DSBs via NHEJ and HR, as well as other types of DNA repair, such as TDP1-mediated cleavage of TOP1-ccs. ATM signalling also controls apoptotic pathways, via its effects on tumour suppressors p53 and p73. Finally, ATM signalling is critical to the repair of DSBs that arise in heterochromatic DNA, wherein ATM-mediated phosphorylation of KAP1 serves to transiently relax the chromatin to enable DSB repair. As well as in response to DSBs, ATM signalling plays a role in R-loop signalling, whereby ATM kinase activity enhances the displacement of the spliceosome. The presence of reactive oxygen species can also activate ATM, which forms an active dimer, bound by disulphide cysteine bonds. The active ATM dimer functions to induce pexophagy by phosphorylating PEX5. In addition, decreased ATM signalling leads to enhanced PP2A activity, and HDAC4 nuclear accumulation. Similarly, ATM deficient neurons also display dysregulated PRC2, which leads to increased levels of the heterochromatic histone mark, H3K27me3. ATM signalling therefore has a diverse number of cellular roles.

4.2. Aims and Hypothesis:

Given that ATM signalling appears to be crucial to neuronal cell function, including DNA repair processes, we aim to investigate whether ATM signalling pathways are altered in C9orf72 models. More specifically, we aim to assess whether:

- ATM activation and accumulation at sites of DNA breaks is altered in cells expressing C9orf72 expansions
- The phosphorylation and recruitment of the ATM effector proteins, 53BP1 and p53, is altered in cells expressing C9orf72 expansions
- C9orf72 expansion-expressing cells display increased levels of TOP1ccs
- The expression of C9orf72 expansions cells leads to increased heterochromatin, and whether this contributes to genome instability
- HDAC4 cellular localisation is altered in cells expressing C9orf72 expansions.

4.3. Results

4.3.1. Expression of C9orf72-related RREs and DPRs leads to defective phosphorylated ATM foci formation in human MRC5 cells.

The growing evidence that links C9orf72 repeat expansions to cerebellar ataxias (Corcia *et al.*, 2016; Lindquist *et al.*, 2013), prompted us to test whether the activation of the master DNA repair kinase, ATM, is dysregulated in cells expressing C9orf72 expansions. While control cells displayed an average of 2 phosphorylated ATM (pATM) foci per nucleus, cells expressing 34 or 69 poly-GA DPRs (Figure 9a, $p=0.002$) or 102 RREs (Figure 9b, $p=0.008$) consistently possessed fewer numbers of pATM foci on average. The reduced number of pATM foci was not an artefact of expressing the V5 epitope tag or transfection associated toxicity, since transfection with a V5 empty plasmid or GFP did not result in defective pATM foci (Figure 9c). It was also not due to reduced ATM expression, as shown by Western blotting (Figure 9d, $p>0.05$).Since the accumulation of oxidative and protein-linked DNA breaks (PDBs) cause neurodegeneration in man (Ashour *et al.*, 2015), we examined if pATM foci would form normally following exposure to CPT or tert-butyl hydroperoxide (TBH). Treatment with CPT or TBH led to a prominent increase in pATM foci in control cells (Figure 9e,f). In a marked contrast, cells expressing 34/69 poly-GA or 102 RREs consistently showed defective pATM foci formation following CPT and TBH treatments (Figure 9 e,f)

Figure 9. Expression of C9orf72 expansions leads to defective ATM activation.

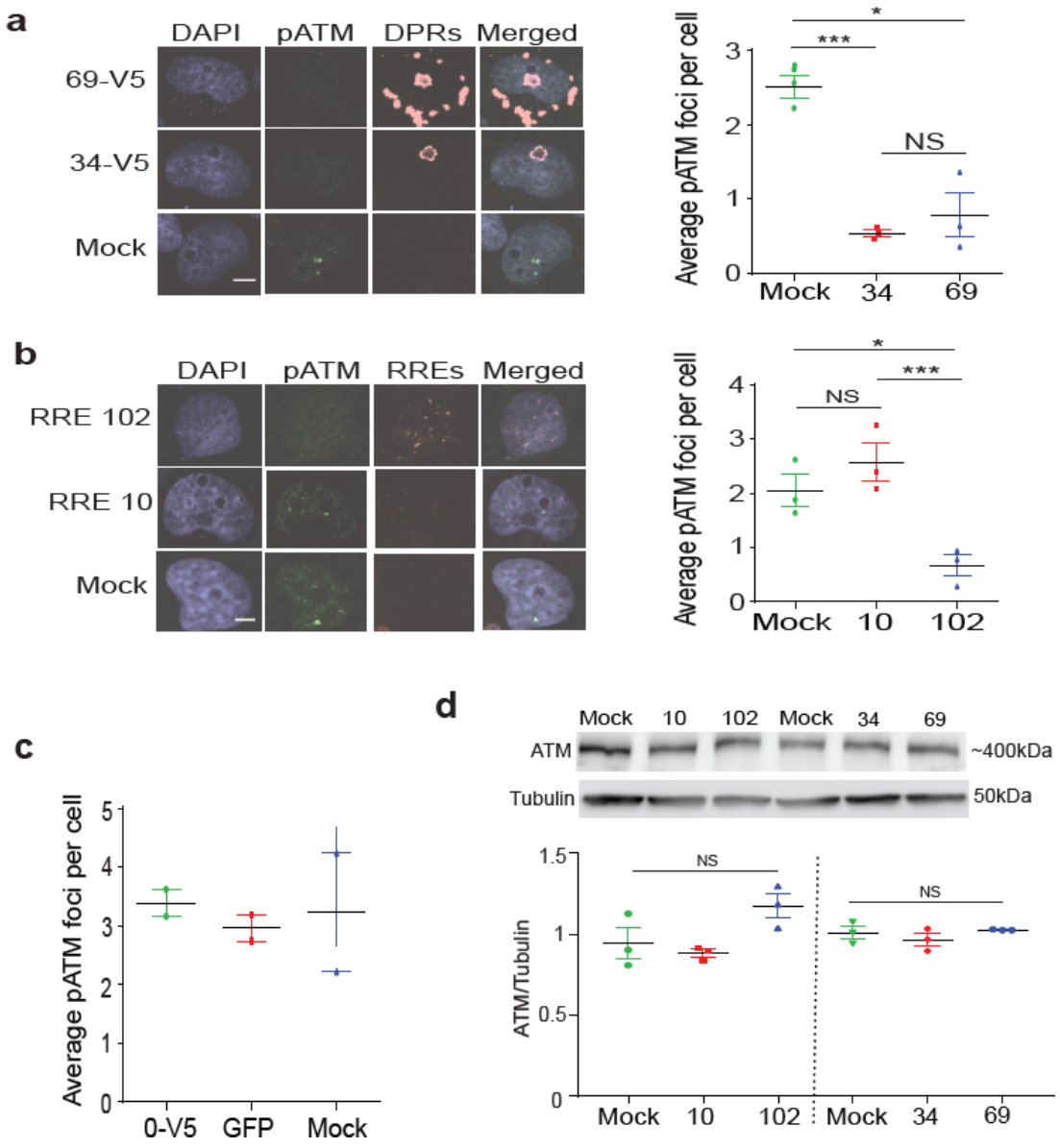

Figure 9: Expression of C9orf72 expansions leads to defective pATM focal accumulation. (a,b) MRC5 cells mock transfected, transfected with 34, 69 DPRs (a), or 10, 102 RREs (b). Cells analysed using immunocytochemistry with anti-phosphorylated ATM 'pATM' and anti-V5 'DPRs' antibodies (a) or with FISH-IF (b). *Left*, Representative images shown, scale bar 5μm. *Right*, The average (± SEM) number of pATM foci per cell was quantified from 3 cell culture replicates, 50 cells each, and analysed using a one-way ANOVA. **(c)** MRC5 cells mock transfected or transfected with 0-V5 empty vector or GFP. Subsequently, cells were immunostained with anti-phosphorylated ATM antibodies. Endogenous GFP signal was visualised without antibody amplification. The number of pATM foci per cell was quantified and presented as average ± range from 2 biological replicates, 50 cells each. **(d)** *Left*, HEK 293T cells were mock transfected 'M' or were transfected constructs encoding 10 or 102 RREs '10, 102' or 34, 69 DPRs '34, 69'. Whole cell lysates were analysed using anti-ATM and α-tubulin antibodies. *Right*, ATM protein expression (normalised to α-tubulin) is presented as average ± SEM from 3 cell culture replicates, and analysed using a one-way ANOVA.

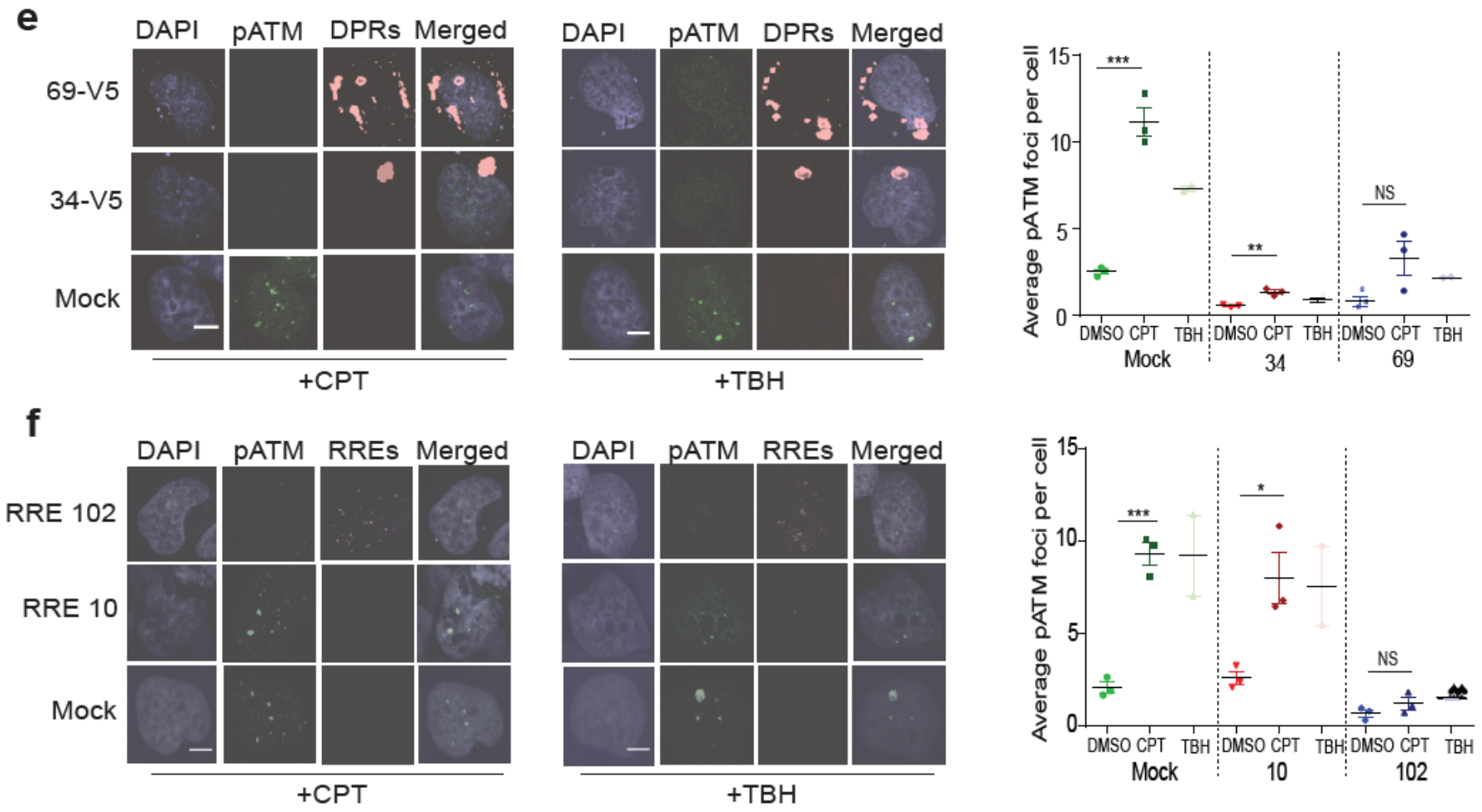

Figure 9: Expression of C9orf72 expansions leads to defective pATM focal accumulation. (e,f) MRC5 cells mock transfected, transfected with constructs encoding 34, 69 DPRs (e), or transfected with constructs encoding for 10, 102 RREs (f). Cells were incubated with 10µM CPT ,0.037% TBH, or DMSO for 1 hour, and analysed by immunocytochemistry as described for (a,b). *Left*, Representative images of 3 cell culture replicates are shown, scale bar 5µm. *Right*, pATM foci were quantified as described for (a,b).

4.3.2. Expression of C9orf72-related RREs and DPRs leads to defective 53BP1 foci formation in human MRC5 cells and rodent cortical neurons.

An important consequence of defective ATM signalling is the defective accumulation of NHEJ repair factors, such as 53BP1, into nuclear foci (Harrigan *et al.*, 2011). As expected, expression of 34 or 69 poly-GA DPRs led to a marked reduction in 53BP1 recruitment to nuclear foci when compared to control cells (Figure10a, p=0.002). As observed with DPRs, expression of 102 RREs also led to the suppression of 53BP1 foci formation, when compared to cells expressing 10 RREs (Figure 10b, p=0.035). Strikingly, whilst CPT induced a significant increase in 53BP1 foci in control cells (Figure 10c, p=0.009), expression of 34 or 69 poly-GA DPRs prevented the CPT-induced increase in 53BP1 foci formation (Figure 10c, p=0.294). Similarly, expression of 102 RREs prevented the CPT-induced increase in 53BP1 foci formation (Figure10d, p=0.496). To test if this was also true in bona fide post-mitotic neurons, we transduced rat cortical neurons with AAV9 viral particles expressing 34, 69 poly-GA DPRs or 10, 102 RREs and examined 53BP1 foci formation following exposure to CPT (Figure 10e,f). Consistent with results using MRC5 cells, whilst control neurons exhibited ~8 53BP1 foci per neuron, those expressing 69 poly-GA DPRs or 102 RREs showed 3 or 1 foci per cell, respectively (Figure 10 e,f, $p<0.01$).

As was the case for pATM, reduced 53BP1 foci was not an artefact of expressing the V5 epitope-tag used to visualise DPRs, nor was it due to transfection-related toxicity, as it was not observed in cells transfected with vectors encoding V5 or GFP (Figure 10 g). Consistent with our transfection data, this was not an artefact of viral transduction as cells transduced with AAV9 encoding V5 or GFP vectors possessed normal level of 53BP1 foci (Figure 10 h). Together, these data demonstrate that the expression of C9orf72-related RREs or DPRs suppress 53BP1 recruitment to DSBs.

Figure 10. Expression of C9orf72 expansions leads to defective 53BP1 foci formation.

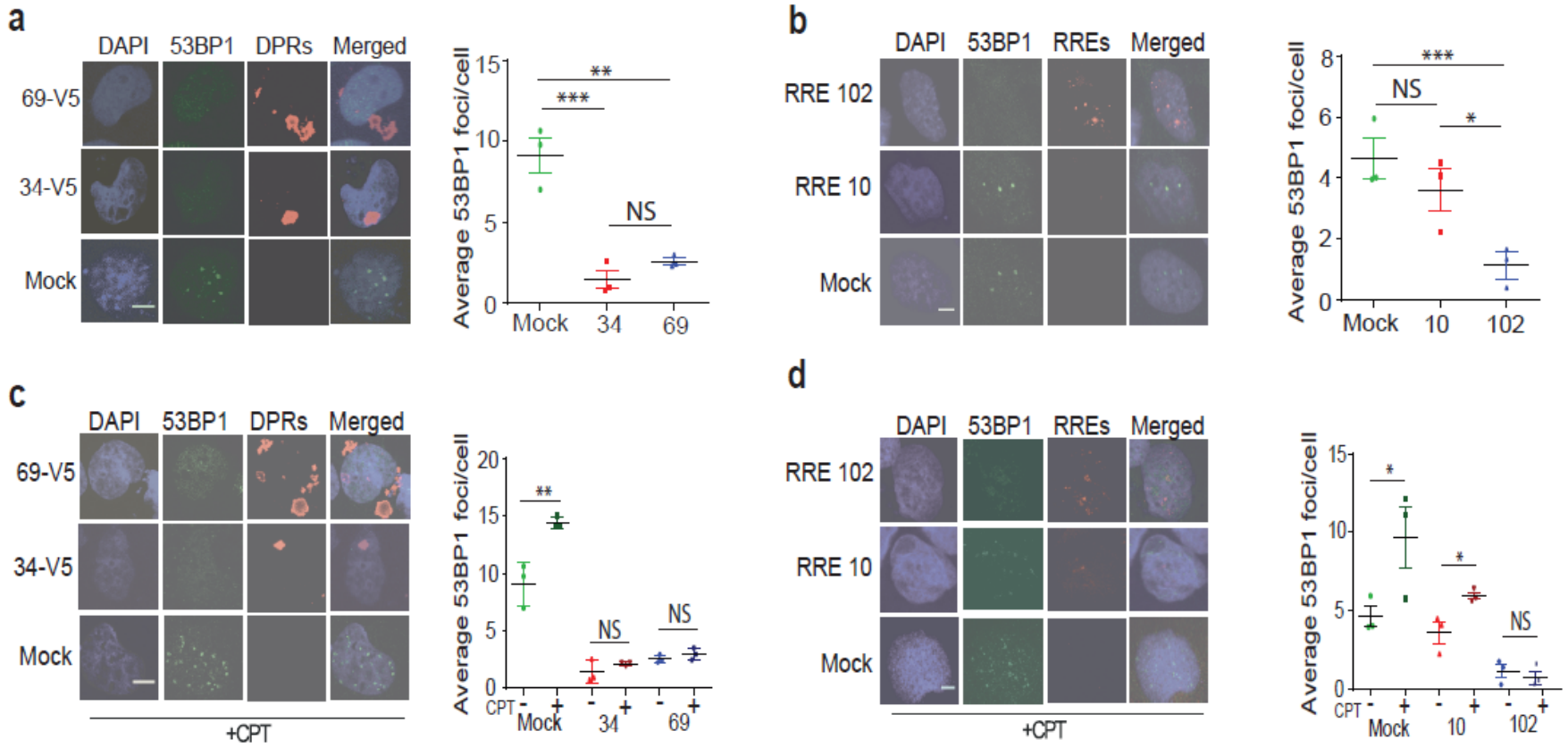

Figure 10: Expression of C9orf72 expansions leads to defective 53BP1 foci formation. (a,b) MRC5 cells mock transfected or transfected with 34 or 69 DPRs (a) or 10, 102 RREs (b), and immunostained with anti-53BP1 antibodies, alongside anti-V5 'DPRs' antibodies or with FISH-IF double-staining 'RNA' (b). *Left*, Representative images are shown, scale bar 5µm. *Right*, The average (± SEM) number of 53BP1 foci per cell was quantified from 3 cell culture replicates, 50 cells each, and analysed using a one-way ANOVA. **(c,d)** MRC5 cells were mock transfected or transfected with constructs encoding 34 or 69 DPRs (c), or 10, 102 RREs (d). Cells were incubated with 10µM CPT or DMSO for 1hour, and immunostained as described for (a,b). *Left*, Representative images are shown, scale bar 5µm. *Right*, 53BP1 foci was quantified as described above and analysed using a Student's t-test.

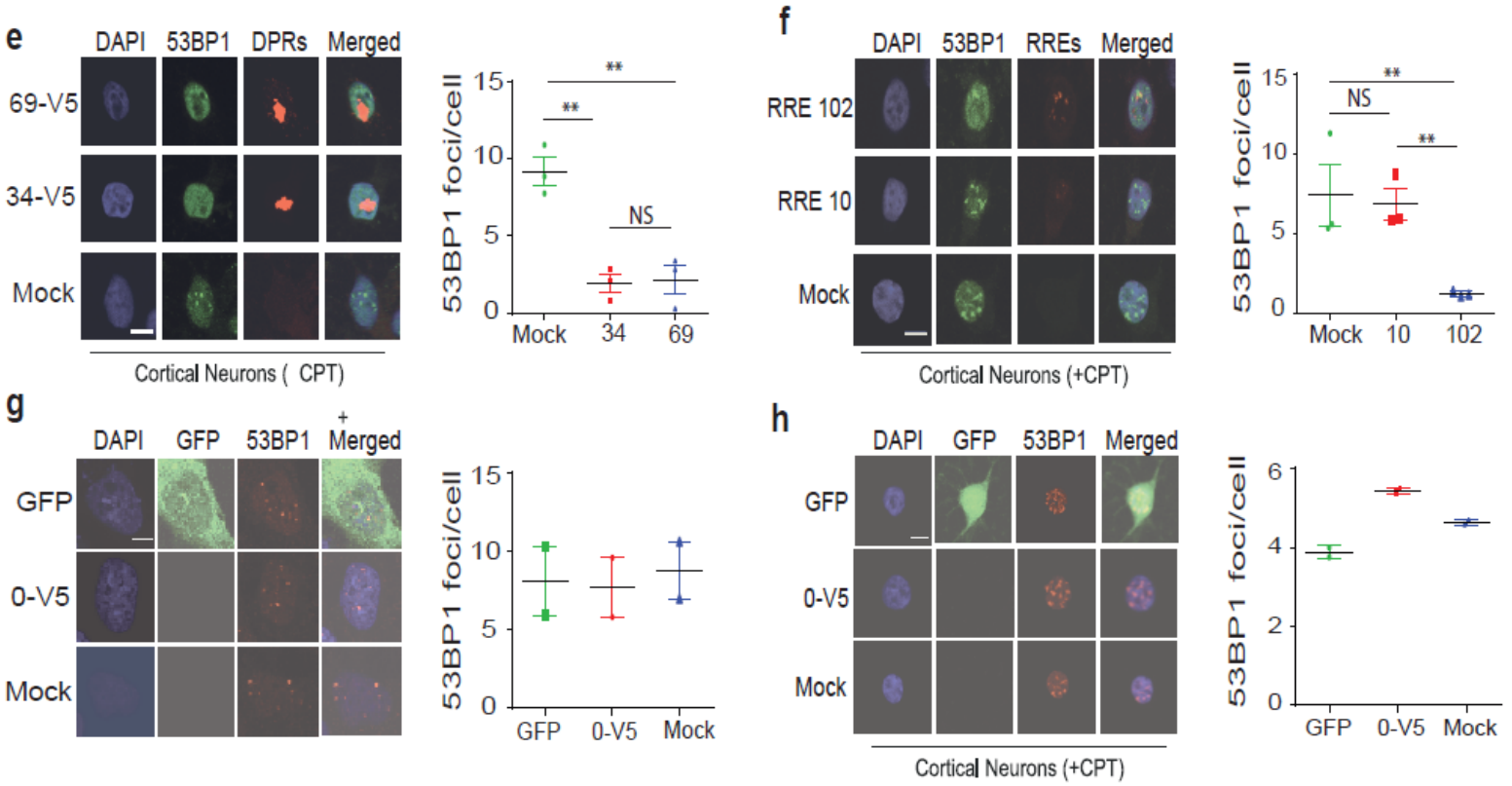

Figure 10: Expression of C9orf72 expansions leads to defective 53BP1 foci formation (e,f) Rat cortical neurons mock transduced or transduced with AAV9 viral-vectors expressing 34 or 69 DPRs (e) or with 10 or 102 RREs (f). Neurons treated with 10μM CPT for 1 hour and analysed by immunocytochemistry as described for (a,b). *Left*, Representative images are shown, scale bar 5μm. *Right*, 53BP1 foci was quantified as described for (a,b), 20 neurons each, and analysed using a one-way ANOVA. **(g)** MRC5 cells were mock transfected or transfected with constructs encoding a 0-V5 empty vector, or GFP. Subsequently, cells were immunostained with anti-53BP1 antibodies. Endogenous GFP signal was visualised without antibody amplification. Left, Representative images of 2 biological replicates are shown, scale bar 5μm. Right, The number of 53BP1 foci per cell was quantified and presented as average ± range from 2 biological replicates, 50 cells each. **(h)** Rat cortical neurons mock transduced or transduced with AAV9 0-V5 or GFP, and were incubated with 10μM CPT '+CPT' for 1 hour. Cells were immunostained with anti-53BP1 antibodies. Left, Representative images of 2 biological replicates are shown, scale bar 5μm. Right, The number of 53BP1 foci per cell was quantified and presented as average ± range from 2 biological replicates, 20 cells each.

4.3.3. Expression of C9orf72-related RREs and DPRs leads to the defective phosphorylation of p53 in human MRC5 cells.

To test whether the expression of C9orf72-related products results in defective phosphorylation of downstream ATM-effector proteins, we next examined the phosphorylation of p53, a known ATM target (Bakkenist & Kastan, 2003). Whilst control cells displayed ~6-fold elevation of p-p53 levels in response to CPT treatment (Figure 11a, $p=0.037$), cells expressing 34 or 69 poly-GA DPRs showed no significant increase above baseline levels (Figure 11a, $p>0.05$). Similarly, cells containing 102 RREs failed to induce p53 phosphorylation following CPT exposure (Figure 11b, $p=0.536$), whilst mock-transfected cells and those expressing the 10 RREs did show a robust p53 response to CPT treatment (Figure 11b; $p=0.0143$ and $p=0.01$, respectively).

Figure 11. Expression of C9orf72 expansions leads to defective p53 phosphorylation.

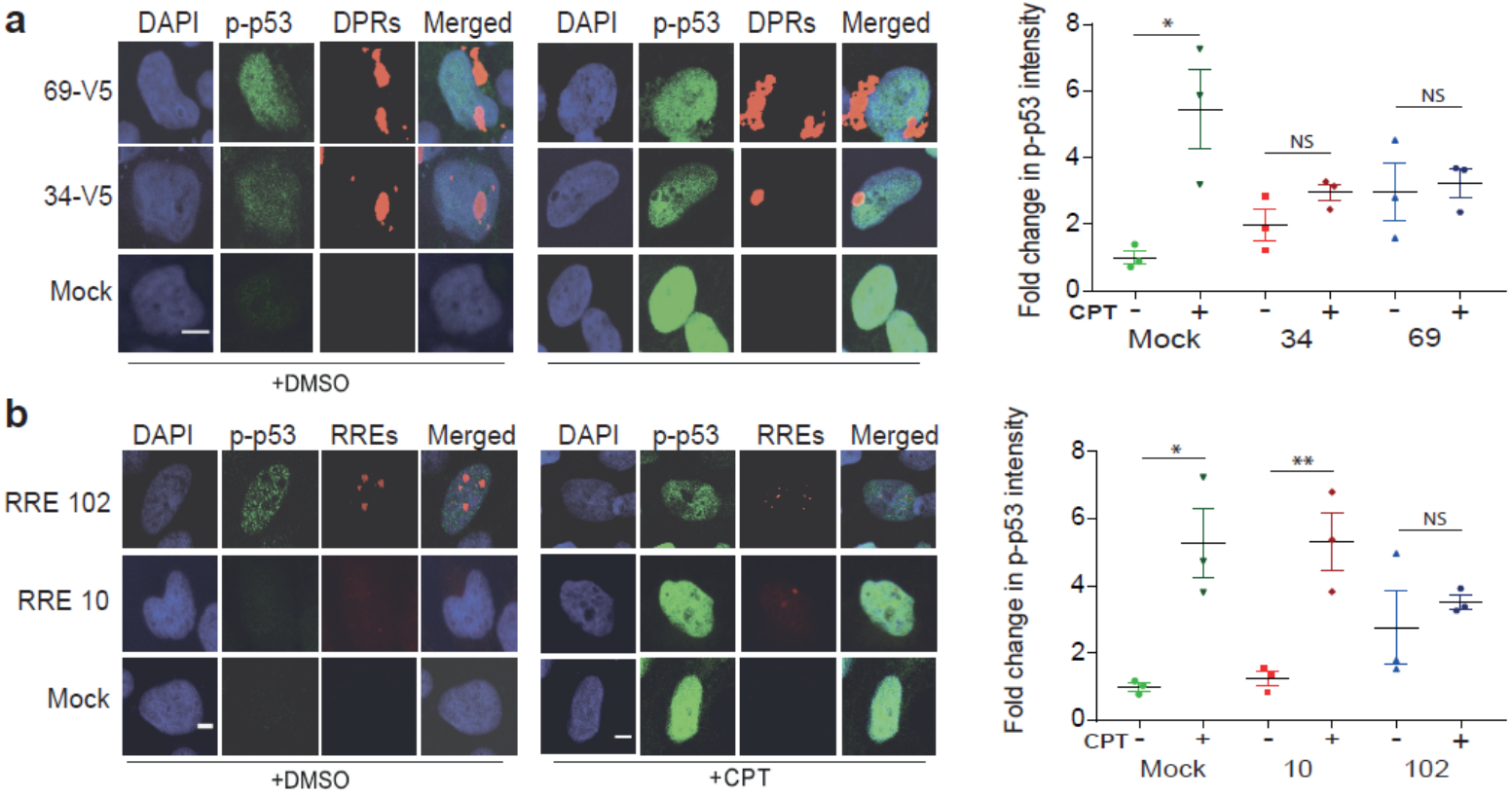

Figure 11: Expression of C9orf72 expansions leads to defective p53 phosphorylation. (a,b) MRC5 cells were mock transfected or transfected with constructs encoding 34 or 69 DPRs (a), or 10, 102 RREs (b) and were then treated with DMSO or with 10μM CPT. Cells were then immunostained with anti-phosphorylated p53 antibodies, alongside anti-V5 'DPRs' antibodies (a) or with FISH-IF double-staining 'RNA' (b). Left, Representative images are shown, scale bar 5μm. Right, The nuclear fluorescence value for 50 nuclei was quantified from 3 cell culture replicates, and presented as the average (± SEM) fold change in nuclear intensity (relative to control cells), and analysed using Student's t-test.

4.3.4. ATM inhibition does not affect 53bp1 and phosphorylated p53 foci in cells expressing C9orf72-related DPRs

After confirming ATM signalling was defective in both DPR and RRE models using three separate read-outs (pATM, 53BP1, and p-p53), we focused on the DPR model and aimed to further demonstrate that ATM-mediated DNA repair processes were defective. Consistent with defective ATM in DPR expressing cells, pre-treatment with the ATM inhibitor Ku55933 significantly impaired pATM and 53BP1 foci formation in control cells, but was epistatic to the suppression of 53BP1 foci that was induced by 34 or 69 poly-GA DPR expression (Figure 12a,b). Consistent with the 53BP1 data, we also observed a defect in the recruitment of p-p53 to nuclear foci in DPR expressing cells, which was mimicked in control cells by pre-treatment with the ATM inhibitor (Figure 12c). Notably, ATM inhibition did not further attenuate p-p53 signalling in DPR-positive cells (Figure 12c, p=0.059 and p=0.49, for 34 and 69, respectively). Whilst we predict that a similar phenomenon would occur with our RNA model, these experiments have not yet been performed.

4.3.5. Expression of C9orf72-related DPRs in human MRC5 cells leads to defective chromatin retention of pATM and 53BP1

In order to validate our key findings (defective pATM and 53BP1 recruitment to repair foci) using a separate technique, we treated MRC5 cells transfected with 0 or 69 poly-GA DPRs with CPT and collected the nuclear soluble and chromatin-bound fractions. We excluded the 34 poly-GA condition since we consistently observe the same phenomenon as with 69 poly-GA DPRs. In-line with our immunocytochemistry data, the chromatin retained levels of 53BP1 and pATM levels were reduced in cells transfected with poly-GA DPRs (Figure 12d, n=2). On the other hand, nuclear soluble fractions from poly-GA transfected cells displayed normal, or possibly increased, levels of 53BP1 and pATM (Figure 12d, n=2). This experiment was repeated 2 times with similar results. These data are consistent with the notion that ATM-mediated DSB repair signalling is defective in cells expressing C9orf72 expansions or DPRs.

Figure 12. Pharmacological inhibition of ATM does not affect 53BP1 and p-p53 repair foci in poly-GA expressing cells, which also display defective chromatin recruitment of 53BP1 and pATM.

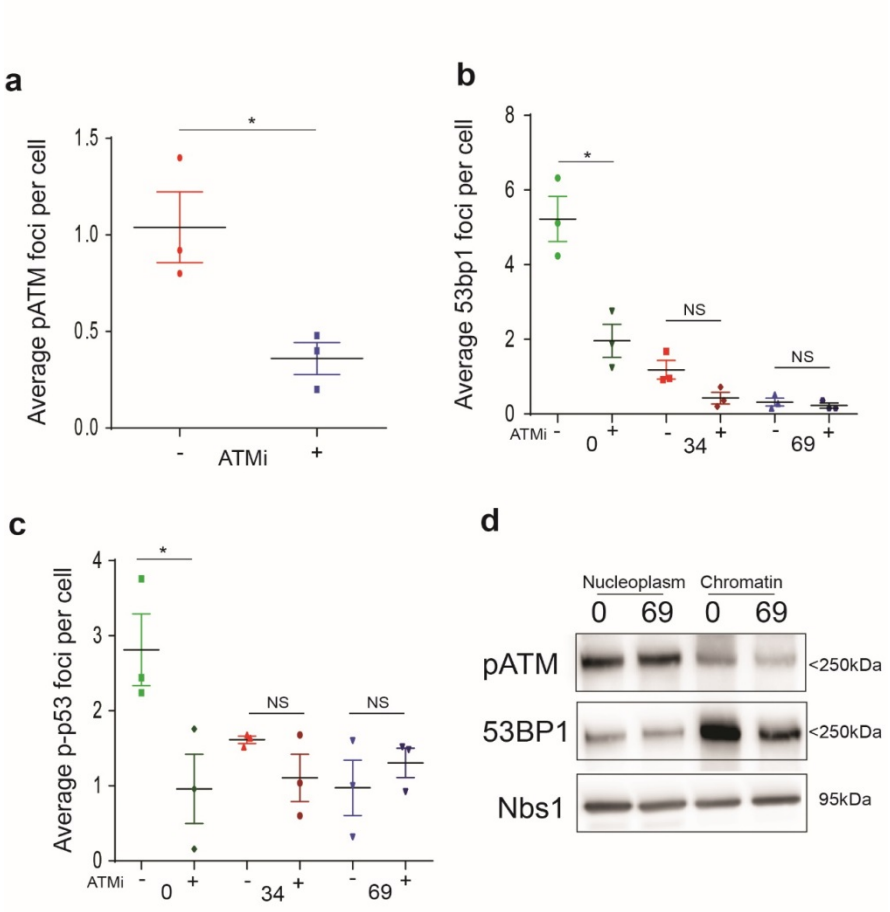

Figure 12: Pharmacological inhibition of ATM does not affect 53BP1 and p-p53 repair foci in poly-GA expressing cells, which also display defective recruitment of 53BP1 and pATM to chromatin. (a) MRC5 cells were treated with Ku5593 (10μM) for 2 hours. Subsequently, cells were analysed by immunocytochemistry, using pATM specific antibodies. The number of pATM nuclear foci was quantified from 3 biological replicates, 25 cells each, and is presented the average +/- SEM. Significance was assessed using a Student's t-test. **(b,c)** MRC5 cells transfected with V5 epitope-tagged 0, 34, or 69 Gly-Ala DPRs for 2 days. Prior to fixation, cells were treated with an Ku5593 (10μM) for 2 hours. Subsequently, cells were analysed by immunocytochemistry using anti-53BP1 (b) or anti-phospho-p53 (c) antibodies. The number of 53BP1 (b) or p-p53 (c) nuclear foci was quantified from 3 biological replicates, 25 cells each, and is presented the average +/- SEM. Significance was assessed using a Student's t-test. **(d)** MRC5 cells were transfected with 0, 69 poly-GA DPRs. 3 days post-transfection, the nuclear soluble and chromatin bound protein fractions were collected and analysed using SDS-PAGE and western blotting with antibodies specific for pATM, 53BP1 and Nbs1. Representative western blot from 2 cell culture replicates is shown.

4.3.6. Expression of C9orf72-related DPRs in rodent neurons leads to the nuclear retention of HDAC4

To further confirm ATM deficits in primary neural cultures we took advantage of the observations in ATM knockout mice and Ataxia Telangiectasia (A-T) patient tissue in which histone deacetylase 4 (HDAC4) is abnormally localised to the nucleus of neurons (Li *et al.*, 2012). To test if the ATM deficits triggered by C9orf72-related DPRs would also cause nuclear accumulation of HDAC4, we transduced rat cortical neurons with AAV9 viral particles expressing 69 poly-GA DPRs and examined the cellular localisation of HDAC4. Whilst HDAC4 appeared cytoplasmic in control neurons, it showed marked nuclear enrichment in neurons expressing 69 poly-GA DPRs (Figure 13a). Subsequent quantification revealed ~3 fold increase in the % of neurons exhibiting nuclear HDAC4 in neurons expressing 69 poly-GA DPRs (Figure 13a, p=0.001). Nuclear accumulation of HDAC4 was not an artefact of viral transduction as neurons transduced with AAV9-V5 or AAV9-GFP displayed normal cytoplasmic HDAC4. Furthermore, pre-treatment with an ATM inhibitor (Ku 55933) similarly caused nuclear HDAC4 re-localisation (Figure 13 b), suggesting that the observed phenotype is due to ATM signalling deficit.

4.3.7. Expression of C9orf72-related RREs and DPRs leads to TOP1cc accumulation

In order to gain further evidence for defective ATM signalling, we next examined the accumulation of TOP1 cleavage complexes (TOP1cc). ATM deficiency in primary neural cultures and in rodent models has been shown to cause elevated levels of TOP1cc, interfering with transcription and contributing to neuronal cell death (Alagoz *et al.*, 2013; Katyal *et al.*, 2014). Consistent with an ATM defect, cells expressing C9orf72-related DPRs or RREs exhibited ~4-fold increase in TOP1cc levels compared to controls (Figure 13c) This experiment was repeated 2 times with similar results and was conducted by Chunyan Liao. Taken together, these experiments reveal that C9orf72-related DPRs or RREs cause defective ATM signalling.

Figure 13. Expression of poly-GA DPRs leads to nuclear HDAC4 enrichment and increased TOP1-ccs

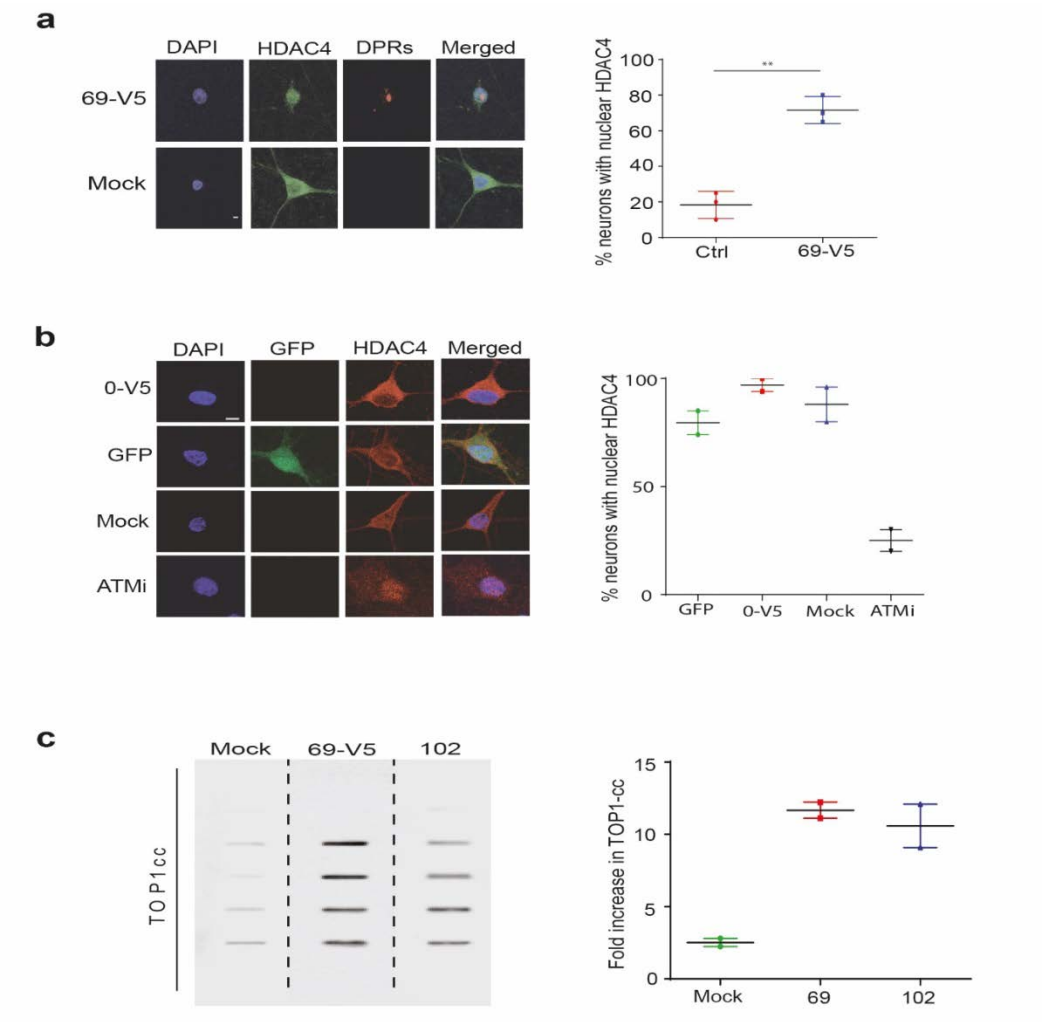

Figure 13. Expression of C9orf72 DPRs leads to nuclear enrichment of HDAC4 and increased TOP1ccs. (a) Rat cortical neurons (5 DIV) mock transduced or transduced with a AAV9-viral vector construct expressing 69 DPRs, and analysed by immunocytochemistry using anti V5 'DPRs' and an anti-HDAC4 antibodies. *Left*, representative images are shown, scale bar 5µm. *Right*, the % of cultured cortical neurons exhibiting nuclear HDAC4 staining was quantified from 3 biological replicates, each replicate represented by a single point on the scatter plot, containing 20 cultured cortical cells and presented as average ± SEM. Significance was assessed using a Student's t-test. **(b)** Rat cortical neurons mock transduced or transduced with AAV9 viral particles encoding a V5 epitope-tag or GFP. Neurons were treated with an ATM inhibitor 'ATMi' (Ku 55933, 10µM) for 1 hour, and subsequently were immunostained with anti-V5 'DPRs' and anti-HDAC4 antibodies. *Left*, representative images of 2 biological replicates are shown, scale bar 5µm. *Right*, The percentage of cells with cytoplasmic HDAC4 was quantified and presented as average ± range from 2 biological replicate, 20 cells each**. (c)** *Left*, HEK 293T cells were mock transfected or were transfected with 69 DPRs or 102 RREs. Cells were treated with 10µM CPT for 40 min, subjected to CsCl step gradients, and fractions were slot blotted with anti-TOP1 antibodies. *Right*, The fold increase in TOP1-ccs, normalised to mock was calculated and presented as the average from 2 cell culture replicates ± range.

4.3.8. Expression of C9orf72-related DPRs in human cells leads to heterochromatin formation, which is linked to genomic instability and cellular toxicity

Given that chromatin compaction has been reported in C9orf72 plasma samples (Belzil *et al.*, 2013), we speculated that an increase in heterochromatin formation might be a hallmark of C9orf72-associated disease. Using H3K9me3 as a marker for heterochromatin, we confirmed that DPR expression increases heterochromatin formation, as measured by ~50% increase in H3K9me3 signals identified by western blotting, in comparison to empty vector control cells (Figure 14a, $p = 0.0001$). We have not yet been able to repeat this experiment with our RNA model. Since ATM has been linked to the repair of heterochromatic DSBs (Goodarzi *et al.*, 2008), we wondered whether promoting chromatin relaxation by Trichostatin A (TSA) would reduce DSBs levels in cells expressing poly-GA DPRs. Indeed, treatment with TSA led to a reduction of H3K9me3 nuclear fluorescence (Figure 14b; $p = 0.002$). TSA treatment also led to a reduction in γH2AX, but not R-loop, foci in cells expressing poly-GA DPRs (Figure 14c,d; $p = 0.001$), suggesting that chromatin relaxation reduces DSB levels. This is in line with the reported role of ATM during the repair of heterochromatic DSBs, in which the DNA repair deficit caused by ATM inhibition is overcome by chromatin relaxation by the inhibition of HDAC1 (Goodarzi *et al.*, 2008). Notably, TSA treatment increased DSB levels in control cells (Figure 4c, $p=0.033$), suggesting that whilst TSA is beneficial in C9orf72 models in which the chromatin is compact, it may confer sensitivity to other types of DNA lesions in cells with non-pathological chromatin arrangements. This is consistent with a recent report from the lab (Meisenberg *et al.*, 2017). Finally, we wondered whether TSA treatment would also have beneficial effects on cell survival in cells expressing poly-GA DPRs. TSA treatment rescued the cellular toxicity triggered by poly-GA DPR expression to a level similar to that observed in DMSO-treated control cells, as measured by both PARP1 cleavage (Figure 14e; $p = 0.0004$) and trypan blue exclusion assays (Figure 14f; $p = 0.003$). These data suggest that C9orf72-related DPRs drive the formation of heterochromatin, thereby exacerbating ATM defects, which contributes to cell death.

Figure 14. Expression of poly-GA DPRs leads to heterochromatin formation, genomic instability and cellular toxicity

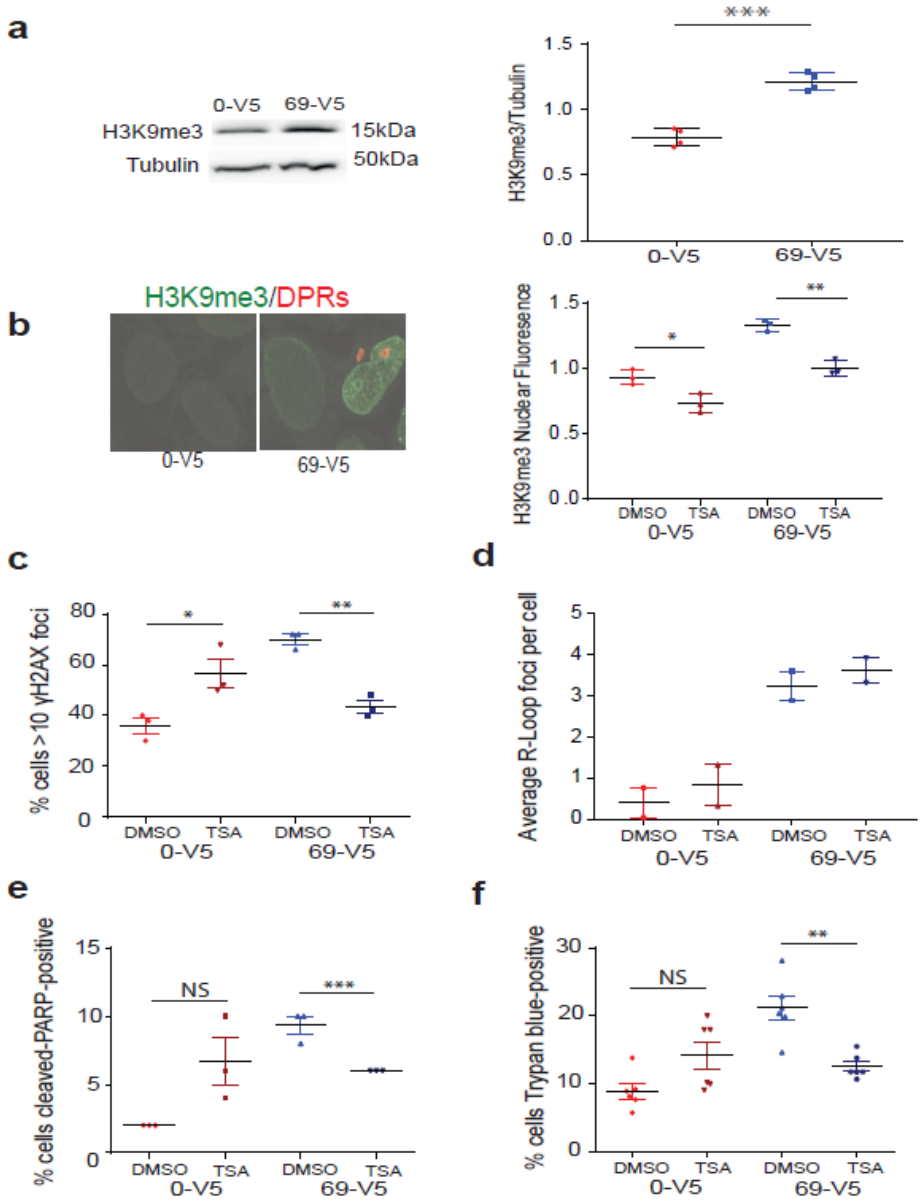

Figure 14: C9orf72-associated DSBs and cellular toxicity can be reduced by chromatin de-condensation. **(a)** *Left*, HEK 293T cells transfected with constructs encoding 0 or 69 DPRs were analysed using Western Blotting with anti-H3K9me3 and anti-GAPDH antibodies. *Right*, H3K9me3 band intensity quantified and normalised to GAPDH, data presented as the average ± SEM from 4 cell culture replicates and analysed using Student's t-test. **(b)** *Left*, MRC5 cells transfected with 0 or 69 DPRs were immunostained with anti-V5 'DPRs' and H3K9me3 antibodies. Representative images of 3 independent cell culture replicates are shown. *Right*, MRC5 cells transfected with 0, 69 DPRs were treated with TSA (100nm) or DMSO and immunostained with

anti-V5 ‘DPRs’ and H3K9me3 antibodies. Nuclear fluorescence intensity was quantified and presented as the average ± SEM from 3 independent cell culture repeats, 25 cells each. Significance was assessed using a Student’s t-test. **(c)** MRC5 cells transfected with 0 or 69 DPRs and were treated with TSA or DMSO. Cells were immunostained with anti-V5 ‘DPRs’ and anti γH2AX antibodies. The average (± SEM) percentage of cells with 10 or more γH2AX foci was quantified from 3 independent cell culture replicates, 50 cells each, and analysed using a Student’s t-test. **(d)** MRC5 cells transfected with 0 or 69 DPRs were treated with TSA or DMSO, and immunostained with anti-V5 ‘DPRs’ and anti S9.6 antibodies. The average (± range) number of R-Loop foci per cell was quantified from 2 independent cellular replicates, 25 cells each. **(e)** MRC5 cells transfected with 0 or 69 DPRs and were treated with TSA or DMSO, and the average (± SEM) percentage of cells positive for cleaved PARP was quantified from 3 independent cell culture replicates, 50 cells each, and analysed using a Student‘s t-test. **(f)** HEK 293T cells transfected with 0 or 69 DPRs were treated with TSA or DMSO. The average (± SEM) percentage of cells permeable to Trypan Blue reagent was quantified from 6 independent replicates, ~200 cells each, and was analysed using a Student’s t-test.

4.3.9. Mice expressing C9orf72 expansions or poly-GA DPRs display elevated levels of genome instability and increased HDAC4 nuclear enrichment

We next examined whether these observations were also true *in vivo*. To achieve this, AAV9 viral vectors encoding 10 or 102 RREs or 0 or 69 V5-tagged DPRs were delivered into the cerebrospinal fluid via cisterna magna of wild-type mice at postnatal day 1. This was performed by Saul Herranz Martin, whom also processed the tissues. As was the case *in vitro*, expression of 102 RREs or 69 poly-GA DPRs in mouse CNS tissue led to HDAC4 nuclear re-localisation and the accumulation of DSBs as measured by increased γH2AX foci (Figure 15a–d; $P < 0.05$). These experiments were performed from mice culled at age 6 months for DPR injected mice and at 12 months for RRE injected mice. Purkinje cells were measured for RRE model experiments, whilst brain-stem nuclei were measured for DPR model experiments. The reason for changing to brainstem for DPR experiments was because the cerebellum was not well transduced by our DPR viral vectors, which is likely the result of viral tropism (since the promoters are identical).

Figure 15. Mice expressing C9orf72 expansions or poly-GA DPRs display elevated levels of genome instability and increased HDAC4 nuclear enrichment

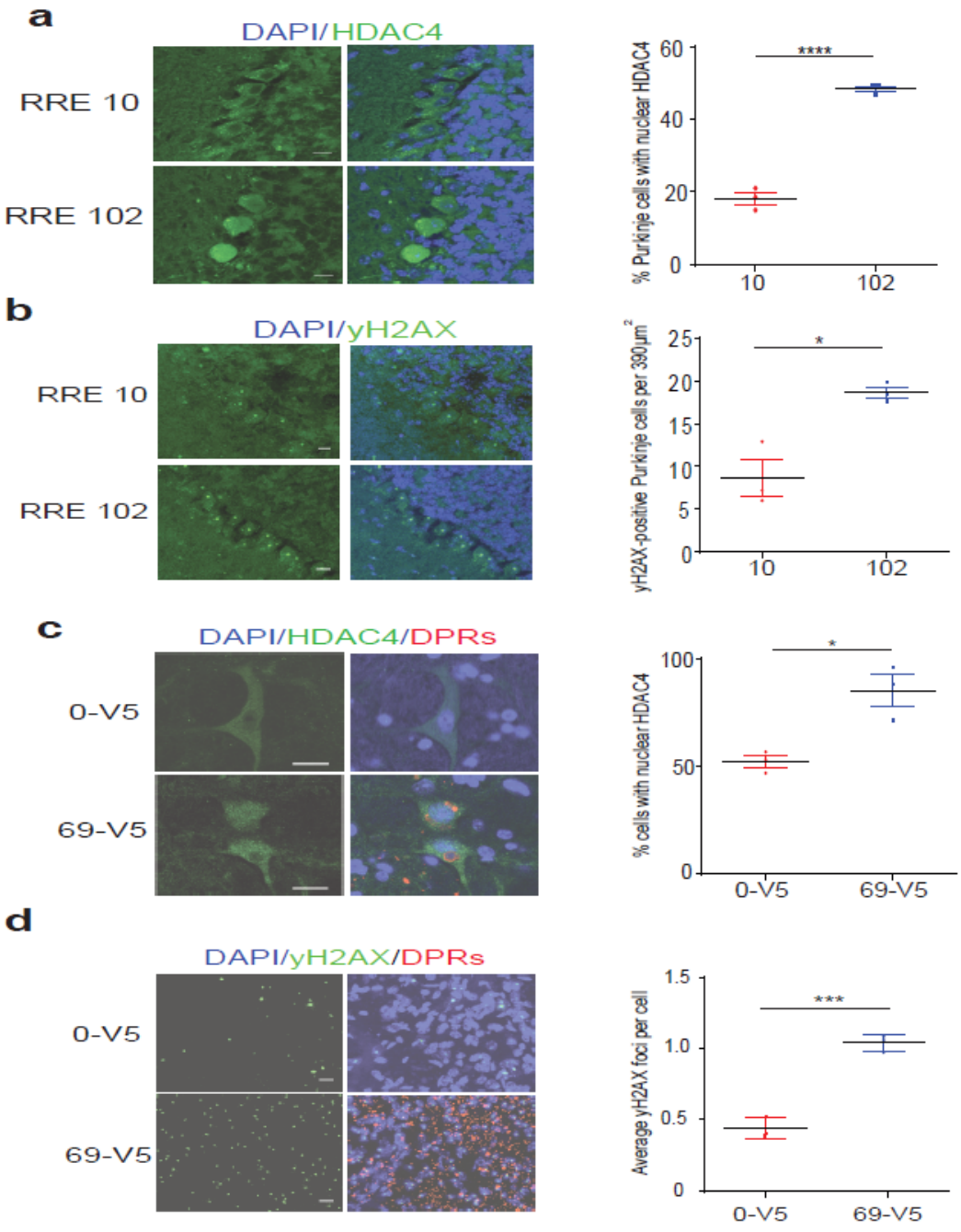

Figure 15: The expression of C9orf72 expansions or poly-GA DPRs in the murine CNS leads to DSBs and nuclear enrichment of HDAC4. (a) Cerebellar sections from mice injected with AAV9-10 or -102 RREs subjected to immunohistochemistry using anti-HDAC4 antibodies. *Left*, Representative images shown, scale bar 10μm. *Right*, the average (± SEM) percentage of Purkinje cells displaying nuclear HDAC4 was calculated for 3

animals per group, 50 Purkinje cells per animal, and analysed using a Student's t-test. **(b)** Cerebellar sections from mice injected with AAV9-10 or -102 RREs subjected to immunohistochemistry using anti- γH2AX antibodies. *Left*, Representative images shown, scale bar 10μm. *Right*, the average (± SEM) number of γH2AX-positive Purkinje cells was calculated from 3 animals per group, 10 images each, and analysed using a Student's t-test. **(c)** Brainstem sections from mice injected with AAV9-0 or -69 poly-GA DPRs were subjected to immunohistochemistry using anti-HDAC4 and anti-V5 antibodies. *Left*, Representative images shown, scale bar 10μm. *Right*, the average (± SEM) percentage of brainstem cells displaying nuclear HDAC4 was calculated for 3 animals per group, 30 HDAC4-positive cells per animal, and analysed using a Student's t-test. **(d)** Brainstem sections from mice injected with AAV9-0 or -69 poly-GA DPRs were subjected to immunohistochemistry using anti-γH2AX and anti-V5 antibodies. *Left*, Representative images shown, scale bar 10μm. *Right*, the average (± SEM) number of γH2AX foci per cell calculated from 3 animals per group, ~1000 cells per animal, and analysed using Student's t-test.

4.3.10. C9orf72-ALS patient motor neurons display elevated levels of nuclear HDAC4

Finally, we examined whether defective ATM signalling observed in human cells, mouse primary neurons and mice were also present in C9orf72-ALS patient tissues. To test this, we subjected post mortem spinal cord sections from controls and C9orf72-ALS patients to HDAC4 immunohistochemistry analyses. Consistent with our cellular and rodent data, we observed a significant increase in the percentage of motor neurons with nuclear HDAC4 staining in C9orf72-ALS sections compared to controls (Figure 16e; $P = 0.0463$), suggesting that ATM signalling was also dysregulated in C9orf72-ALS patient motor neurons.

Figure 16. C9orf72-ALS patient motor neurons display elevated levels of nuclear HDAC4

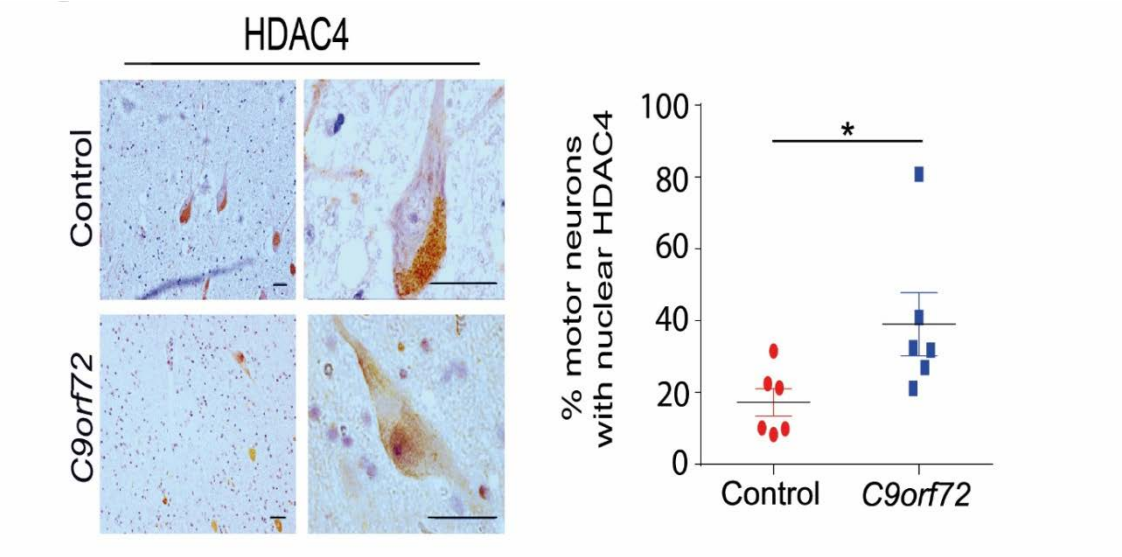

Figure 16. Spinal Cord Motor Neurons from C9orf72-ALS post-mortem show elevated levels of nuclear HDAC4. *Left*, Human spinal cord sections were analysed by immunohistochemistry using anti-HDAC4 antibodies. Representative images from 6 C9orf72 patient and 6 control sections are presented, scale bar 5 µm. *Right*, The % of motor neurons displaying HDAC4 enrichment in the nucleus was quantified from 6 C9orf72 patient and 6 control sections and is presented as average ± SEM, with ~50 cells each. Significance assessed using a Student's t-test.

4.4. Discussion

In summary, we demonstrate that human cells and rodent neurons expressing C9orf72 poly-GA DPRs and RNA repeat expansions display reduced ATM signalling. As evidence of this, we show that C9orf72 expansions and poly-GA DPRs lead to impaired pATM, 53BP1 and p-p53 repair foci (Figures 9, 10, 12c), impaired p53 phosphorylation in response to CPT (Figure 11), as well as reduced levels of pATM and 53BP1 in the chromatin fraction extracted from CPT treated cells (Figure 12d). Moreover, poly-GA mediated decreases in 53BP1 and p-p53 foci were epistatic to decreased 53BP1 and p-p53 that was induced by ATM inhibitors (Figure 12a-c), in-line with a pre-existing ATM defect in cells expressing poly-GA DPRs.

We further validated our finding using other readouts for ATM signalling that did not rely on the canonical ATM signalling pathway: We report the presence of increased TOP1ccs (Figure 13c) as well as the nuclear enrichment of HDAC4 (Figure 13a). Both of these phenomena are reported consequences of ATM dysfunction and promote neurodegeneration in mammals (Alagoz *et al.*, 2013; Li *et al.*, 2012). We validated these findings *in vivo*, demonstrating genome instability and increased HDAC4 nuclear localisation in CNS tissues from mice (Figure 15a-d) and C9orf72-ALS patients (Figure 16).

4.4.1. C9orf72 expansions and poly-GA DPRs lead to defective pATM repair foci and recruitment to chromatin

Since we observed an increase in DSBs in cells expressing C9orf72 expansions in chapter 1 (Figure 4e-h), the identification that pATM DNA repair foci were decreased in the same cells, was unexpected. This likely represents a defect in DSB repair signalling, since, even after CPT treatment, the recruitment of pATM to repair foci was severely defective (Figure 9e,f). We confirmed that pATM recruitment to damaged chromatin was defective by assessing the levels of pATM in the chromatin-bound fraction of cell lysates that had been treated with CPT. In-line with decreased pATM repair foci in cells expressing poly-GA DPRs, we similarly found that cells expressing poly-GA DPRs displayed less chromatin-bound pATM (Figure 12d). Taken together, these data demonstrate that the activation and/or the recruitment of pATM to DNA damage is defective in cells expressing C9orf72 expansions. Importantly, though, additional experimental repeats of the fractionated western blotting experiments are required in order to obtain statistical confidence in this particular

piece of data. Moreover, these experiments should be repeated with the C9orf72 RNA expansion constructs, in order to confirm the same phenomenon in this model.

4.4.2. C9orf72 expansions and poly-GA DPRs impair 53BP1 foci and p53 phosphorylation

The discovery that 53BP1 foci formation was defective in MRC5 cells expressing C9orf72 expansions and poly-GA DPRs indicated that NHEJ-mediated DSB repair was defective (Figure 10). Alike pATM foci, 53BP1 foci were not induced by CPT treatment in cells expressing C9orf72 expansions or poly-GA DPRs (Figure 10c,d). Importantly, since MRC5 cells are dividing, it is feasible that error-free HR was compensating for the observed defect in NHEJ. Crucially, primary neurons also displayed a defect in 53BP1-mediated DNA repair (Figure 10e,f). Since neuronal cells are not able to execute HR, this ultimately represents a defect in DSB repair processing.

As previously mentioned, one of the most well-documented ATM effector molecules is the tumour suppressor, p53, which is phosphorylated on serine 15 by ATM kinase activity (Bakkenist & Kastan, 2003; Canman *et al.*, 1998). In line with defective ATM signalling, CPT treatment failed to induce a significant increase in p-p53 nuclear fluorescence in cells expressing C9orf72 expansions and poly-GA DPRs. In-line with our γH2AX data, p-p53 levels were elevated in C9orf72 expansion and DPR-expressing cells endogenously. This is likely due to the influence of other PIKK family kinase members, such as ATR, which are also capable of phosphorylating p53 (Matsuoka *et al.*, 2007). Indeed, the elevated levels of p53 phosphorylation under basal conditions are synonymous with increased levels of DNA damage, which we previously demonstrated with γH2AX and neutral comet analysis (Figure 4e-h).

ATM-mediated DSB repair was confirmed to be defective in additional experiments, since 53BP1 and p-p53 foci were not further perturbed in cells expressing poly-GA DPRs by treatment with ATM inhibitors (Figure 12a-c). Taken together, we conclude that canonical ATM signalling in response to DNA damage is defective in C9orf72 RRE and poly-GA-expressing cells.

4.4.3. Non-canonical ATM signalling pathways are defective in cells expressing C9orf72 expansions and poly-GA DPRs

In addition to demonstrating the disruption of ATM-mediated DSB repair signalling, we also found evidence for defects in non-canonical forms of ATM-mediated repair, including increased topoisomerase-1 cleavage complexes (Alagoz *et al.*, 2013). Whilst this is likely the result of ATM signalling dysfunction, this result could conceivably be due to other phenomena, such as increased endogenous levels of aldehydes, which are known to induce TOP-ccs (Vaz *et al.*, 2016). This could be assessed by assessing whether TOP1-ccs are further enhanced by ATM inhibitors. Indeed, if ATM signalling disruption is the cause of elevated TOP1-ccs, then treatment with ATM inhibitors should be epistatic to the increased levels of TOP1-ccs observed in C9orf72 cells.

Additional evidence of non-canonical ATM signalling perturbations was provided by evidence that HDAC4 is aberrantly localised to the nucleus in neurons expressing poly-GA DPRs. This has previously been demonstrated in cortical neurons derived from ATM null mice, as well as in A-T patient Purkinje cells (Li *et al.*, 2012), suggesting that HDAC4 nuclear enrichment in C9orf72 cell models might be the result of reduced ATM signalling. In ATM null mice, the enrichment of HDAC4 into the nucleus was found to be the consequence of increased PP2A phosphatase activity. Critically, PP2A activity is regulated by numerous different post-translational modifications (Seshacharyulu *et al.*, 2013) and HDAC4 phosphorylation has been shown to be controlled by other kinases, such as PKC (Wu *et al.*, 2016). Thus, in C9orf72 models, it is feasible that the nuclear accumulation of HDAC4 is a consequence of other dysregulated phenomena, not necessarily ATM signalling.

4.4.4. C9orf72-related poly-GA DPRs induce heterochromatin formation, DSBs and cellular toxicity

In-line with previous reports, which demonstrated increased H3K9me3 in C9orf72-ALS samples (Belzil *et al.*, 2013), we similarly found an increase in H3K9me3 in cells expressing poly-GA DPRs by western blotting and immunocytochemistry (Figure 14a,b). We were able to reduce levels of heterochromatin by treatment with the HDAC inhibitor TSA, which also reduced DSB levels, and alleviated cellular toxicity (Figure 14b-f). The reduction of DSBs by HDAC inhibition in poly-GA cells (defective in ATM signalling) is in-line with previous work demonstrating a role for ATM signalling in the repair of heterochromatic DNA breaks

(Goodarzi *et al.*, 2008). Elegantly, HDAC1 genetic inhibition was able to compensate for the increased number of heterochromatic DSBs induced by ATM inhibitors. By this logic, it can be explained that TSA is able to reduce DSBs in poly-GA expressing cells, by reducing the demand placed upon ATM signalling. Moreover, this may represent a good drug target, since TSA treatment was able to consistently reduce cellular toxicity associated with poly-GA expression in human cells. Critically though, TSA inhibits all class I HDACs, and so it is not clear as to the mechanisms by which TSA exerts therapeutic benefit in our models. For example, previous work has implied that HDAC4 inhibition by TSA is therapeutic in mouse models of A-T (Li *et al.*, 2012). Moreover, our experimentation did not observe whether DSBs occur in heterochromatin, which is clearly a prerequisite for this explanation being correct. As such, more experiments are needed to test this model. Nonetheless, the finding that TSA reduces DSBs in poly-GA expressing cells, but not control cells, is in-line with the idea that ATM signalling is defective in cells expressing C9orf72-related poly-GA DPRs.

4.4.5. The nuclear accumulation of HDAC4 is also observed in vivo in mouse CNS sections and in C9orf72-ALS patient spinal cord motor neurons

Importantly, evidence of ATM signalling defects was also found in mice CNS tissues derived from mice injected with C9orf72 expansions or poly-GA DPRs (Figure 15). In mice expressing the longer C9orf72 expansion, the Purkinje cells were clearly enriched with nuclear HDAC4, which also occurs in A-T patients and ATM null mice strains (Li *et al.*, 2012). We observed a similar phenomenon in the brainstem of DPR-expressing mice brains (Figure 15c,d), though the Purkinje cells seldom expressed poly-GA DPRs and so we did not examine HDAC4 localisation in these cells. Importantly, these data demonstrate in the mammalian CNS, C9orf72 expansions and poly-GA DPRs lead to decreased ATM signalling.

Whilst these mouse models recapitulate our findings *in vivo*, they are still non-physiological in the sense that they are overexpression systems and artificial expression constructs. However, we also identified an increase in nuclear HDAC4 in the motor neurons of C9orf72-ALS patient spinal cord sections (Figure 16). We note that nuclear accumulation of HDAC4 could also result from other factors, such as increased activity of the inhibitor of PP2A (I2PP2A). Indeed, increase I2PP2A activity has been shown in sALS patients (Wang *et al.*, 2014). In other neurodegenerative diseases, the nuclear accumulation of HDAC4 has also been observed, and was found to be the result of decreased protein kinase C activity (Wu *et*

al., 2016). As such, whilst this data indicates that ATM signalling may be defective in C9orf72-ALS cases, more experiments are required to fully confirm this point.

A recent report demonstrated that pATM nuclear fluorescence was elevated in C9orf72-ALS spinal cord tissues (Farg et al, 2017). It is difficult to account for these data alongside our HDAC4 staining, which are both performed on the same subject material. Since this is the first published evidence of pATM staining using immunohistochemistry, it is possible that the staining is not specific for pATM. Indeed, according to the published micrographs, pATM did not form foci in these tissues (Farg *et al.*, 2017), which raises concerns about antibody specificity. Another explanation is that, since this is pan nuclear levels of pATM, ATM-mediated DSB repair is still defective, despite levels of pATM in the nucleoplasm being increased. More experimentation is required to understand the reason for these conflicting results, though since post-mortem tissues cannot be challenged or treated with inhibitors, it is particularly difficult to study signalling cascades in these sections.

The same report found an increase in 53BP1 protein levels by western blotting from whole cell lysates (Farg *et al.*, 2017). Critically, the lysis protocol used in these experiments did not extract the chromatin bound fraction of these tissues, which is where active 53BP1 (engaged in the process of DNA repair) is localised. It is therefore feasible that, in the control samples, a significant portion of 53BP1 protein is chromatin bound. In C9orf72-ALS cases, however, less chromatin bound 53BP1 may be present (based on our result that 53BP1 recruitment to chromatin is defective, Figure 12d) and thus falsely appears to be increased in their *whole-cell lysates.*

As such, it is clear that more research is required in post-mortem tissues to understand whether DSB repair is defective. An interesting experiment would be to assess whether C9orf72-ALS patient motor neurons have decreased 53BP1 repair foci. Moreover, fractionated western blotting could be used to measure chromatin bound 53BP1/pATM. Problematically, it is not possible to induce additional DNA damage in these tissues, and so it may be the case that the basal levels of 53BP1 foci is too low in control sections to observe a defect in DSB repair in ALS cases. Another important consideration for experiments using tissue homogenates is that, in the spinal cord and motor cortex of ALS samples, most of the motor neurons have already degenerated. It may be more practical therefore to use cerebellar

sections, since the cerebellum contains the highest levels of C9orf72-related pathologies (Davidson *et al.*, 2014).

4.4.6. Assessing ATM signalling in patient IPSC-derived neurons and C9orf72-BAC mouse models

In addition to further experimentation in patient tissues, future research should focus on patient IPSC-derived neuronal cultures. Indeed these cells have been shown to display elevated levels of genome instability (Lopez-Gonzalez *et al.*, 2016). It would be interesting to assess 53BP1/pATM repair foci and HDAC4 localisation in these cells, which are physiological and can be challenged with DNA damaging agents. Assessing p53 phosphorylation after DNA damage would also be interesting in this cell-type, since, alike in our DPR and RRE models, basal p-p53 levels are reported to be increased in C9orf72 patient IPSC-derived neurons (Lopez-Gonzalez *et al.*, 2016). These experiments would be a useful way to address the above disagreements in C9orf72 post-mortem tissues.

In addition to IPSC-derived neuronal cultures, ATM signalling should be assessed in phenotypic C9orf72-BAC mouse models in order to confirm these findings are true *in vivo* in a physiological context (Jiang *et al.*, 2016; Liu *et al.*, 2016). Moreover, understanding when ATM signalling becomes dysregulated in BAC mouse models (in relation to the disease progression) would be important for assessing the potential usefulness of designing therapeutic strategies that target this defect.

4.4.7. Avenues for future research

We therefore demonstrate that C9orf72 expansions or poly-GA DPRs lead to defects in ATM-coordinated DSB repair signalling. It remains unclear as to why both constructs, one encoding RNA repeats and the other encoding only DPRs, recapitulate the same finding. A feasible explanation is that the non-ATG expansion construct also produces poly-GA DPRs (Herranz-Martin *et al.*, 2017). Alternatively, this may be a general consequence of both C9orf72 RNA- and DPR- species. This could be assessed using expansion constructs which contain 5’ STOP codons (in each frame). Such constructs have been shown to abrogate DPR production (Mizielinska *et al.*, 2014), thereby isolating RNA-mediated effects from those of

DPRs. Alternatively, SRSF1 depletion could be used to reduce DPR production, and similarly isolate RNA toxicity from that of DPRs (Hautbergue *et al.*, 2017).

In addition to isolating RNA from DPR toxicity in non-ATG models, it would be interesting to repeat these experiments with cells expressing poly-GR and poly-PR DPRs, which are generally considered to be the most toxic DPR species. This is particularly important since data generated elsewhere argues that poly-PR and poly-GR DPRs *do not* have a defect in pATM focal recruitment (Farg *et al.*, 2017). In fact, this study reports increased pATM levels in cells expressing poly-PR and poly-GR DPRs. The reason for this disparity is currently unclear. One explanation is that poly-PR and poly-GR DPRs are biochemically different to poly-GA DPRs, and therefore do not impair ATM signalling. Future research should therefore aim to investigate whether ATM-mediated DSB repair is defective across all C9orf72-associated poly-DPR constructs.

4.4.8. Concluding remarks

We therefore identify defective ATM signalling as a pathological process in C9orf72-related disease models. Future research should attempt to investigate whether ATM signalling is perturbed in poly-PR and poly-GR models. The dysregulation of ATM signalling and ATM-mediated repair pathways are known to cause neurodegeneration in A-T, ATLD and SCAN-1, making our findings an attractive explanation for neurodegeneration in C9orf72-ALS/FTD. In addition, our data is an extremely attractive explanation for cases of C9orf72-linked cerebellar ataxia (Corcia *et al.*, 2016; Lindquist *et al.*, 2013).

Chapter 5: C9orf72 expansions couple defective DSB signalling to dysregulated autophagy

5.1. Introduction

5.1.1. The MRN complex induces ATM activation in response to DSBs

Mre11, Rad50 and Nbs1 form a trimeric complex known as the MRN complex, which has been shown by several researchers to be important for the activation of ATM by DSBs (Buscemi *et al.*, 2001; Girard *et al.*, 2002; Lim *et al.*, 2000; Uziel *et al.*, 2003; Yazdi *et al.*, 2002). It was initially postulated that ATM and the MRN complex were situated on the same pathway, since NBS, A-T and ATLD patients all bear remarkably similar clinical phenotypes, including radiosensitivity and genomic instability and cell-cycle checkpoint dysfunction. Girard and colleagues, as well as Uziel and colleagues, both demonstrated that serine 15 phosphorylation of p53 in response to DNA damage was defective in NBS and ATLD cells, respectively, demonstrating that ATM signalling in response to DSBs is MRN complex dependant (Girard *et al.*, 2002; Uziel *et al.*, 2003).

Berkovich *et al.* also found that Nbs1 was required for the activation of ATM, but also the recruitment of ATM to DSBs (Berkovich, Monnat, & Kastan, 2007). In-line with this, Lee & Paull found that ATM interacts with the MRN complex *in vitro* and that the presence of the MRN complex increases the kinase activity of ATM towards its substrates, p53 and Chk2, profoundly (~13-fold) (Lee & Paull, 2005).

A major breakthrough in understanding how ATM becomes activated was provided by Bakkenist & Kastan (Bakkenist & Kastan, 2003), whom demonstrate that ATM exists as an inactive dimer, but becomes monomerised by the presence of DSBs, and serine 1981 autophosphorylation was demonstrated to be critical for ATM monomerisation. In agreement with this, purified dimeric ATM does not have kinase activity, even in the presence of the MRN complex, and requires linear DNA to be activated (Lee & Paull, 2005). Thus, the MRN complex likely acts as an initial sensor for DSBs, and functions upstream of ATM to induce its activation.

5.1.2. Regulation of ATM by 53BP1/BRCA1 and RNF168

Whilst ATM activation is typically described as an upstream process in DSB repair signalling, and ATM inhibition clearly decreases 53BP1-mediated DSB repair (Figure 12b), recent evidence has demonstrated that there is a reciprocal relationship between ATM and 53BP1, whereby 53BP1 recruitment to DSBs is equally as important for ATM signalling in response to DSBs (Lee *et al.*, 2010; Noon *et al.*, 2010; Wang *et al.*, 2002). As well as 53BP1, BRCA1 has also been shown to be required for optimal ATM signalling (Kitagawa *et al.*, 2004; Lee *et al.*, 2010). The requirement of 53BP1 and/or BRCA1 for the recruitment of pATM to sites of DSBs (Kitagawa *et al.*, 2004; Noon *et al.*, 2010), suggests that the *sustained* recruitment of active ATM at sites of DSBs requires many more co-factors than just the MRN complex.

RIDDLE (Radiosensitivity, ImmunoDeficiency Dysmorphic features and LEarning difficulties) syndrome is an extremely rare genetic disorder that is caused by mutations in the gene, RNF168 (Stewart *et al.*, 2007). Its gene product is an E3 ubiquitin ligase with a well-documented function in DSB repair. Following DSB induction, the phosphorylation of γH2AX serves as a docking station for MDC1. MDC1 phosphorylation in turn facilitates the docking of RNF8, which mono-ubiquitylates H2A(X) on Lysines 13 and 15 (Huen *et al.*, 2010; Kolas *et al.*, 2007; Mailand *et al.*, 2007). This serves to recruit RNF168, another E3 ligase that amplifies the ubiquitylation signalling cascade, by further mono and poly-ubiquitylating H2A(X) (Stewart *et al.*, 2009). H2A(X) ubiquitylation thereby permits the binding and focal accumulation of BRCA1 and 53BP1 to DSBs (Ciccia & Elledge, 2010; Stewart *et al.*, 2009).

Evidently, RIDDLE cells and RNF168$^{-/-}$ mice display extremely impaired 53BP1 and BRCA1 foci (Noon *et al.*, 2010). Curiously, quiescent RIDDLE cells also display defective ATM signalling, impaired ATM foci accumulation by immunocytochemistry, and impaired ATM recruitment to chromatin by fractionated Western blotting (Noon *et al.*, 2010). This work also demonstrated that defects in ATM signalling were caused by improper 53BP1 recruitment to DNA breaks, a process that is highly dependent on RNF168 activity, since siRNA to 53BP1 led to similar defects in pATM accumulation to foci/chromatin (Noon *et al.*, 2010). These data suggest that sustained ATM signalling at sites of DSBs is highly dependent on the function of downstream effector proteins, including 53BP1 and RNF168.

These data appear paradoxical, since, canonically, ATM activation and recruitment to DNA breaks is upstream and independent of 53BP1 and RNF168 recruitment. To account for these data, ATM signalling in response to DSBs is now viewed to occur in at least two separate waves: An initial wave that is mediated by interactions with Nbs1, and a secondary wave that is RNF168-dependant and mediated by 53BP1 (and perhaps BRCA1 in some cases).

5.1.3. ATM activation in the absence of DSBs

In addition to its activation by DNA damage, ATM can also be activated by changes in the chromatin structure. This was first reported in seminal work by Bakkenist and Kastan (Bakkenist & Kastan, 2003). Here, it was shown that chloroquine, a DNA intercalating agent, or low salt conditions were able to phosphorylate and monomerise ATM to the same extent as ionising radiation. Since chloroquine and low salt conditions did not induce any DNA breaks, as measured by γH2AX foci, this data suggests that ATM can be activated in the absence of DSBs by the presence of relaxed chromatin.

Interestingly, it has been shown that the activation of ATM by chloroquine leads to its association with ATMIN (ATM interacting) (Kanu & Behrens, 2007). ATMIN depletion led to a decrease in chloroquine-mediated p53 activation, suggesting that ATMIN induces ATM activity after cellular stressors that do not induce DSBs. These data were consistent with previous reports, which linked ATM activation to chromatin relaxation (Bakkenist & Kastan, 2003).

As well as in response to chromatin modulating drugs, non-canonical ATM activation has been observed following oxidation (in the absence of the MRN complex and DSBs). Elegantly, ATM activation in response to oxidative stress occurs by the detection of oxidative disulfide cross-links occurring directly between two ATM dimers (Guo *et al.*, 2010). A key cysteine residue on each ATM molecule was shown to be required for this phenomenon, and mutation of this domain results in abrogation of this pathway. To date, little is known about the biological significance of this signalling pathway. Given that ROS handling is central to CNS health, and given that ROS-induced DNA damage has been reported in C9orf72 models (Lopez-Gonzalez *et al.*, 2016), it is likely that ROS-induced ATM signalling is important in neurodegenerative disease and may be defective in C9orf72-associated disease. Distinct mechanisms of ATM activation are summarised in Figure 17.

Remarkably, further evidence of non-canonical ATM signalling pathways have been identified. Tresini and colleagues demonstrate that ATM activation is induced by the presence of R-loops, which can be induced by UV irradiation or RNASE H1/H2 depletion (Tresini *et al.*, 2015). In response to UV radiation, RNASE H1/2 depletion, or CPT treatment, the late spliceosome components U2 and U5 were mobilised (displaced), leading to intron retention. Curiously, ATM activation in response to UV radiation or RNASE H1/2 depletion was shown to be dependent on spliceosome mobility (Tresini *et al.*, 2015). More curiously, ATM signalling was also shown to enhance spliceosome displacement signalling transduction (but was not necessary for its initiation). Counter-intuitively, ATM signalling functions to promote intronic retention, since treatment with ATM inhibitors increases splicing fidelity in the presence of UV radiation or RNASE H1/2 depletion (Tresini *et al.*, 2015). Whilst the biological function of this non-canonical ATM signalling pathway is unknown, it is tempting to speculate that such events occur in order to facilitate R-loop resolution. As such, cells might sacrifice splicing fidelity in order to overcome a more dangerous threat - R-loop-mediated genome instability. It should be noted, however, that ATM signalling has not yet been implicated in the process of R-loop resolution.

Figure 17. Mechanisms of ATM activation

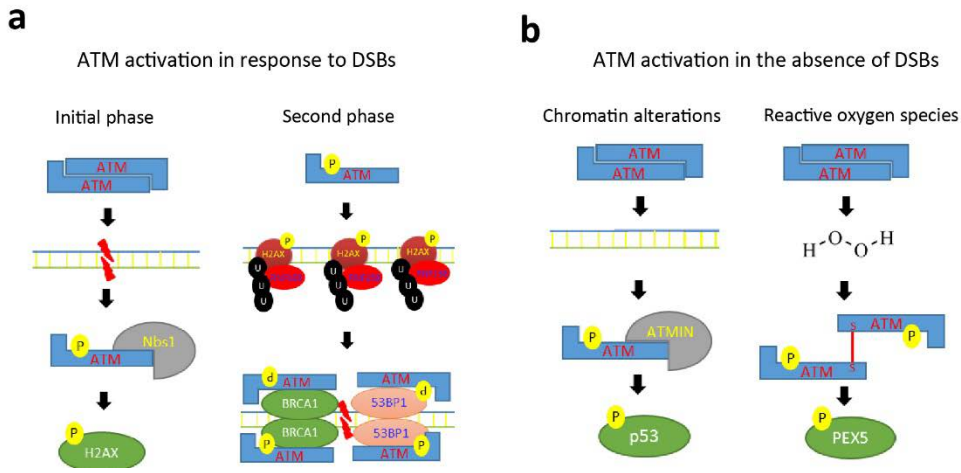

Figure 17. Mechanisms of ATM activation. (a) *Left*, initially, ATM is activated following double-stranded DNA breaks by the focal accumulation of the MRN complex, leading to ATM-Nbs1 interactions and ATM phosphorylation. Amongst other things, this promotes H2AX phosphorylation by ATM. *Right*, in addition to MRN complex-mediated activation of ATM, sustained ATM activation at sites of DSBs is dependent on the focal accumulation of 53BP1 or BRCA1, which are recruited to DSB sites by RNF168-mediated H2A(X) ubiquitylation. Thus, ATM signalling is also dependent upon "down-stream" effector proteins, RNF168, 53BP1 and BRCA1 **(b)** *Left*, **i**n the absence of DNA damage, ATM dimer dissociation and activation can be induced by chloroquine or hypotonic solutions, which lead to altered chromatin states. This form of ATM activation involves ATMIN, as opposed to Nbs1, interactions. *Right*, reactive oxygen species, such as hydrogen peroxide, can induce ATM activation directly, by promoting the formation of disulphide bridges on a key cysteine residue on the ATM molecule. This form of ATM activation has been shown to promote peroxisomal biogenesis factor 5 (PEX5) phosphorylation, which induces pexophagy. Adapted from (Kanu & Behrens, 2007).

5.1.4. Autophagy regulates the DNA damage response

Autophagy is a process by which unwanted cytoplasmic phenomena are targeted to lysosomes for their degradation (Klionsky, 2007; Mizushima, Yoshimori, & Ohsumi, 2011). In response to cellular stress, including DNA damage (Eapen *et al.*, 2017; Eliopoulos *et al.*, 2016), autophagic processing is increased in order to remove harmful cytoplasmic components but also to maintain energy balance in the cell (Green & Levine, 2014; Mizushima & Komatsu, 2011). Though autophagy is generally considered to be non-selective, there is accumulated evidence that the process of selective autophagy is used to clear proteins or organelles in a specific manner (Stolz *et al.*, 2014).

5.1.5. P62 regulates DSB repair

P62/SQSTM1 (herein P62) is a protein with ubiquitin and LC3-binding capacity, and has been implicated in the process of selective autophagy and signal transduction (Ichimura *et al.*, 2008; Pankiv *et al.*, 2007) (Summarised in Figure 18). Work in mice and Drosophila have demonstrated that P62 is required for the clearance of ubiquitinated cytosolic aggregates, and that ubiquitylated substrates are a requisite for p62-mediated selective autophagy (Komatsu *et al.*, 2007; Nezis *et al.*, 2008). Interestingly, in ALS patients, p62 accumulates in CNS sections (Davidson *et al.*, 2014; Mann *et al.*, 2013), suggesting a dysregulation of autophagic processing occurs during the disease.

Recently, a seminal discovery demonstrated that the nuclear accumulation of the ALS-associated protein, p62, functions in the nucleus as a regulator of the DSB repair signalling (Wang *et al.*, 2016). Initially, it was discovered using immunofluorescence microscopy that p62 depletion leads to increased levels of ubiquitylated protein foci in the nucleus of human cells. Furthermore, the opposing effect was found by p62 overexpression, which was also shown to impair H2A ubiquitylation on lysine 13 and 15 (Wang *et al.*, 2016). P62 overexpression also prevented 53BP1 and BRCA1 focal accumulation in response to DNA lesions. These findings could be recapitulated using the autophagy inhibitor, 3-methyladenine (3-MA). Importantly, 3-MA did not induce DSB repair defects in p62 depleted cells, suggesting that 3-MA leads to increased p62 accumulation due to defective autophagic clearance, which then leads to DSB repair inhibition (Wang *et al.*, 2016). The chemical inhibition of DNA repair by 3-MA is thought to be mediated by the nuclear accumulation of

p62, since the overexpression of p62 mutants lacking the NLS motifs, or the overexpression of other key autophagy proteins, does not impair DNA repair signalling.

Biochemical assays demonstrated that p62 was capable of binding to RNF168 (Wang *et al.*, 2016), an E3 ubiquitin ligase that functions upstream of 53BP1 and BRCA1, to recruit them to DNA breaks (Stewart, 2009). Importantly p62-mediated defects in H2A(X) ubiquitylation were partly restored by RNF168 overexpression and were epistatic with RNF168 but not RNF8 depletion. P62 was shown to bind the MIU (motif interacting with ubiquitin) domain of RNF168, which is the domain that mediates RNF168 E3 ligase activity. Evidently, deletion of this domain prevented its association with p62 (Wang *et al.*, 2016). Moreover, the LIM-binding (LB) domain of p62 (residues 170-220) was shown to promote RNF168 binding and inhibition, since deletion of this domain similarly prevented its association with RNF168 and led to normal DSB repair signalling. This is promising since the LM domain of p62 is likely to be redundant for p62-mediated autophagy and for p62-mediated signalling cascades. In-line with this idea, other animals, such as the zebrafish and Drosophila, do not possess this domain in p62, implying that it may be dispensable for the function of p62 in autophagy. These data demonstrate that p62 interacts with and controls the DNA damage response via non-canonical interactions with RNF168.

In-line with an important role for the LB domain in DSB repair, the overexpression of p62-WT, but not p62 lacking the LB domain, led to radiosensitivity in human tumours (Wang *et al.*, 2016). Excitingly to the field of ALS, p62 accumulation is a disease hallmark (Al-Sarraj *et al.*, 2011; Troakes *et al.*, 2012). Moreover, p62 proteinopathy is known to be particularly elevated in C9orf72-ALS/FTD, when compared to sporadic disease forms (Troakes *et al.*, 2012). Since ATM signalling is dependent on functional RNF168 and 53BP1 (Noon *et al.*, 2010), ATM signalling defects may also arise as a consequence of p62 accumulation.

Figure 18. Structure of the P62 protein

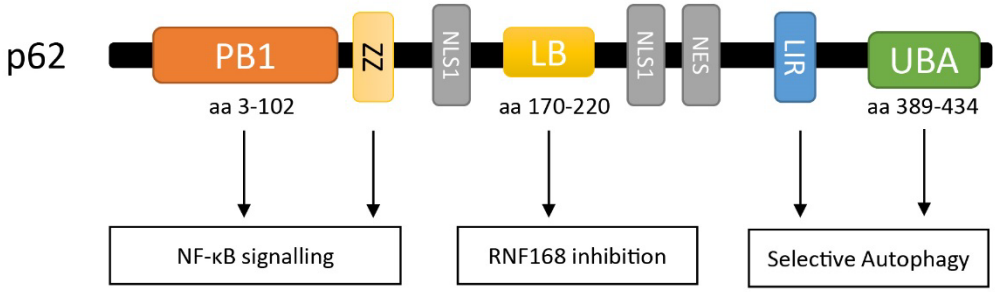

Figure 18. Key domains of the p62 protein and their cellular functions. The Phox1 and Bem1p (PB1) domain of p62 can oligomerise with other proteins containing this domain, such as Next to BRCA1 1 (Nbr1). Atypical protein kinase C also interacts with the PB1 domain of p62, whilst Receptor-interacting protein (RIP) interacts with the zinc finger (ZZ) domain, both of which are likely involved with The Nuclear Factor NF-κB (NF-κB) signalling. The LIM-binding (LB) domain of p62 has recently been shown to interact with and inhibit the E3 ubiquitin ligase, RNF168. This leads to defective histone ubiquitylation and DSB repair defects. The ubiquitin-associated (UBA) domain of p62 binds to poly-ubiquitylated proteins, whilst the LC3-interacting region (LIR) domain interacts with the Microtubule-associated protein 1A/1B-light chain 3 (LC3). Thus, the UBA and LIR domains of p62 are involved in the process of selective autophagy. Adapted from (Katsuragi *et al.*, 2015).

5.2. Aims and Hypothesis:

The principle aim of this chapter is to understand why ATM-mediated DNA repair is defective and to attempt to restore ATM signalling in C9orf72 disease models. In addition, we aim to investigate other aspects of ATM signalling, such as whether ATM is responsive to chromatin modulating drugs like chloroquine. We hypothesise that if ATM signalling is specific to DSBs, then other ATM signalling pathways should be functional.

5.3. Results

5.3.1. Nbs1 foci accumulation is not defective in poly-GA expressing cells

In response to DNA damage, ATM signalling is mediated by the Mre11–Rad50–Nbs1 (MRN) complex, which forms foci at sites of DSBs, facilitating interactions between ATM and Nbs1 and thereby enhancing ATM phosphorylation (Williams & Tainer, 2007). Thus, we speculated that defective ATM signalling might be a consequence of upstream Nbs1 disruption. In contrast to 53BP1 and pATM, Nbs1 foci formed normally in cells expressing poly-GA DPRs (Figure 19a). Similar to γH2AX, expression of 69 poly-GA DPRs led to an increase in Nbs1 foci formation (Figure 19a; $p = 0.001$). These data argue against the failure of Nbs1 recruitment as a cause for the C9orf72-related ATM defect.

Ub-H2A foci and protein levels are reduced in poly-GA expressing cells

Central to efficient ATM-mediated signalling is a cascade of post-translational histone modifications required for efficient and sustained DSB repair (Paull, 2015). Part of this cascade is the ubiquitylation of histone H2A by the E3 ubiquitin ligase RNF168, which plays an important role in the recruitment of 53BP1 to DSBs. Notably, RNF168-mediated H2A ubiquitylation and subsequent 53BP1 recruitment has also been shown to maintain efficient ATM signalling (Noon *et al.*, 2010). We thus examined whether *C9orf72* expansions would impact H2A ubiquitylation, which could explain the observed ATM signalling defect. Consistent with previous reports, western blot analyses using H2A-specific antibodies revealed multiple ubiquitylated species (Figure 19b). The extent of H2A ubiquitylation, however, was attenuated in cells expressing poly-GA DPRs, which showed ~2-fold less H2A ubiquitylation in comparison to controls (Figure 19b; $p = 0.0042$). Consistent with the western blotting data, immunostaining with ubiquitylated H2A (ub-H2A) antibodies also revealed reduced levels of ub-H2A foci in cells expressing 69 poly-GA DPRs when compared to control cells (Figure 19c, $p = 0.013$). Notably, although DPR-positive cells

exhibited fewer ub-H2A foci, we noticed co-localization between DPRs and ub-H2A (Figure 19c).

5.3.2. RNF168 overexpression rescues 53BP1 and pATM nuclear foci

Since RNF168 is the key ubiquitin ligase driving H2A ubiquitylation (Stewart *et al.*, 2009), we wondered whether the defective ATM signalling was due to the decreased availability of RNF168. Consistent with this idea, increasing the pool of RNF168 by overexpression of GFP-RNF168 in cells expressing poly-GA DPRs restored 53BP1 (Figure 19d, $p = 0.0003$) and increased pATM (Figure 19e, $p = 0.006$) foci formation. Moreover, these experiments revealed that RNF168 was also sequestered into DPRs (Figure 19d, arrowhead), explaining the observed co-localization between DPRs and ub-H2A.

5.3.3. P62 depletion similarly restores 53BP1 and pATM nuclear foci

Inspired by a recent seminal report showing that an ALS-associated autophagy protein, p62, perturbs RNF168 function and impairs H2A ubiquitylation-mediated DNA repair (Wang *et al.*, 2016), we wondered whether the defective ATM signalling in C9orf72 models could result from a p62-mediated attenuation of H2A ubiquitylation. This hypothesis was particularly attractive since p62 accumulation is a hallmark pathology of C9orf72-related disease. If this is true, we predicted that depletion of p62 in cells expressing poly-GA DPRs would recapitulate the effect of RNF168 overexpression. Indeed, p62 depletion with siRNA (Figure 19f) led to restoration of 53BP1 (Figure 19g; $p = 0.047$) and pATM (Figure 19h; $p = 0.003$) foci. These data are fully in line with reports that p62 accumulation impairs RNF168-mediated H2A ubiquitylation (Wang *et al.*, 2016) and with studies that highlight the role of H2A ubiquitylation in ATM signalling (Noon *et al.*, 2010).

5.3.4. P62 depletion leads to reduced R-loops and reduced DSBs

Since p62 depletion was able to restore DSB repair foci, we wondered whether this would also be able to reduce DSB levels, as measured by γH2AX foci. As expected, the restoration of ATM-mediated repair in DPR expressing cells by p62 depletion suppressed the number of DSBs (Figure 19i; $P = 0.029$) and the aberrant accumulation of R-loops (Figure 19j; $P = 0.037$). The latter is consistent with the recently reported reciprocal functional interaction between R-loops and ATM signalling (Tresini *et al.*, 2015).

5.3.5. ATM activation by chloroquine is not defective

In addition to DNA damage, ATM can also be activated in the absence of DNA damage by the drug chloroquine, a DNA intercalating agent (Bakkenist & Kastan, 2003). Since the accumulation of P62 and inhibition of H2A ubiquitylation led to dysfunctional ATM signalling in C9orf72 cells, we reasoned that ATM activation by chloroquine, which is not linked to sensing DNA damage, would not be defective. Thus, we tested whether chloroquine-induced chromatin relaxation could restore ATM signalling in DPR-positive cells. As predicted, whilst DPR-positive cells did not display any ATM phosphorylation under normal conditions, chloroquine treatment led to pan-nuclear ATM phosphorylation (Figure 20a; $p = 0.004$), indicating that DPR-positive cells were indeed responsive to chloroquine and, consequently, able to activate ATM. To test whether the ensuing ATM signalling was restored by chloroquine treatment in bona fide primary neuronal cells, we next examined the localization of HDAC4, which we demonstrated above is localized to the nucleus of neurons expressing DPRs. As predicted, whilst DPR-positive neurons displayed nuclear HDAC4, the addition of chloroquine led to HDAC4 being relocalized to the cytoplasm (Figure 20b). Whilst only ~40% of DPR-positive neurons displayed cytoplasmic HDAC4 without chloroquine treatment, the number of neurons with cytoplasmic HDAC4 increased to almost 100% after cell treatment with chloroquine (Figure 20b; $p = 0.014$). These data demonstrate that ATM can be activated by inducing chromatin relaxation and are consistent with our previous data linking dysfunctional ATM signalling to a defect in histone ubiquitylation.

5.3.6. R-loop-mediated genome instability is distinguishable from genomic instability caused by DSB repair defects

The above data suggest that p62 accumulation and the consequential defect in ATM signalling act together with expansion-driven R-loops to trigger genome instability, though it is not clear whether they constitute distinct or epistatic pathways. To address this question, we examined whether SETX overexpression would further suppress the elevated level of DSBs in P62-depleted cells. Consistent with our previous data, overexpression of SETX or depletion of P62 was capable of reducing γH2AX foci in DPR-positive cells (Figure 19k; $p = 0.0013$ and $p = 0.0146$, respectively). However, the concomitant overexpression of SETX and depletion of P62 further reduced DSB levels compared to levels observed by SETX overexpression or P62 depletion alone (Figure 19k; $p = 0.0433$ and $p = 0.0045$, respectively)

Together, these data identify two separate pathways that drive genome instability in C9orf72 poly-GA expressing cells: One is driven by P62 accumulation, defective H2A ubiquitylation and the subsequent ATM signalling defect; the other is driven by repeat-associated R-loop accumulation (Figure 21). Whilst the two pathways are distinct, crosstalk does exist, due to the reciprocal functional interaction between R-loops and ATM signalling (Tresini *et al.*, 2015).

Figure 19. Defective ATM-mediated DNA repair can be restored by RNF168 overexpression or p62 depletion.

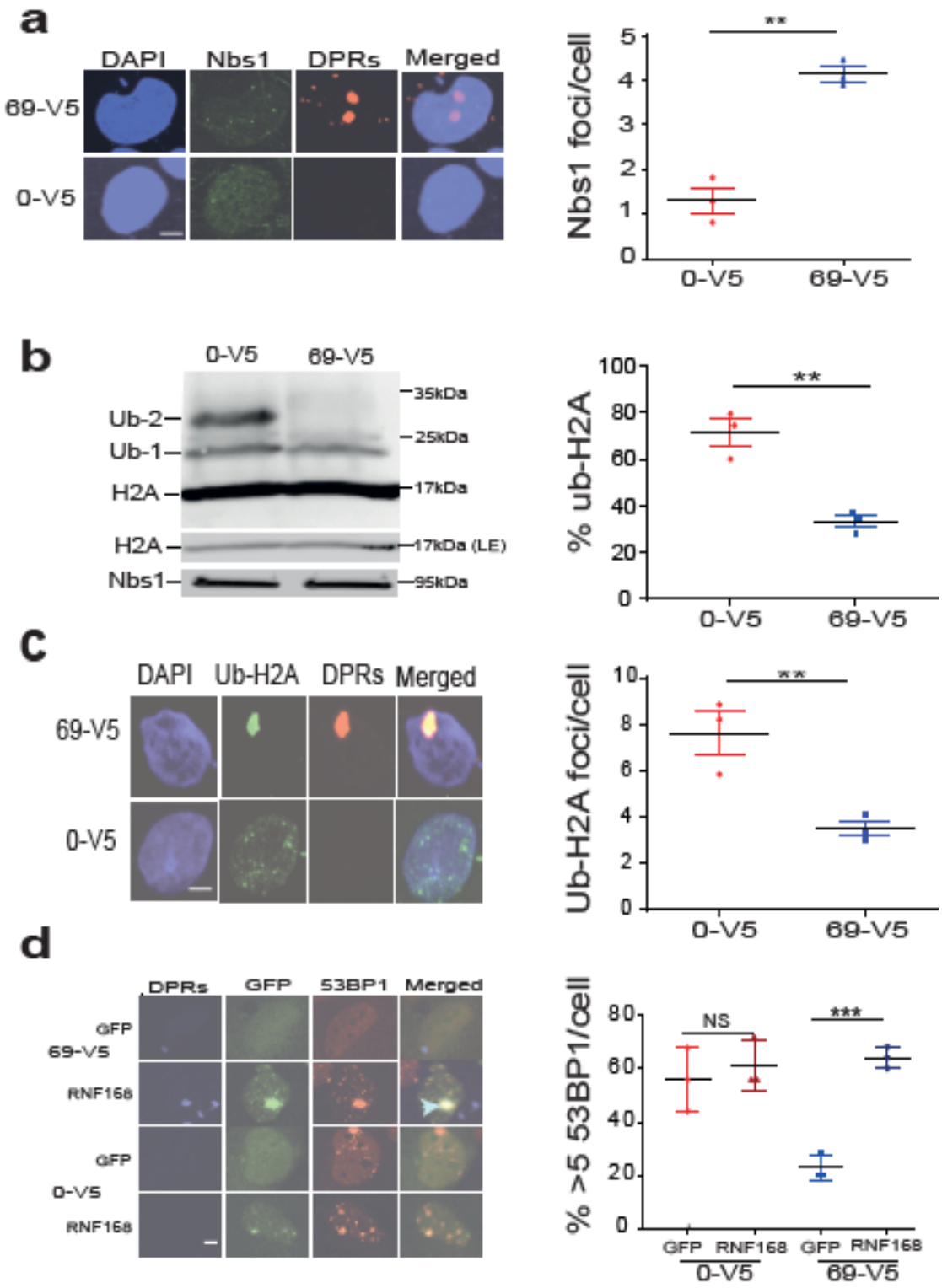

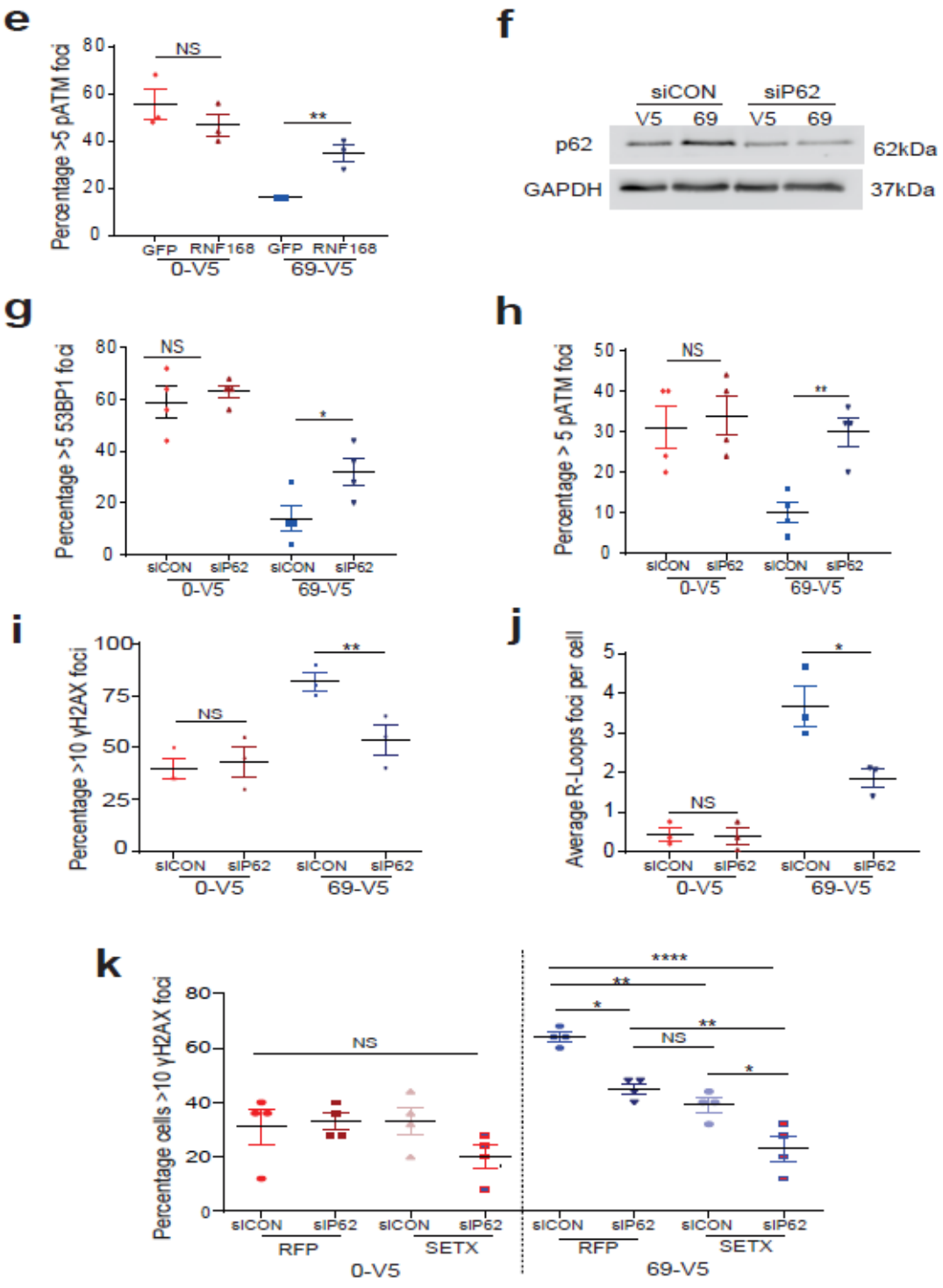

Figure 19: Defective ATM-mediated DNA repair can be restored by RNF168 overexpression or p62 depletion. (a) MRC5 cells transfected with 0 or 69 DPRs, and immunostained with anti-V5 'DPRs' and anti-Nbs1 antibodies. *Left*, Representative images are shown, scale bar 5µm. *Right*, the average (± SEM) number of Nbs1 foci per cell was quantified from 3 cell culture replicates, 50 cells each, and analysed using a Student's t-test. **(b)** *Left*, Chromatin fractions from MRC5 cells transfected with 0 or 69 DPRs analysed with Western blotting using antibodies specific to H2A. Low exposure (LE) H2A and Nbs1 bands show equal loading. *Right*, the average (± SEM) percentage of H2A that was ubiquitylated was quantified from 3 cell culture replicates and analysed using Student's t-test. **(c)** *Left*, MRC5 cells transfected with constructs encoding 0 or 69 DPRs, and immunostained with anti-V5 'DPRs' and anti-Ubiquinated-H2A 'Ub-H2A' antibodies.

Representative images are shown, scale bar 5μm. *Right*, Ub-H2A foci were quantified, 25 cells each, presented and analysed as described for (a). **(d)** MRC5 cells transfected with constructs encoding 0 or 69 DPRs, and with control-GFP or RNF168-GFP, were immunostained with anti-V5 and anti-53BP1 antibodies. Left, Representative images are shown. Right, the percentage of cells with 5 or more 53BP1 foci was quantified (25 cells each), presented, and analysed as described for (a). **(e)** MRC5 cells transfected with constructs encoding 0 or 69 DPRs, and with control-GFP or RNF168-GFP plasmids, were immunostained with anti-V5 and anti-pATM antibodies. The percentage of cells with 5 or more pATM foci was quantified (25 cells each), presented and analysed as described for (a). **(f)** MRC5 cells transfected with constructs encoding 0 or 69 DPRs, with either control siRNA particles or p62 siRNA particles, were analysed with western blotting using antibodies specific to p62 and GAPDH. **(g)** MRC5 cells transfected with constructs encoding 0 or 69 DPRs, and with control siRNA particles or p62 siRNA particles, were immunostained with anti-V5 and anti-53BP1 antibodies. The percentage of cells with 5 or more 53BP1 foci was quantified from 4 cell culture replications (25 cells each), presented and analysed as described for (a). **(h)** MRC5 cells transfected with constructs encoding 0 or 69 DPRs, and with control siRNA particles or p62 siRNA particles, were immunostained with anti-V5 and anti-pATM antibodies. The percentage of cells with 5 or more pATM foci were quantified from 4 cell culture replicates (25 cells each), presented and analysed as described for (a). **(i)** MRC5 cells transfected with constructs encoding 0 or 69 DPRs, with control siRNA particles or p62 siRNA particles. Cells were immunostained with anti-V5 'DPRs' and anti--γH2AX antibodies. The percentage of cells with 10 or more γH2AX foci was quantified (25 cells each), presented, and analysed as described for (a). **(j)** MRC5 cells transfected with constructs encoding 0 or 69 DPRs, with control siRNA particles or p62 siRNA particles, were immunostained with anti-V5 'DPRs' and anti—S9.6 antibodies. R-Loop foci were quantified, presented and analysed as described for (a). **(k)** MRC5 cells transduced with adenoviral vectors encoding for SETX or RFP, transfected with constructs encoding 0 or 69 DPRs, with control siRNA or p62 siRNA particles, were immunostained with anti-V5 and anti--γH2AX antibodies. Nuclei were counterstained with DAPI. The average (± SEM) percentage of cells with 10 or more γH2AX foci was quantified from 4 cell culture replicates (25 cells each), and analysed using a one-way ANOVA.

Figure 20. ATM activation by chloroquine is not defective in cells expressing poly-GA DPRs

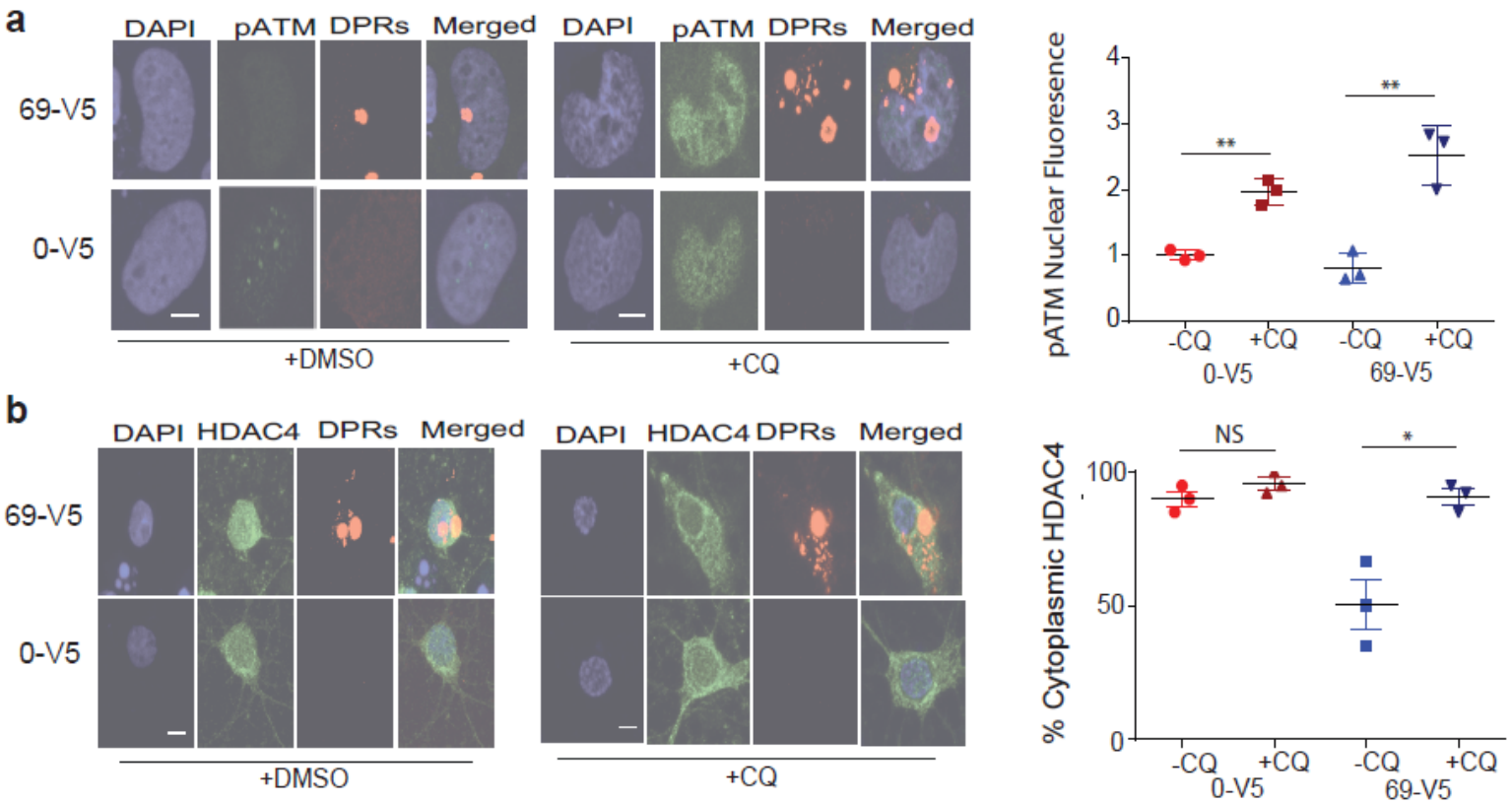

Figure 20: Chloroquine, a DNA intercalating agent, increases ATM activation and restores cytoplasmic HDAC4 localisation in DPR-expressing cells. (a) *Left*, MRC5 cells were transfected with constructs encoding 0 or 69 repeat GA dipeptides. 48 hours post transfection, cells were treated with chloroquine (320µg/ml) '+CQ' or DMSO '+DMSO' for 4 hours. Subsequently, cells were immunostained with anti-V5 'DPRs' and anti-ATM 'pATM' antibodies. Nuclei were counterstained with DAPI and representative images of 3 biological replicates are shown, scale bar 5µm. *Right*, Nuclear fluorescence intensity was quantified and data presented as the average ± SEM from 3 biological repeats, 25 cells each. Significance was assessed using a Student's t-test. **(b)** *Left*, Rat cortical neurons (5 DIV) were transduced with a AAV9-viral vector construct expressing V5-epitope tagged Gly-Ala 0 or 69 DPRs, and analysed by immunocytochemistry using anti V5 'DPRs' and an anti-HDAC4 antibodies. 7 days post transduction, cells were treated with chloroquine (320µg/ml) '+CQ' or DMSO '+DMSO' for 4 hours. Nuclei were counterstained with DAPI and representative images are shown, scale bar 5µm. *Right*, The % of cultured cortical neurons exhibiting cytoplasmic HDAC4 staining was quantified from 3 biological replicates, each replicate containing 20 cultured cortical cells and presented as average ± SEM. Significance was assessed using a Student's t-test.

Figure 21. Model describing how C9orf72 expansions cause genomic instability.

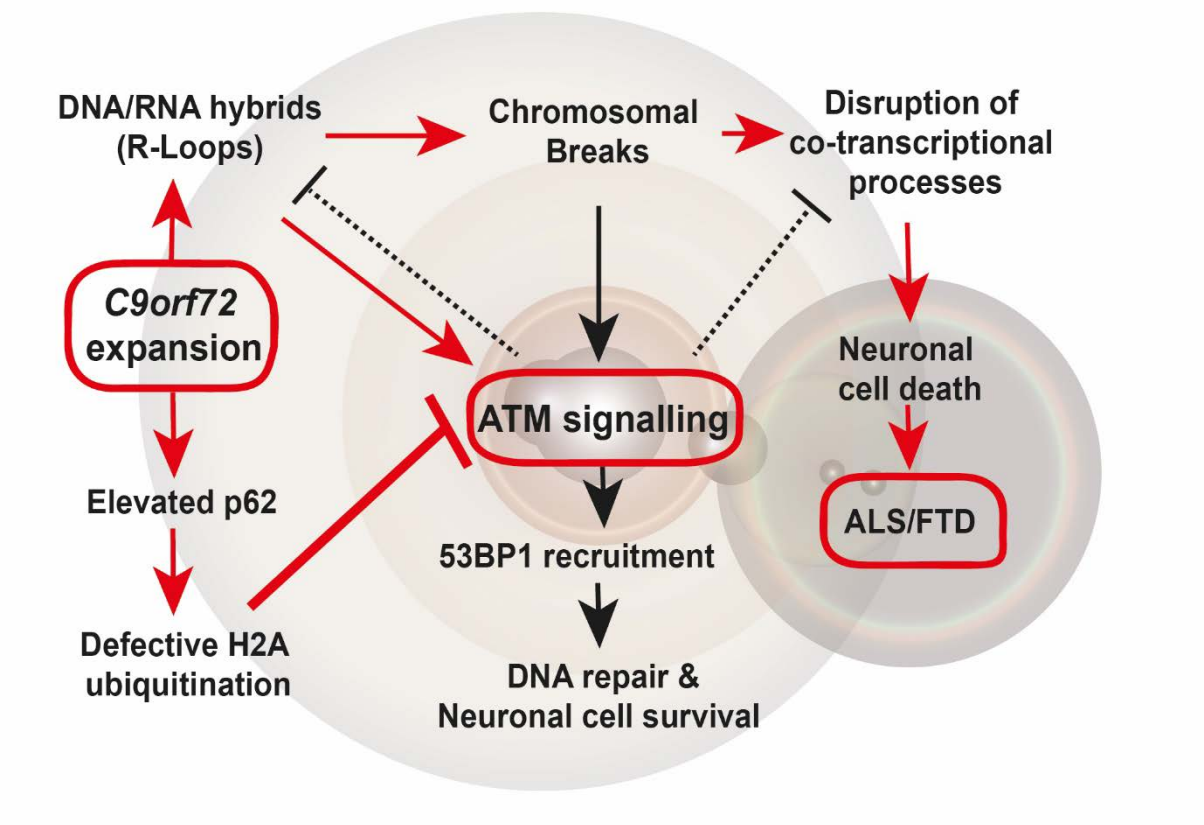

Figure 21: Model describing how C9orf72 expansions cause genomic instability. Transcription of C9orf72 repeat expansions causes elevated R-loop levels, leading to chromosomal breaks. Concomitantly, C9orf72 expansions cause the hallmark accumulation of p62, which inhibits H2A ubiquitination, and disrupts ATM signalling. Defective ATM signalling prevents 53BP1-mediated DNA repair, exacerbating the genomic instability driven by R-loops. R-loops and defective ATM signalling are distinguishable, yet interlinked, pathways that contribute to genome instability, leading to the disruption of co-transcriptional processing, and, ultimately, neuronal cell death in ALS/FTD. (Walker *et al.*, 2017).

5.4. Discussion

Expression of C9orf72-related poly-GA DPRs leads to defective ATM-mediated DSB signalling (Figure 9-16). In this chapter, we demonstrate that defective DNA repair is due to the accumulation of p62 (Figure 19g,h), which leads to defective H2A ubiquitylation (Figure 19b,c). The defect is likely due to p62-mediated RNF168 sequestration, since defective DSB repair can also be resolved by RNF168 overexpression (Figure 19d,e). These data can explain why pATM and 53BP1, but not Nbs1, are defective (Figure 19a-c). Moreover, activation of ATM by chloroquine, which does not require DSB repair signalling cascades (Bakkenist & Kastan, 2003; Kanu & Behrens, 2007), is normal (Figure 20), and is fully in-line with this model.

5.4.1. P62 inhibits the DNA damage response in C9orf72-ALS models

In-line with previous reports, which demonstrated a role for p62 in regulating histone ubiquitination by inhibiting RNF168 (Wang *et al.*, 2016), p62 accumulation in cells expressing C9orf72-related poly-GA DPRs was shown to impair 53BP1 and pATM foci accumulation (Figure 19g,h). Moreover, RNF168 overexpression recapitulated the same effect, which supports a model in which a balance between RNF168 and p62 protein levels mediate DSB repair signalling (Figure 19d,e). In future experiments, the epistasis between p62 depletion and RNF168 overexpression should be assessed, using γH2AX or the neutral COMET assay as a readout of genomic instability.

Whilst p62 depletion was able to partially rescue 53BP1 foci (Figure 19g), RNF168 overexpression was able to fully rescue 53BP1 foci (Figure 19d). A likely explanation for this difference is that there may still be an increase in p62 protein in cells expressing poly-GA DPRs after siRNA transfection. Though our western blotting analysis does not appear to suggest this, it is possible that the remaining p62 resides in the insoluble fraction. Using CRISPR/Cas9 technology, future experiments should aim to reassess 53BP1 and pATM foci levels after poly-GA expression, in cells that are $p62^{-/-}$, which would overcome the issue with siRNA-mediated knock-down. P62 knock-out human cells are viable since they have been used previously (Wang *et al.*, 2016).

In addition to measuring pATM, 53BP1 and γH2AX foci, which were the main readouts of DSB repair used in this study, future experiments should assess whether p-p53 signalling is

restored by p62 depletion/deletion. In addition, non-canonical forms of ATM signalling, such as the nuclear accumulation of HDAC4 and the accumulation of TOP1-ccs, should be assessed after p62 depletion/deletion and RNF168 overexpression.

As mentioned previously, other reports have indicated that poly-PR and poly-GR DPRs do not induce ATM signalling defects (Farg *et al.*, 2017). It may be explained that poly-PR and poly-GR do not induce ATM signalling defects because they are not substrates for p62-mediated selective autophagy, and hence do not induce p62 accumulation. Indeed, defective autophagy is not reported to be associated with poly-PR or poly-GR DPR expression. Thus, in future work, research should assess whether poly-PR and poly-GR DPRs induce elevated levels of p62, and whether this has any notable effect on DSB repair signalling.

5.4.2. P62 depletion reduces R-loops

Unexpectedly, p62 depletion was also shown to decrease R-loop foci in cells expressing C9orf72 poly-GA DPRs (Figure 19j). This could be due to the reciprocal relationship between R-loop accumulation and ATM signalling, described recently (Tresini *et al.*, 2015). These data may suggest that ATM signalling helps to resolve R-loops or prevent R-loop accumulation. Alternatively, it may imply a role for H2A ubiquitylation by RNF168 in regulating R-loop homeostasis. In addition, this result could be explained by the reciprocal relationship between R-loops and DNA breaks: Since DNA lesions obstruct RNA polymerase elongation, it is possible that the reduced DSB levels (Figure 19i) prevents polymerase pausing/stalling, and thereby reduce R-loop levels indirectly. A fourth, less likely option, is that p62 accumulation directly induces R-loops via an unknown mechanism.

Future research should therefore aim to understand why p62 depletion appears to prevent R-loop accumulation in C9orf72 poly-GA expressing cells. One experiment would be to repeat this experiment in the presence of an ATM inhibitor, which would determine whether this finding is due to the restoration of ATM signalling. Problematically, this would not determine whether this finding is related directly to ATM, since ATM inhibition will also impair RNF168 (as well as many other DSB effector proteins).

5.4.3. R-loop- and p62-mediated DNA damage are distinct

As well as reducing R-loop levels, p62 depletion also reduced DSBs, as measured by γH2AX foci (Figure 19i). The result is likely due to the restoration of DSB repair signalling, but may also reflect the above finding that p62 depletion can also reduce R-loop levels (Figure 19j). Moreover, SETX overexpression reduced DSB levels, as previously demonstrated in chapter 1. Interestingly, SETX overexpression was able to further reduce DSB levels in poly-GA expressing cells that were depleted of p62, suggesting that R-loop-driven DSBs occur via a separate mechanism to p62-driven DSBs (Figure 19k).

Whilst this is an attractive hypothesis, it is not clear whether this result simply reflects the fact, that p62 is only depleted and may still be increased in cells expressing poly-GA DPRs. Thus, the additional effect of SETX overexpression may be because p62-mediated genomic instability is not fully ablated by p62 siRNA. CRISPR/Cas9-mediated deletion of p62, and subsequent poly-GA and SETX overexpression, would therefore represent a more elegant experiment to confirm this result.

In addition, SETX may be involved in DSB repair (Yuce & West, 2013), since it is shown to co-localise with a number of DSB repair factors, including 53BP1 and γH2AX, after DNA damaging agents. As such, the role of SETX may not necessarily be specific to R-loop resolution and may also contribute to DSB repair. RNASE H1 overexpression may therefore represent a more direct way to test epistasis between R-loop- and p62-mediated damage, though we consistently observed considerable toxicity using RNASE H1 transfections and transductions. We therefore preferred to use SETX as opposed to RNASE H1.

5.4.4. P62 as a therapeutic target

P62 has a number of cellular roles, including its role in selective autophagy and signal transduction pathways (Katsuragi *et al.*, 2015). As such, is unlikely that p62 depletion strategies would confer therapeutic benefit to C9orf72-ALS patients. Small peptide inhibitors targeting the LB domain of p62, however, may represent a promising drug target, since this domain is not linked to its function in autophagy, but is essential for its role in RNF168 inhibition. Small peptides targeting this domain should therefore prevent p62-mediated DNA damage, without disrupting other functions of p62. Future research should therefore seek to investigate the potential of small peptides inhibitors.

5.4.5. Understanding the nature of p62 accumulation in IPSC-derived neuronal cells and C9orf72-BAC mouse models

Since our data demonstrates that p62 drives the pathological dysregulation of DSB repair in C9orf72-ALS, it would be interesting to assess when during the disease progression p62 begins to accumulate. BAC mouse models would therefore be useful for characterising the time course during which p62 accumulates (Jiang *et al.*, 2016; Liu *et al.*, 2016). It is also unclear as to the pattern of p62 accumulation in C9orf72-ALS IPSC-derived neurons, and whether p62 accumulation impedes DSB repair in these cells. Finally, BAC mouse models and IPSC-derived neuronal culture would be good models to assess the therapeutic potential of small peptide inhibitors that disrupt the p62-RNF168 interaction.

5.4.6. The LB domain of P62 is not conserved

Interestingly, poly-GA DPRs are not toxic in drosophila (Mizielinska *et al.*, 2014) and the p62 drosophila analogue of p62 lacks the LB domain that induces DSB repair defects. Thus, poly-GA DPRs may not be toxic in drosophila because ATM-mediated DSB repair is not dysfunctional. In mice, whom do express the LB domain, poly-GA DPRs clearly induce neurodegeneration (Walker *et al.*, 2017; Zhang *et al.*, 2016). Since p62 is a hallmark feature of ALS and ALS disease models, our finding highlights an important consideration for future research. Given the diverse role of ATM signalling, it may be the case that important features of C9orf72-ALS (as well as other ALS subtypes) are missed by using model systems whose endogenous p62 isoform lacks the LB domain.

5.4.7. P62 accumulation in non-C9orf72-ALS and other neurodegenerative diseases

Promisingly, C9orf72-ALS is not the only ALS subtype that displays p62 accumulation. Indeed, p62 accumulation is a feature of sporadic-ALS cases (Mizuno *et al.*, 2006; Sasaki, 2011), which comprise 90% of the disease. As such, DSB repair signalling is likely defective across the spectrum of ALS subtypes, and thus the targeted modulation of p62-RNF168 interactions may confer therapeutic benefit to most ALS patients – not just C9orf72-ALS cases.

In addition to ALS, the expression of poly-glutamine (polyQ) aggregates (which are linked to Huntington's disease, Friedreich's ataxia, and spinocerebellar ataxias) have been linked to

p62 dysfunction (Sutovsky *et al.*, 2016). It has been shown that p62 targets polyQ aggregates for degradation (Matsumoto *et al.*, Nukina, 2011), and these aggregates appear to be p62-positive in some cases (Bjørkøy *et al.*, 2005; Nagaoka *et al.*, 2004). As such, it is possible that DSB repair and ATM signalling is defective in such disorders. In line with this idea, previous reports have demonstrated that polyQ aggregates impair 53BP1 repair foci, and that this could be partly rescued by ubiquitin overexpression (Ben Yehuda *et al.*, 2017), which is fully in-line with our model by which p62 accumulation impairs H2A(X) ubiquitylation by RNF168. Indeed dysfunctional ATM signalling would be an elegant explanation for the clinical phenotype of Friedreich's ataxia and spinocerebellar ataxias, wherein the neurological symptoms of patients are similar to that of A-T (i.e. cerebellar ataxia).

5.4.8. Concluding Remarks

In this chapter, it was demonstrated that defective ATM-mediated DNA repair was a consequence of p62 accumulation. Our data builds upon a previous seminal discovery, that p62 impairs the DDR (Wang *et al.*, 2016), and expands the physiological relevance of their work. Moreover, our data associate a hallmark feature of ALS/FTD, p62 accumulation, to decreased ATM signalling. Future work should therefore aim to utilise this molecular understanding to develop therapeutic strategies, possibly using small peptide competing inhibitors.

Chapter 6: General Discussion

6.1. Genomic Instability is an emerging paradigm in ALS

We have therefore shown that C9orf72 repeat expansions and poly-GA DPRs lead to R-loop accumulation and defective ATM-mediated DSB repair, both of which drive genomic instability. Whilst R-loops actively drive the formation of DSBs, defects in DSB repair passively exacerbate the increased levels of damage, ultimately leading to cellular toxicity in C9orf72 cellular models. Interestingly, a number of ALS-linked proteins (TDP-43 FUS-ALS, SMA, and SETX) have now been linked to a role in regulating R-loop homeostasis (Hill *et al.*, 2016; Jangi *et al.*, 2017; Yuce & West, 2013; Zhao *et al.*, 2016), suggesting that elevated R-loop levels may be a common disease mechanism.

Crucially, targeted depletion of R-loops may be therapeutic for C9orf72-ALS/FTD, since SETX overexpression of our C9orf72 models reduced cell death. Moreover, since other ALS-linked proteins have been associated with R-loop resolution/prevention, SETX viral vectors may confer therapeutic potential for other ALS patients, widening the potential applicability of our research.

6.2. P62 proteinopathy connects dysregulated autophagy to defective DNA repair

In addition to R-loop-mediated damage, we unravelled the mechanism by which ATM signalling was dysfunctional in C9orf72 models, which was linked to the hallmark accumulation of p62, impaired histone H2A ubiquitylation, and defective RNF168-mediated DNA repair. Our findings highlight, for the first time, a direct pathological consequence of p62 accumulation in ALS. Moreover, this interaction between p62 and the DNA damage response may represent a promising strategy for therapeutic intervention. Whilst p62 plays an integral role in autophagy, the LM domain that impairs DNA repair is likely to be dispensable for this function, making small peptide competitors for this domain a feasible way to prevent p62-mediated DSB repair dysfunction (without compromising autophagy). Excitingly, since p62 accumulation is observed in other ALS/FTD subtypes (Al-Sarraj *et al.*, 2011; Troakes *et al.*, 2012), including sporadic cases, we predict ATM signalling will be similarly dysfunction in other ALS/FTD patients, again widening the potential impact of our research.

6.3. C9orf72 expansions and cancer

In addition to cerebellar ataxia, a feature of A-T is cancer predisposition, namely lymphomas (Taylor *et al.*, 2004). Thus, it remains unclear why C9orf72-ALS patients, which likely have defects in ATM signalling, are not predisposed to cancer. A plausible explanation is that dividing cells do not accumulate p62 proteinopathy. An alternative option may be that ATM-mediated cell cycle control is not defective, and thus proliferating cells with DSB repair defects become senescent rather than cancerous. Thirdly, homologous recombination may not be defective, though based on the previous work of Wang *et al.* (Wang *et al.*, 2016), p62 accumulation appears to disrupt both HR and NHEJ. Assessing ATM signalling pathways in non-CNS tissues derived from C9orf72-ALS patients, and studying ATM-mediated control of checkpoint kinases Chk1/2, should therefore be the focus of future research.

Importantly, A-T patients, cell cultures and mouse models are highly radiosensitive, as is the RNF168 knock-out mouse model (Bohgaki *et al.*, 2011; Taylor *et al.*, 2004). It is not currently known whether C9orf72-ALS patients are also radiosensitive, but clearly has important clinical implications. In a similar manner, it is unclear whether other forms of ALS are also radiosensitive, since p62 accumulation is a feature of these diseases as well (Al-Sarraj *et al.*, 2011; Troakes *et al.*, 2012). Curiously, Huntington's and Friedreich's ataxia cell cultures are reported to be radiosensitive (Chamberlain & Lewis, 1982; Ferlazzo *et al.*, 2014; Lewis, Corr, Arlett, & Harcourt, 1979), suggesting a possible link to ATM signalling disruption. As such, future research should aim to assess whether C9orf72 expansions or other ALS-causing gene mutations make cells radiosensitive.

Appendix

Table 3. Statistical information for each Figure used in this report

Figure	Statistical test used	Replicates	P Value	Degrees of freedom & F/T value
4a	one-way ANOVA	3 cell culture replicates	M-10=0.78 M-102=0.004 10-102=0.009	F (2, 6) = 16.32
4b	one-way ANOVA	3 cell culture replicates	M-34=0.046 M-69=0.003 34-69=0.100	F(2,6)=1.412
4c	one-way ANOVA	3 cell culture replicates	M-10=0.31 M-102=0.004 10-102=0.018	F (2, 6) = 16.09
4d	one-way ANOVA	3 cell culture replicates	M-34=0.001 M-69=0.0002 34-69=0.07	F (2, 6) = 48.39
4e	one-way ANOVA	3 cell culture replicates	M-10=0.062 M-102=0.0005 10-102=0.005	F (2, 6) = 32.91
4f	one-way ANOVA	3 cell culture replicates	M-10=0.32 M-102=0.001 10-102=0.006	F (2, 6) = 23.59
4g	one-way ANOVA	3 cell culture replicates	M-34=0.006 M-69=0.0008 34-69=0.13	F (2, 6) = 27.96
4h	one-way ANOVA	3 cell culture replicates	M-34=0.0007 M-69=0.0003 34-69=0.4959	F (2, 6) = 45.32

5b	student's t-test	3 cell culture replicates	10(-+)=0.355 102(-+)=0.01 V5(-+)=0.807 69(-+)=0.022	t=1.044 df=4 t=4.6 df=4 t=0.6456 df=4 t=3.542 df=4
5c	student's t-test	3 cell culture replicates	10(-+)=0.62 102(-+)=0.037	t=0.2613 df=4 t=4.689 df=4
5d	student's t-test	6 cell culture replicates	10(-+)=0.806 102(-+)=0.009	t=0.2509 df=10 t=2.714 df=10
5e	student's t-test	3 cell culture replicates	V5(-+)=0.999 69(-+)=0.0394	t=0 df=4 t=3.015 df=4
5f	student's t-test	4 cell culture replicates	V5(-+)=0.6544 69(-+)=0.0025	t=0.4708 df=6 t=4.964 df=6
6a	student's t-test	6 cases per group	0.0038	t=3.755 df=10
6b	student's t-test	6 cases per group	0.0268	t=2.592 df=10
9a	one-way ANOVA	3 cell culture replicates	M-34=0.0009 M-69=0.0019 34-69=0.66	F (2, 6) = 30.18
9b	one-way ANOVA	3 cell culture replicates	M-10=0.4525 M-102=0.0348 10-102=0.008	F (2, 6) = 11.55
9d	one-way ANOVA	2 cell culture replicates	M-10=0.8052 M-102=0.1372 10-102=0.061 M-34=0.6263 M-69=0.9253 34-69=0.4276	F (2, 6) = 4.669 F (2, 6) = 0.9504
9e	student's t-test	3 cell culture replicates	M(-+)=0.0005 34(-+)=0.0032 69(-+)=0.0708	t=10.19 df=4 t=6.316 df=4 t=2.446 df=4
9f	student's t-test	3 cell culture replicates	M(-+)=0.0005 10(-+)=0.019	t=10.35 df=4 t=3.762 df=4

			102(-+)=0.249	t=1.369 df=4
10a	one-way ANOVA	3 cell culture replicates	M-34=0.0007 M-69=0.0016 34-69=0.5561	F (2, 6) = 32.94
10b	one-way ANOVA	3 cell culture replicates	M-10=0.4525 M-102=0.0348 10-102=0.008	F (2, 6) = 11.55
10c	student's t-test	3 cell culture replicates	M(-/+)=0.0094 34(-+)=0.2983 69(-+)=0.2943	t=4.681 df=4 t=1.194 df=4 t=1.206 df=4
10d	student's t-test	3 cell culture replicates	M(-+)=0.0179 10(-+)=0.0331 102(-+)=0.496	t=3.879 df=4 t=3.195 df=4 t=0.7481 df=4
10e	one-way ANOVA	3 cell culture replicates	M-34=0.0022 M-69=0.0026 34-69=0.9728	F (2, 6) = 23.89
10f	one-way ANOVA	3 cell culture replicates	M-10=0.8478 M-102=0.0023 10-102=0.004	F (2, 6) = 22.30
11a	student's t-test	3 cell culture replicates	M(-+)=0.0371 34(-+)=0.1334 69(-+)=0.3659	t=2.402 df=4 t=1.289 df=4 t=0.3676 df=4
11b	student's t-test	3 cell culture replicates	M(-+)=0.0143 10(-+)=0.0100 102(-+)=0.536	t=4.146 df=4 t=4.608 df=4 t=0.6749 df=4
12a	student's t-test	3 cell culture replicates	0.0278	t=3.378 df=4
12b	student's t-test	3 cell culture replicates	V5=0.0119 34=0.0593 69=0.4970	t=4.375 df=4 t=2.613 df=4 t=0.7462 df=4

12c	student's t-test	3 cell culture replicates	V5=0.0492 34=0.1854 69=0.4693	t=2.792 df=4 t=1.597 df=4 t=0.7986 df=4
13a	student's t-test	3 cell culture replicates	0.001	t=8.552 df=4
14a	student's t-test	4 cell culture replicates	0.0001	t=8.822 df=6
14b	student's t-test	3 cell culture replicates	V5=0.0221 69=0.0016	t=3.634 df=4 t=7.565 df=4
14c	student's t-test	3 cell culture replicates	V5(-/+)=0.033 69(-/+)=0.001	t=3.197 df=4 t=8.528 df=4
14e	student's t-test	3 cell culture replicates	V5(-+)=0.057 69(-+)=0.0004	t=2.646 df=4 t=11.00 df=4
14f	student's t-test	6 cell culture replicates	V5(-/+)=0.105 69(-/+)=0.003	t=1.908 df=6 t=4.786 df=6
15a	student's t-test	3 mice per group	<0.0001	t=16.19 df=4
15b	student's t-test	3 mice per group	0.0113	t=4.449 df=4
15c	student's t-test	3 mice per group	0.0363	t=3.097 df=4
15d	student's t-test	3 mice per group	0.0004	t=10.91 df=4
16	student's t-test	6 cases per group	0.0463	t=2.274 df=10
19a	student's t-test	3 cell culture replicates	0.0011	t=8.495 df=4
19b	student's t-test	3 cell culture replicates	0.0132	t=4.246 df=4
19c	student's t-test	3 cell culture replicates	0.0042	t=5.891 df=4
19d	student's t-test	3 cell culture replicates	V5(-+)=0.57 69(-+)=0.0003	t=0.61 df=4 t=11.72 df=4
19e	student's t-test	3 cell culture replicates	V5(-+)=0.3381 69(-+)=0.0061	t=1.087 df=4 t=5.292 df=4
19g	student's t-test	4 cell culture replicates	V5(-+)=0.5598 69(-+)=0.0468	t=0.4229 df=6 t=2.496 df=6
19h	student's t-test	4 cell culture replicates	V5(-+)=0.6871	t=0.2524 df=6

			69(-+)=0.0036	t=4.629 df=6
10i	student's t-test	3 cell culture replicates	V5=0.7247 69=0.0290	t=0.378 df=4 t=3.334 df=4
19j	student's t-test	3 cell culture replicates	V5=0.8512 69=0.0307	t=0.2 df=4 t=3.274 df=4
19k	one-way ANOVA	4 cell culture replicates	v5 siCON vs. 69 siCON <0.0001 v5 siCON vs. v5 siP62 0.9242 v5 siCON vs. v5 SETX 0.9242 v5 siCON vs. v5 siP62 SETX 0.2249 69 siCON vs. 69 siP62 0.0146 69 siCON vs. 69 SETX 0.0013 69 siCON vs. 69 siP62 SETX <0.0001 69 SETX vs. 69 siP62 SETX 0.0433 69 siP62 vs. 69 siP62 SETX 0.0045 69 siP62 vs. 69 SETX 0.6506	F (7, 24) = 12.17
20a	student's t-test	3 cell culture replicates	V5=0.0013 69=0.0042	t=8.095 df=4 t=5.869 df=4
20b	student's t-test	3 cell culture replicates	V5=0.1903 69=0.0139	t=1.575 df=4 t=4.18 df=4

Table 4: Abbreviations list

Abbreviations	Full length name
3-MA	3-Methyladenine
53BP1	p53 binding-protein-1
AAV	Adeno-associated virus
AAV9	Adeno-associated virus serotype 9
a-EJ	alternative end-joining
AID	Activation-induced cytidine deaminase
ALS	Amyotrophic Lateral Sclerosis
aly-REF	THO complex subunit 4
ANOVA	Analysis of variance
A-T	Ataxia-Telangiectasia
A-TLD	Ataxia-Telangiectasia like disorder
ATM	Ataxia-telangiectasia mutated
ATMIN	ataxia-telangiectasia mutated interacting
ATR	Ataxia telangiectasia and Rad3-related
BAC	Bacterial artificial chromosome
BER	Base excision repair
BRCA1	Breast cancer associated 1
BRCA2	Breast cancer associated 2
C9orf72	Chromosome 9 open read frame 72
Cas9	CRISPR-associated system-9
ChIP	Chromatin immunoprecipitation
CNF	Corrected nuclear fluorescence

CPT	Camptothecin
CQ	Chloroquine
CRISPR	Clustered Regularly Interspaced Short Palindromic Repeats
CS	Cockayne Syndrome
CsCl	Caesium chloride
DDR	DNA damage response
DIV	Days in vitro
DMEM	Dulbecco's modified essential medium
DMSO	Dimethyl sulfoxide
DNA-PK	DNA dependant protein kinase
DNA-PKcs	DNA dependant protein kinase catalytic subunit
DPRs	Dipeptide repeats
DRIP	DNA/RNA immunoprecipitation
DSB	Double-stranded break
EAAT2	Excitatory amino acid transporter 2
ECL	Electrochemilluminesence
EDTA	Ethylenediaminetetraacetic acid
EZH2	Enhancer of zeste homolog 2
fALS	familial ALS
FAT	FRAP, ATM, TRRAP
FAT-C	FRAP, ATM, TRRAP carboxyl
FBS	Foetal Bovine Syndrome
FISH	Fluorescence in situ hybridisation
FISH-ICC	Fluorescence in situ hybridisation - immunocytochemistry

FTD	Frontotemporal dementia
FUS	Fused in Sarcoma
GA	Glycine-alanine
GR	Glycine-arginine
H2A	Histone H2A
H3K9	Histone H3 Lysine 9
H3K9me2	Histone H3 Lysine 9 dimethylation
H3K9me3	Histone H3 Lysine 9 trimethylation
H3S10P	Histone H3 Serine 10 phosphorylation
HBSS	Hanks balanced salt solution
HDAC1	Histone deacetylase 1
HDAC4	Histone deacetylase 4
HEK 293T	Human embryonic kidney 293 expressing the SV40 large T antigen
HR	Homologous recombination
I2PP2A	Inhibitor-2 Of Protein Phosphatase-2A
ICC	Immunocytochemistry
IND	Integrated density
KAP1	KRAB-associated protein-1
LB	Lim-binding domain
LC3	Microtubule-associated protein 1A/1B-light chain 3
LIR	LC3-interacting region
MEFs	Mouse embryonic fibroblasts
MEM	Minimum essential medium
MFB	Mean fluorescence background

LC3	Microtubule-associated protein 1A/1B-light chain 3
MIU	Motif interacting with ubiquitin
MMR	Mismatch repair
MRC5	Medical research council-5
MRN	Mre11 Rad50 Nbs1
NA	Nuclear Area
Nbr1	Next to BRCA1 gene 1
NBS	Nijmegen breakage syndrome
NER	Nucleotide excision repair
NF-κB	Nuclear Factor κB
NHEJ	Non-homologous end-joining
NLS	Nuclear Localisation Signal
PARP1	Poly ADP ribose polymerase 1
pATM	Phosphorylated ataxia-telangiectasia mutated
PB1	Phox1 and Bem1p
PBS	Phosphate buffer saline
PEI	Polyethylenimine
PEX5	peroxisomal biogenesis factor 5
PFA	Paraformaldehyde
PI3K	Phosphatidylinositol-4,5-bisphosphate 3-kinase
PIKK	Phosphatidylinositol 3-kinase-related kinase
PNKP	Polynucleotide kinase 3'-phosphatase
POL2	RNA polymerase 2
polyQ	Poly-glutamine

PP2A	Protein phosphatase 2A
PP5	Protein phosphatase 5
p-p53	Phosphorylated p53
PR	Proline-arginine
PRC2	Polycomb repressive complex 2
RFP	Red fluorescent protein
RIP	Receptor-interacting protein
RNF168	Ring finger protein 168
RNF8	Ring finger protein 8
RPA	Replication protein A
RREs	RNA repeat expansions
sALS	sporadic ALS
scAAV9	Self-complimenting adeno-associated virus serotype 9
SCAN1	Spinocerebellar ataxia with axonal neuropathy-1
SETX	Senataxin
siRNA	Small interfering RNA
SMA	Spinal muscular atrophy
SQSTM1	Sequestosome-1
SRSF1	Serine-rich splicing factor 1
SSA	Single strand annealing
SSB	Single strand break
SSC	Saline-sodium citrate
TBST	Tris buffered saline with tween 20
TDP1	Tyrosyl-DNA phosphodiesterase 1

TDP-43	Tar DNA-binding protein-43
TOP1	Topoisomerase 1
TSA	Trichostatin A
TSS	Transcriptional start site
TTS	Transcriptional termination site
UBA	ubiquitin-associated
ub-H2A	Ubiquitylated histone H2A
UPS	Ubiquitin proteasome system
UV	Ultraviolet
V(D)J	Variable (diversity) joining
vg	Viral genomes
vWA	von Willebrand
WDR41	WD repeat-containing protein 41
Wip1	Wild-type p53-induced phosphatase 1
WT	Wild-type
XP	Xeroderma pigmentosum
XRCC4	X-ray repair cross complementing 4
XRN2	Exoribonuclease 2
ZZ	Zinc finger

References

Aguilera, A. (2002). The connection between transcription and genomic instability. *Embo j, 21*(3), 195-201.

Aguilera, A., & Garcia-Muse, T. (2012). R loops: from transcription byproducts to threats to genome stability. *Mol Cell, 46*(2), 115-124.

Ahel, I., Rass, U., El-Khamisy, S. F., Katyal, S., Clements, P. M., McKinnon, P. J., . . . West, S. C. (2006). The neurodegenerative disease protein aprataxin resolves abortive DNA ligation intermediates. *Nature, 443*(7112), 713-716.

Al-Sarraj, S., King, A., Troakes, C., Smith, B., Maekawa, S., Bodi, I., . . . Shaw, C. E. (2011). p62 positive, TDP-43 negative, neuronal cytoplasmic and intranuclear inclusions in the cerebellum and hippocampus define the pathology of C9orf72-linked FTLD and MND/ALS. *Acta Neuropathol, 122*(6), 691-702.

Alagoz, M., Chiang, S. C., Sharma, A., & El-Khamisy, S. F. (2013). ATM deficiency results in accumulation of DNA-topoisomerase I covalent intermediates in neural cells. *PLoS One, 8*(4), e58239.

Alzu, A., Bermejo, R., Begnis, M., Lucca, C., Piccini, D., Carotenuto, W., . . . Liberi, G. (2012). Senataxin associates with replication forks to protect fork integrity across RNA-polymerase-II-transcribed genes. *Cell, 151*(4), 835-846.

Andegeko, Y., Moyal, L., Mittelman, L., Tsarfaty, I., Shiloh, Y., & Rotman, G. (2001). Nuclear retention of ATM at sites of DNA double strand breaks. *J Biol Chem, 276*(41), 38224-38230.

Arning, L., Epplen, J. T., Rahikkala, E., Hendrich, C., Ludolph, A. C., & Sperfeld, A. D. (2013). The SETX missense variation spectrum as evaluated in patients with ALS4-like motor neuron diseases. *Neurogenetics, 14*(1), 53-61.

Ashour, M. E., Atteya, R., & El-Khamisy, S. F. (2015). Topoisomerase-mediated chromosomal break repair: an emerging player in many games. *Nat Rev Cancer, 15*(3), 137-151. Ayala, Y. M., De Conti, L., Avendano-Vazquez, S. E., Dhir, A., Romano, M., D'Ambrogio, A., . . . Baralle, F. E. (2011). TDP-43 regulates its mRNA levels through a negative feedback loop. *Embo j, 30*(2), 277-288.

Bakkenist, C. J., & Kastan, M. B. (2003). DNA damage activates ATM through intermolecular autophosphorylation and dimer dissociation. *Nature, 421*(6922), 499-506.

Banin, S., Moyal, L., Shieh, S., Taya, Y., Anderson, C. W., Chessa, L., . . . Ziv, Y. (1998). Enhanced phosphorylation of p53 by ATM in response to DNA damage. *Science, 281*(5383), 1674-1677.

Barker, H. V., Niblock, M., Lee, Y. B., Shaw, C. E., & Gallo, J. M. (2017). RNA Misprocessing in C9orf72-Linked Neurodegeneration. *Front Cell Neurosci, 11*, 195.

Barmada, S. J., Skibinski, G., Korb, E., Rao, E. J., Wu, J. Y., & Finkbeiner, S. (2010). Cytoplasmic mislocalization of TDP-43 is toxic to neurons and enhanced by a mutation associated with familial amyotrophic lateral sclerosis. *J Neurosci, 30*(2), 639-649. oi:10.1523/jneurosci.4988-09.2010

Basu, U., Meng, F.-L., Keim, C., Grinstein, V., Pefanis, E., Eccleston, J., . . . Alt, F. W. (2011). The RNA Exosome Targets the AID Cytidine Deaminase to Both Strands of Transcribed Duplex DNA Substrates. *Cell, 144*(3), 353-363.

Belzil, V. V., Bauer, P. O., Prudencio, M., Gendron, T. F., Stetler, C. T., Yan, I. K., . . . Petrucelli, L. (2013). Reduced C9orf72 gene expression in c9FTD/ALS is caused by histone trimethylation, an epigenetic event detectable in blood. *Acta Neuropathologica, 126*(6), 895-905.

Ben Yehuda, A., Risheq, M., Novoplansky, O., Bersuker, K., Kopito, R. R., Goldberg, M., & Brandeis, M. (2017). Ubiquitin Accumulation on Disease Associated Protein Aggregates Is Correlated with Nuclear Ubiquitin Depletion, Histone De-Ubiquitination and Impaired DNA Damage Response. *PLoS One, 12*(1), e0169054.

Benson, F. E., Baumann, P., & West, S. C. (1998). Synergistic actions of Rad51 and Rad52 in recombination and DNA repair. *Nature, 391*(6665), 401-404.

Berkovich, E., Monnat, R. J., Jr., & Kastan, M. B. (2007). Roles of ATM and NBS1 in chromatin structure modulation and DNA double-strand break repair. *Nat Cell Biol, 9*(6), 683-690.
Biton, S., Barzilai, A., & Shiloh, Y. (2008). The neurological phenotype of ataxia-telangiectasia: solving a persistent puzzle. *DNA Repair (Amst), 7*(7), 1028-1038.
Bjørkøy, G., Lamark, T., Brech, A., Outzen, H., Perander, M., Øvervatn, A., . . . Johansen, T. (2005). p62/SQSTM1 forms protein aggregates degraded by autophagy and has a protective effect on huntingtin-induced cell death. *The Journal of Cell Biology, 171*(4), 603.
Blackford, A. N., & Jackson, S. P. (2017). ATM, ATR, and DNA-PK: The Trinity at the Heart of the DNA Damage Response. *Mol Cell, 66*(6), 801-817.
Blokhuis, A. M., Groen, E. J. N., Koppers, M., van den Berg, L. H., & Pasterkamp, R. J. (2013). Protein aggregation in amyotrophic lateral sclerosis. *Acta Neuropathologica, 125*(6), 777-794.
Bohgaki, T., Bohgaki, M., Cardoso, R., Panier, S., Zeegers, D., Li, L., . . . Hakem, R. (2011). Genomic instability, defective spermatogenesis, immunodeficiency, and cancer in a mouse model of the RIDDLE syndrome. *PLoS Genet, 7*(4), e1001381.
Bouwman, P., Aly, A., Escandell, J. M., Pieterse, M., Bartkova, J., van der Gulden, H., . . . Jonkers, J. (2010). 53BP1 loss rescues BRCA1 deficiency and is associated with triple-negative and BRCA-mutated breast cancers. *Nat Struct Mol Biol, 17*(6), 688-695.
Brady, O. A., Meng, P., Zheng, Y., Mao, Y., & Hu, F. (2011). Regulation of TDP-43 aggregation by phosphorylation and p62/SQSTM1. *J Neurochem, 116*(2), 248-259.
Brcic, J., & Plavec, J. (2017). ALS and FTD linked GGGGCC-repeat containing DNA oligonucleotide folds into two distinct G-quadruplexes. *Biochim Biophys Acta, 1861*(5 Pt B), 1237-1245.
Britton, S., Coates, J., & Jackson, S. P. (2013). A new method for high-resolution imaging of Ku foci to decipher mechanisms of DNA double-strand break repair. *J Cell Biol, 202*(3), 579-595.
Bunting, S. F., Callen, E., Wong, N., Chen, H. T., Polato, F., Gunn, A., . . . Nussenzweig, A. (2010). 53BP1 inhibits homologous recombination in Brca1-deficient cells by blocking resection of DNA breaks. *Cell, 141*(2), 243-254.
Burghes, A. H. M., & Beattie, C. E. (2009). Spinal Muscular Atrophy: Why do low levels of SMN make motor neurons sick? *Nature reviews. Neuroscience, 10*(8), 597-609.
Buscemi, G., Savio, C., Zannini, L., Micciche, F., Masnada, D., Nakanishi, M., . . . Delia, D. (2001). Chk2 activation dependence on Nbs1 after DNA damage. *Mol Cell Biol, 21*(15), 5214-5222. Cadet, J., Ravanat, J. L., TavernaPorro, M., Menoni, H., & Angelov, D. (2012). Oxidatively generated complex DNA damage: tandem and clustered lesions. *Cancer Lett, 327*(1-2), 5-15.
Caldecott, K. W. (2003). XRCC1 and DNA strand break repair. *DNA Repair (Amst), 2*(9), 955-969.
Canman, C. E., Lim, D. S., Cimprich, K. A., Taya, Y., Tamai, K., Sakaguchi, K., . . . Siliciano, J. D. (1998). Activation of the ATM kinase by ionizing radiation and phosphorylation of p53. *Science, 281*(5383), 1677-1679.
Carson, C. T., Schwartz, R. A., Stracker, T. H., Lilley, C. E., Lee, D. V., & Weitzman, M. D. (2003). The Mre11 complex is required for ATM activation and the G2/M checkpoint. *Embo j, 22*(24), 6610-6620.
Castellano-Pozo, M., Santos-Pereira, J. M., Rondon, A. G., Barroso, S., Andujar, E., Perez-Alegre, M., . . . Aguilera, A. (2013). R loops are linked to histone H3 S10 phosphorylation and chromatin condensation. *Mol Cell, 52*(4), 583-590.
Celeste, A., Fernandez-Capetillo, O., Kruhlak, M. J., Pilch, D. R., Staudt, D. W., Lee, A., . . . Nussenzweig, A. (2003). Histone H2AX phosphorylation is dispensable for the initial recognition of DNA breaks. *Nat Cell Biol, 5*(7), 675-679.
Cerritelli, S. M., & Crouch, R. J. (2009). Ribonuclease H: the enzymes in eukaryotes. *Febs j, 276*(6), 1494-1505.
Cerritelli, S. M., Frolova, E. G., Feng, C., Grinberg, A., Love, P. E., & Crouch, R. J. (2003). Failure to produce mitochondrial DNA results in embryonic lethality in Rnaseh1 null mice. *Mol Cell, 11*(3), 807-815.

Chamberlain, S., & Lewis, P. D. (1982). Studies of cellular hypersensitivity to ionising radiation in Friedreich's ataxia. *J Neurol Neurosurg Psychiatry, 45*(12), 1136-1138.

Champoux, J. J. (2001). DNA topoisomerases: structure, function, and mechanism. *Annu Rev Biochem, 70*, 369-413.

Chang, H. H. Y., Pannunzio, N. R., Adachi, N., & Lieber, M. R. (2017). Non-homologous DNA end joining and alternative pathways to double-strand break repair. *Nat Rev Mol Cell Biol, 18*(8), 495-506.

Chang, Y. J., Jeng, U. S., Chiang, Y. L., Hwang, I. S., & Chen, Y. R. (2016). The Glycine-Alanine Dipeptide Repeat from C9orf72 Hexanucleotide Expansions Forms Toxic Amyloids Possessing Cell-to-Cell Transmission Properties. *J Biol Chem, 291*(10), 4903-4911.

Chapman, J. R., & Jackson, S. P. (2008). Phospho-dependent interactions between NBS1 and MDC1 mediate chromatin retention of the MRN complex at sites of DNA damage. *EMBO Rep, 9*(8),

Chen, Y. Z., Bennett, C. L., Huynh, H. M., Blair, I. P., Puls, I., Irobi, J., . . . Chance, P. F. (2004). DNA/RNA helicase gene mutations in a form of juvenile amyotrophic lateral sclerosis (ALS4). *Am J Hum Genet, 74*(6), 1128-1135.

Chew, J., Gendron, T. F., Prudencio, M., Sasaguri, H., Zhang, Y. J., Castanedes-Casey, M., . . . Petrucelli, L. (2015). Neurodegeneration. C9ORF72 repeat expansions in mice cause TDP-43 pathology, neuronal loss, and behavioral deficits. *Science, 348*(6239), 1151-1154.

Chiang, S. C., Meagher, M., Kassouf, N., Hafezparast, M., McKinnon, P. J., Haywood, R., & El-Khamisy, S. F. (2017). Mitochondrial protein-linked DNA breaks perturb mitochondrial gene transcription and trigger free radical-induced DNA damage. *Sci Adv, 3*(4), e1602506.

Chiarle, R., Zhang, Y., Frock, Richard L., Lewis, Susanna M., Molinie, B., Ho, Y.-J., . . . Alt, Frederick W. (2011). Genome-wide Translocation Sequencing Reveals Mechanisms of Chromosome Breaks and Rearrangements in B Cells. *Cell, 147*(1), 107-119.

Chio, A., Logroscino, G., Hardiman, O., Swingler, R., Mitchell, D., Beghi, E., & Traynor, B. G. (2009). Prognostic factors in ALS: A critical review. *Amyotroph Lateral Scler, 10*(5-6), 310-323.

Chon, H., Sparks, J. L., Rychlik, M., Nowotny, M., Burgers, P. M., Crouch, R. J., & Cerritelli, S. M. (2013). RNase H2 roles in genome integrity revealed by unlinking its activities. *Nucleic Acids Res, 41*(5), 3130-3143.

Ciccia, A., & Elledge, S. J. (2010). The DNA damage response: making it safe to play with knives. *Mol Cell, 40*(2), 179-204.

Ciura, S., Lattante, S., Le Ber, I., Latouche, M., Tostivint, H., Brice, A., & Kabashi, E. (2013). Loss of function of C9orf72 causes motor deficits in a zebrafish model of amyotrophic lateral sclerosis. *Ann Neurol, 74*(2), 180-187.

Clements, P. M., Breslin, C., Deeks, E. D., Byrd, P. J., Ju, L., Bieganowski, P., . . . Caldecott, K. W. (2004). The ataxia-oculomotor apraxia 1 gene product has a role distinct from ATM and interacts with the DNA strand break repair proteins XRCC1 and XRCC4. *DNA Repair (Amst), 3*(11), 1493-1502.

Conlon, E. G., Lu, L., Sharma, A., Yamazaki, T., Tang, T., Shneider, N. A., & Manley, J. L. (2016). The C9ORF72 GGGGCC expansion forms RNA G-quadruplex inclusions and sequesters hnRNP H to disrupt splicing in ALS brains. *Elife, 5*.

Cooper-Knock, J., Bury, J. J., Heath, P. R., Wyles, M., Higginbottom, A., Gelsthorpe, C., . . . Shaw, P. J. (2015c). C9ORF72 GGGGCC Expanded Repeats Produce Splicing Dysregulation which Correlates with Disease Severity in Amyotrophic Lateral Sclerosis. *PLoS One, 10*(5), e0127376.

Cooper-Knock, J., Hewitt, C., Highley, J. R., Brockington, A., Milano, A., Man, S., . . . Shaw, P. J. (2012). Clinico-pathological features in amyotrophic lateral sclerosis with expansions in C9ORF72. *Brain, 135*(Pt 3), 751-764.

Cooper-Knock, J., Higginbottom, A., Stopford, M. J., Highley, J. R., Ince, P. G., Wharton, S. B., . . . Shaw, P. J. (2015a). Antisense RNA foci in the motor neurons of C9ORF72-ALS patients are associated with TDP-43 proteinopathy. *Acta Neuropathol, 130*(1), 63-75.

Cooper-Knock, J., Kirby, J., Highley, R., & Shaw, P. J. (2015b). The Spectrum of C9orf72-mediated Neurodegeneration and Amyotrophic Lateral Sclerosis. *Neurotherapeutics, 12*(2), 326-339.
Cooper-Knock, J., Walsh, M. J., Higginbottom, A., Robin Highley, J., Dickman, M. J., Edbauer, D., . . . Shaw, P. J. (2014). Sequestration of multiple RNA recognition motif-containing proteins by C9orf72 repeat expansions. *Brain, 137*(Pt 7), 2040-2051.
Corcia, P., Vourc'h, P., Guennoc, A. M., Del Mar Amador, M., Blasco, H., Andres, C., . . . Meininger, V. (2016). Pure cerebellar ataxia linked to large C9orf72 repeat expansion. *Amyotroph Lateral Scler Frontotemporal Degener, 17*(3-4), 301-303.
Couratier, P., Corcia, P., Lautrette, G., Nicol, M., & Marin, B. (2017). ALS and frontotemporal dementia belong to a common disease spectrum. *Revue Neurologique, 173*(5), 273-279.
Das, B. B., Antony, S., Gupta, S., Dexheimer, T. S., Redon, C. E., Garfield, S., . . . Pommier, Y. (2009). Optimal function of the DNA repair enzyme TDP1 requires its phosphorylation by ATM and/or DNA-PK. *Embo j, 28*(23), 3667-3680.
Davidson, Y., Robinson, A. C., Liu, X., Wu, D., Troakes, C., Rollinson, S., . . . Mann, D. M. (2016). Neurodegeneration in frontotemporal lobar degeneration and motor neurone disease associated with expansions in C9orf72 is linked to TDP-43 pathology and not associated with aggregated forms of dipeptide repeat proteins. *Neuropathol Appl Neurobiol, 42*(3), 242-254.
Davidson, Y. S., Barker, H., Robinson, A. C., Thompson, J. C., Harris, J., Troakes, C., . . . Mann, D. M. (2014). Brain distribution of dipeptide repeat proteins in frontotemporal lobar degeneration and motor neurone disease associated with expansions in C9ORF72. *Acta Neuropathol Commun, 2*, 70.
Davis, A. J., & Chen, D. J. (2013). DNA double strand break repair via non-homologous end-joining. *Translational cancer research, 2*(3), 130-143.
DeJesus-Hernandez, M., Mackenzie, I. R., Boeve, B. F., Boxer, A. L., Baker, M., Rutherford, N. J., . . . Rademakers, R. (2011). Expanded GGGGCC hexanucleotide repeat in noncoding region of C9ORF72 causes chromosome 9p-linked FTD and ALS. *Neuron, 72*(2), 245-256.
Diaper, D. C., Adachi, Y., Lazarou, L., Greenstein, M., Simoes, F. A., Di Domenico, A., . . . Hirth, F. (2013). Drosophila TDP-43 dysfunction in glia and muscle cells cause cytological and behavioural phenotypes that characterize ALS and FTLD. *Hum Mol Genet, 22*(19), 3883-3893.
Difilippantonio, S., Celeste, A., Fernandez-Capetillo, O., Chen, H. T., Reina San Martin, B., Van Laethem, F., . . . Nussenzweig, A. (2005). Role of Nbs1 in the activation of the Atm kinase revealed in humanized mouse models. *Nat Cell Biol, 7*(7), 675-685.
Dobbs, T. A., Tainer, J. A., & Lees-Miller, S. P. (2010). A structural model for regulation of NHEJ by DNA-PKcs autophosphorylation. *DNA Repair (Amst), 9*(12), 1307-1314.
Dols-Icardo, O., Garcia-Redondo, A., Rojas-Garcia, R., Sanchez-Valle, R., Noguera, A., Gomez-Tortosa, E., . . . Clarimon, J. (2014). Characterization of the repeat expansion size in C9orf72 in amyotrophic lateral sclerosis and frontotemporal dementia. *Hum Mol Genet, 23*(3), 749-754.
Donnelly, C. J., Zhang, P. W., Pham, J. T., Haeusler, A. R., Mistry, N. A., Vidensky, S., . . . Rothstein, J. D. (2013). RNA toxicity from the ALS/FTD C9ORF72 expansion is mitigated by antisense intervention. *Neuron, 80*(2), 415-428.
Douglas, P., Cui, X., Block, W. D., Yu, Y., Gupta, S., Ding, Q., . . . Meek, K. (2007). The DNA-dependent protein kinase catalytic subunit is phosphorylated in vivo on threonine 3950, a highly conserved amino acid in the protein kinase domain. *Mol Cell Biol, 27*(5), 1581-1591.
Downs, J. A., & Jackson, S. P. (2004). A means to a DNA end: the many roles of Ku. *Nat Rev Mol Cell Biol, 5*(5), 367-378.
Duquette, M. L., Handa, P., Vincent, J. A., Taylor, A. F., & Maizels, N. (2004). Intracellular transcription of G-rich DNAs induces formation of G-loops, novel structures containing G4 DNA. *Genes Dev, 18*(13), 1618-1629.
Eapen, V. V., Waterman, D. P., Bernard, A., Schiffmann, N., Sayas, E., Kamber, R., . . . Haber, J. E. (2017). A pathway of targeted autophagy is induced by DNA damage in budding yeast. *Proc Natl Acad Sci U S A, 114*(7), E1158-e1167.

Eder, P. S., Walder, R. Y., & Walder, J. A. (1993). Substrate specificity of human RNase H1 and its role in excision repair of ribose residues misincorporated in DNA. *Biochimie, 75*(1), 123-126.
El-Khamisy, S. F., & Caldecott, K. W. (2007). DNA single-strand break repair and spinocerebellar ataxia with axonal neuropathy-1. *Neuroscience, 145*(4), 1260-1266.
El-Khamisy, S. F., Saifi, G. M., Weinfeld, M., Johansson, F., Helleday, T., Lupski, J. R., & Caldecott, K. W. (2005). Defective DNA single-strand break repair in spinocerebellar ataxia with axonal neuropathy-1. *Nature, 434*(7029), 108-113.
Eliopoulos, A. G., Havaki, S., & Gorgoulis, V. G. (2016). DNA Damage Response and Autophagy: A Meaningful Partnership. *Front Genet, 7*, 204.
Esashi, F., Christ, N., Gannon, J., Liu, Y., Hunt, T., Jasin, M., & West, S. C. (2005). CDK-dependent phosphorylation of BRCA2 as a regulatory mechanism for recombinational repair. *Nature, 434*(7033), 598-604.
Falck, J., Coates, J., & Jackson, S. P. (2005). Conserved modes of recruitment of ATM, ATR and DNA-PKcs to sites of DNA damage. *Nature, 434*(7033), 605-611. doi:10.1038/nature03442
Farg, M. A., Konopka, A., Soo, K. Y., Ito, D., & Atkin, J. D. (2017). The DNA damage response (DDR) is induced by the C9orf72 repeat expansion in amyotrophic lateral sclerosis. *Hum Mol Genet, 26*(15), 2882-2896.
Farg, M. A., Sundaramoorthy, V., Sultana, J. M., Yang, S., Atkinson, R. A., Levina, V., . . . Atkin, J. D. (2014). C9ORF72, implicated in amytrophic lateral sclerosis and frontotemporal dementia, regulates endosomal trafficking. *Hum Mol Genet, 23*(13), 3579-3595.
Fecto, F., Yan, J., Vemula, S. P., Liu, E., Yang, Y., Chen, W., . . . Siddique, T. (2011). SQSTM1 mutations in familial and sporadic amyotrophic lateral sclerosis. *Arch Neurol, 68*(11), 1440-1446.
Ferlazzo, M. L., Sonzogni, L., Granzotto, A., Bodgi, L., Lartin, O., Devic, C., . . . Foray, N. (2014). Mutations of the Huntington's disease protein impact on the ATM-dependent signaling and repair pathways of the radiation-induced DNA double-strand breaks: corrective effect of statins and bisphosphonates. *Mol Neurobiol, 49*(3), 1200-1211.
Ferrari, R., Kapogiannis, D., Huey, E. D., & Momeni, P. (2011). FTD and ALS: a tale of two diseases. *Curr Alzheimer Res, 8*(3), 273-294.
FitzGerald, J. E., Grenon, M., & Lowndes, N. F. (2009). 53BP1: function and mechanisms of focal recruitment. *Biochem Soc Trans, 37*(Pt 4), 897-904.
Fratta, P., Mizielinska, S., Nicoll, A. J., Zloh, M., Fisher, E. M., Parkinson, G., & Isaacs, A. M. (2012). C9orf72 hexanucleotide repeat associated with amyotrophic lateral sclerosis and frontotemporal dementia forms RNA G-quadruplexes. *Sci Rep, 2*, 1016.
Freibaum, B. D., Lu, Y., Lopez-Gonzalez, R., Kim, N. C., Almeida, S., Lee, K. H., . . . Taylor, J. P. (2015). GGGGCC repeat expansion in C9orf72 compromises nucleocytoplasmic transport. *Nature, 525*(7567), 129-133.
Galanty, Y., Belotserkovskaya, R., Coates, J., Polo, S., Miller, K. M., & Jackson, S. P. (2009). Mammalian SUMO E3-ligases PIAS1 and PIAS4 promote responses to DNA double-strand breaks. *Nature, 462*(7275), 935-939.
Gallia, G. L., Johnson, E. M., & Khalili, K. (2000). Puralpha: a multifunctional single-stranded DNA- and RNA-binding protein. *Nucleic Acids Res, 28*(17), 3197-3205.
García-Pichardo, D., Cañas, J. C., García-Rubio, M. L., Gómez-González, B., Rondón, A. G., & Aguilera, A. (2017). Histone Mutants Separate R Loop Formation from Genome Instability Induction. *Molecular Cell, 66*(5), 597-609.e595.
Genois, M.-M., Paquet, E. R., Laffitte, M.-C. N., Maity, R., Rodrigue, A., Ouellette, M., & Masson, J.-Y. (2014). DNA Repair Pathways in Trypanosomatids: from DNA Repair to Drug Resistance. *Microbiology and Molecular Biology Reviews : MMBR, 78*(1), 40-73.
Georgakilas, A. G., O'Neill, P., & Stewart, R. D. (2013). Induction and repair of clustered DNA lesions: what do we know so far? *Radiat Res, 180*(1), 100-109.
Gijselinck, I., Van Langenhove, T., van der Zee, J., Sleegers, K., Philtjens, S., Kleinberger, G., . . . Van Broeckhoven, C. (2012). A C9orf72 promoter repeat expansion in a Flanders-Belgian cohort

with disorders of the frontotemporal lobar degeneration-amyotrophic lateral sclerosis spectrum: a gene identification study. *Lancet Neurol, 11*(1), 54-65.
Gijselinck, I., Van Mossevelde, S., van der Zee, J., Sieben, A., Engelborghs, S., De Bleecker, J., . . . Van Broeckhoven, C. (2016). The C9orf72 repeat size correlates with onset age of disease, DNA methylation and transcriptional downregulation of the promoter. *Mol Psychiatry, 21*(8), 1112-1124.
Ginno, P. A., Lim, Y. W., Lott, P. L., Korf, I., & Chedin, F. (2013). GC skew at the 5' and 3' ends of human genes links R-loop formation to epigenetic regulation and transcription termination. *Genome Res, 23*(10), 1590-1600.
Ginno, P. A., Lott, P. L., Christensen, H. C., Korf, I., & Chedin, F. (2012). R-loop formation is a distinctive characteristic of unmethylated human CpG island promoters. *Mol Cell, 45*(6), 814-825.
Girard, P. M., Riballo, E., Begg, A. C., Waugh, A., & Jeggo, P. A. (2002). Nbs1 promotes ATM dependent phosphorylation events including those required for G1/S arrest. *Oncogene, 21*(27), 4191-4199.
Gomez-Gonzalez, B., & Aguilera, A. (2007). Activation-induced cytidine deaminase action is strongly stimulated by mutations of the THO complex. *Proc Natl Acad Sci U S A, 104*(20), 8409-8414.
Goodarzi, A. A., Block, W. D., & Lees-Miller, S. P. (2003). The role of ATM and ATR in DNA damage-induced cell cycle control. *Prog Cell Cycle Res, 5*, 393-411.
Goodarzi, A. A., Noon, A. T., Deckbar, D., Ziv, Y., Shiloh, Y., Lobrich, M., & Jeggo, P. A. (2008). ATM signaling facilitates repair of DNA double-strand breaks associated with heterochromatin. *Mol Cell, 31*(2), 167-177.
Gottlieb, T. M., & Jackson, S. P. (1993). The DNA-dependent protein kinase: requirement for DNA ends and association with Ku antigen. *Cell, 72*(1), 131-142.
Grawunder, U., Wilm, M., Wu, X., Kulesza, P., Wilson, T. E., Mann, M., & Lieber, M. R. (1997). Activity of DNA ligase IV stimulated by complex formation with XRCC4 protein in mammalian cells. *Nature, 388*(6641), 492-495.
Green, Douglas R., & Levine, B. (2014). To Be or Not to Be? How Selective Autophagy and Cell Death Govern Cell Fate. *Cell, 157*(1), 65-75.
Gregory, R. I., Yan, K. P., Amuthan, G., Chendrimada, T., Doratotaj, B., Cooch, N., & Shiekhattar, R. (2004). The Microprocessor complex mediates the genesis of microRNAs. *Nature, 432*(7014), 235-240.
Groh, M., Lufino, M. M., Wade-Martins, R., & Gromak, N. (2014). R-loops associated with triplet repeat expansions promote gene silencing in Friedreich ataxia and fragile X syndrome. *PLoS Genet, 10*(5), e1004318.
Grundy, G. J., Rulten, S. L., Zeng, Z., Arribas-Bosacoma, R., Iles, N., Manley, K., . . . Caldecott, K. W. (2013). APLF promotes the assembly and activity of non-homologous end joining protein complexes. *Embo j, 32*(1), 112-125.
Guo, Z., Kozlov, S., Lavin, M. F., Person, M. D., & Paull, T. T. (2010). ATM activation by oxidative stress. *Science, 330*(6003), 517-521.
Haeusler, A. R., Donnelly, C. J., Periz, G., Simko, E. A., Shaw, P. G., Kim, M. S., . . . Wang, J. (2014). C9orf72 nucleotide repeat structures initiate molecular cascades of disease. *Nature, 507*(7491), 195-200.
Hammel, M., Yu, Y., Mahaney, B. L., Cai, B., Ye, R., Phipps, B. M., . . . Tainer, J. A. (2010). Ku and DNA-dependent protein kinase dynamic conformations and assembly regulate DNA binding and the initial non-homologous end joining complex. *J Biol Chem, 285*(2), 1414-1423.
Hamperl, S., Bocek, M. J., Saldivar, J. C., Swigut, T., & Cimprich, K. A. (2017). Transcription-Replication Conflict Orientation Modulates R-Loop Levels and Activates Distinct DNA Damage Responses. *Cell, 170*(4), 774-786.e719.
Harper, J. W., & Elledge, S. J. (2007). The DNA damage response: ten years after. *Mol Cell, 28*(5), 739-745.

Harrigan, J. A., Belotserkovskaya, R., Coates, J., Dimitrova, D. S., Polo, S. E., Bradshaw, C. R., . . . Jackson, S. P. (2011). Replication stress induces 53BP1-containing OPT domains in G1 cells. *The Journal of Cell Biology, 193*(1), 97-108.

Hartlerode, A. J., & Scully, R. (2009). Mechanisms of double-strand break repair in somatic mammalian cells. *Biochem J, 423*(2), 157-168.

Hatchi, E., Skourti-Stathaki, K., Ventz, S., Pinello, L., Yen, A., Kamieniarz-Gdula, K., . . . Livingston, D. M. (2015). BRCA1 recruitment to transcriptional pause sites is required for R-loop-driven DNA damage repair. *Mol Cell, 57*(4), 636-647.

Hautbergue, G. M., Castelli, L. M., Ferraiuolo, L., Sanchez-Martinez, A., Cooper-Knock, J., Higginbottom, A., . . . Shaw, P. J. (2017). SRSF1-dependent nuclear export inhibition of C9ORF72 repeat transcripts prevents neurodegeneration and associated motor deficits. *Nat Commun, 8*, 16063.

Helmink, B. A., & Sleckman, B. P. (2012). The response to and repair of RAG-mediated DNA double-strand breaks. *Annu Rev Immunol, 30*, 175-202.

Herranz-Martin, S., Chandran, J., Lewis, K., Mulcahy, P., Higginbottom, A., Walker, C., . . . Azzouz, M. (2017). Viral delivery of C9orf72 hexanucleotide repeat expansions in mice leads to repeat-length-dependent neuropathology and behavioural deficits. *Dis Model Mech, 10*(7), 859-868.

Hill, S. J., Mordes, D. A., Cameron, L. A., Neuberg, D. S., Landini, S., Eggan, K., & Livingston, D. M. (2016). Two familial ALS proteins function in prevention/repair of transcription-associated DNA damage. *Proc Natl Acad Sci U S A, 113*(48), E7701-e7709.

Hoch, N. C., Hanzlikova, H., Rulten, S. L., Tétreault, M., Komulainen, E., Ju, L., . . . Caldecott, K. W. (2017). XRCC1 mutation is associated with PARP1 hyperactivation and cerebellar ataxia. *Nature, 541*(7635), 87-91.

Hodroj, D., Serhal, K., & Maiorano, D. (2017). Ddx19 links mRNA nuclear export with progression of transcription and replication and suppresses genomic instability upon DNA damage in proliferating cells. *Nucleus*, 1-7.

Hoeijmakers, J. H. (2009). DNA damage, aging, and cancer. *N Engl J Med, 361*(15), 1475-1485.

Hsiang, Y. H., Hertzberg, R., Hecht, S., & Liu, L. F. (1985). Camptothecin induces protein-linked DNA breaks via mammalian DNA topoisomerase I. *J Biol Chem, 260*(27), 14873-14878.

Hsu, J. Y., Sun, Z. W., Li, X., Reuben, M., Tatchell, K., Bishop, D. K., . . . Allis, C. D. (2000). Mitotic phosphorylation of histone H3 is governed by Ipl1/aurora kinase and Glc7/PP1 phosphatase in budding yeast and nematodes. *Cell, 102*(3), 279-291.

Huen, M. S., Grant, R., Manke, I., Minn, K., Yu, X., Yaffe, M. B., & Chen, J. (2007). RNF8 transduces the DNA-damage signal via histone ubiquitylation and checkpoint protein assembly. *Cell, 131*(5), 901-914.

Huen, M. S., Sy, S. M., & Chen, J. (2010). BRCA1 and its toolbox for the maintenance of genome integrity. *Nat Rev Mol Cell Biol, 11*(2), 138-148.

Huertas, P., & Aguilera, A. (2003). Cotranscriptionally formed DNA:RNA hybrids mediate transcription elongation impairment and transcription-associated recombination. *Mol Cell, 12*(3), 711-721.

Ichimura, Y., Kumanomidou, T., Sou, Y. S., Mizushima, T., Ezaki, J., Ueno, T., . . . Komatsu, M. (2008). Structural basis for sorting mechanism of p62 in selective autophagy. *J Biol Chem, 283*(33), 22847-22857.

Ishimura, R., Nagy, G., Dotu, I., Zhou, H., Yang, X.-L., Schimmel, P., . . . Ackerman, S. L. (2014). Ribosome stalling induced by mutation of a CNS-specific tRNA causes neurodegeneration. *Science (New York, N.Y.), 345*(6195), 455-459.

Iyama, T., & Wilson, D. M., 3rd. (2013). DNA repair mechanisms in dividing and non-dividing cells. *DNA Repair (Amst), 12*(8), 620-636.

Jackson, S. P., & Bartek, J. (2009). The DNA-damage response in human biology and disease. *Nature, 461*(7267), 1071-1078.

James, P. A., & Talbot, K. (2006). The molecular genetics of non-ALS motor neuron diseases. *Biochim Biophys Acta, 1762*(11-12), 986-1000.

Jangi, M., Fleet, C., Cullen, P., Gupta, S. V., Mekhoubad, S., Chiao, E., . . . Staropoli, J. F. (2017). SMN deficiency in severe models of spinal muscular atrophy causes widespread intron retention and DNA damage. *Proc Natl Acad Sci U S A, 114*(12), E2347-e2356.

Ji, A. L., Zhang, X., Chen, W. W., & Huang, W. J. (2017). Genetics insight into the amyotrophic lateral sclerosis/frontotemporal dementia spectrum. *J Med Genet, 54*(3), 145-154.

Jiang, J., Zhu, Q., Gendron, T. F., Saberi, S., McAlonis-Downes, M., Seelman, A., . . . Lagier-Tourenne, C. (2016). Gain of toxicity from ALS/FTD-linked repeat expansions in C9ORF72 is alleviated by antisense oligonucleotides targeting GGGGCC-containing RNAs. *Neuron, 90*(3), 535-550.

Jiricny, J. (2006). The multifaceted mismatch-repair system. *Nat Rev Mol Cell Biol, 7*(5), 335-346.

Johnson, E. M. (2003). The Pur protein family: clues to function from recent studies on cancer and AIDS. *Anticancer Res, 23*(3a), 2093-2100.

Johnson, E. M., Kinoshita, Y., Weinreb, D. B., Wortman, M. J., Simon, R., Khalili, K., . . . Gordon, J. (2006). Role of Pur alpha in targeting mRNA to sites of translation in hippocampal neuronal dendrites. *J Neurosci Res, 83*(6), 929-943.

Jovicic, A., Mertens, J., Boeynaems, S., Bogaert, E., Chai, N., Yamada, S. B., . . . Gitler, A. D. (2015). Modifiers of C9orf72 dipeptide repeat toxicity connect nucleocytoplasmic transport defects to FTD/ALS. *Nat Neurosci, 18*(9), 1226-1229.

Kaidi, A., & Jackson, S. P. (2013). KAT5 tyrosine phosphorylation couples chromatin sensing to ATM signalling. *Nature, 498*(7452), 70-74.

Kanno, S., Kuzuoka, H., Sasao, S., Hong, Z., Lan, L., Nakajima, S., & Yasui, A. (2007). A novel human AP endonuclease with conserved zinc-finger-like motifs involved in DNA strand break responses. *Embo j, 26*(8), 2094-2103.

Kanu, N., & Behrens, A. (2007). ATMIN defines an NBS1-independent pathway of ATM signalling. *Embo j, 26*(12), 2933-2941.

Kastan, M. B., & Lim, D. S. (2000). The many substrates and functions of ATM. *Nat Rev Mol Cell Biol, 1*(3), 179-186.

Katsuragi, Y., Ichimura, Y., & Komatsu, M. (2015). p62/SQSTM1 functions as a signaling hub and an autophagy adaptor. *Febs j, 282*(24), 4672-4678.

Katyal, S., el-Khamisy, S. F., Russell, H. R., Li, Y., Ju, L., Caldecott, K. W., & McKinnon, P. J. (2007). TDP1 facilitates chromosomal single-strand break repair in neurons and is neuroprotective in vivo. *Embo j, 26*(22), 4720-4731.

Katyal, S., Lee, Y., Nitiss, K. C., Downing, S. M., Li, Y., Shimada, M., . . . McKinnon, P. J. (2014). Aberrant topoisomerase-1 DNA lesions are pathogenic in neurodegenerative genome instability syndromes. *Nat Neurosci, 17*(6), 813-821.

Kawauchi, J., Mischo, H., Braglia, P., Rondon, A., & Proudfoot, N. J. (2008). Budding yeast RNA polymerases I and II employ parallel mechanisms of transcriptional termination. *Genes Dev, 22*(8), 1082-1092.

Kenna, K. P., van Doormaal, P. T., Dekker, A. M., Ticozzi, N., Kenna, B. J., Diekstra, F. P., . . . Landers, J. E. (2016). NEK1 variants confer susceptibility to amyotrophic lateral sclerosis. *Nat Genet, 48*(9), 1037-1042.

Khanna, K. K., & Jackson, S. P. (2001). DNA double-strand breaks: signaling, repair and the cancer connection. *Nat Genet, 27*(3), 247-254.

Kienker, L. J., Shin, E. K., & Meek, K. (2000). Both V(D)J recombination and radioresistance require DNA-PK kinase activity, though minimal levels suffice for V(D)J recombination. *Nucleic Acids Research, 28*(14), 2752-2761.

Kim, S. T., Lim, D. S., Canman, C. E., & Kastan, M. B. (1999). Substrate specificities and identification of putative substrates of ATM kinase family members. *J Biol Chem, 274*(53), 37538-37543.

Kitagawa, R., Bakkenist, C. J., McKinnon, P. J., & Kastan, M. B. (2004). Phosphorylation of SMC1 is a critical downstream event in the ATM-NBS1-BRCA1 pathway. *Genes Dev, 18*(12), 1423-1438.

Klionsky, D. J. (2007). Autophagy: from phenomenology to molecular understanding in less than a decade. *Nat Rev Mol Cell Biol, 8*(11), 931-937.
Kolas, N. K., Chapman, J. R., Nakada, S., Ylanko, J., Chahwan, R., Sweeney, F. D., . . . Durocher, D. (2007). Orchestration of the DNA-damage response by the RNF8 ubiquitin ligase. *Science, 318*(5856), 1637-1640.
Kolb, S. J., & Kissel, J. T. (2011). Spinal muscular atrophy: A timely review. *Archives of Neurology, 68*(8), 979-984.
Komatsu, M., Waguri, S., Koike, M., Sou, Y.-s., Ueno, T., Hara, T., . . . Tanaka, K. (2007). Homeostatic Levels of p62 Control Cytoplasmic Inclusion Body Formation in Autophagy-Deficient Mice. *Cell, 131*(6), 1149-1163.
Koppers, M., Blokhuis, A. M., Westeneng, H. J., Terpstra, M. L., Zundel, C. A., Vieira de Sa, R., . . . Pasterkamp, R. J. (2015). C9orf72 ablation in mice does not cause motor neuron degeneration or motor deficits. *Ann Neurol, 78*(3), 426-438.
Kovacs, G. G., van der Zee, J., Hort, J., Kristoferitsch, W., Leitha, T., Hoftberger, R., . . . Matej, R. (2016). Clinicopathological description of two cases with SQSTM1 gene mutation associated with frontotemporal dementia. *Neuropathology, 36*(1), 27-38.
Kozlov, S. V., Graham, M. E., Peng, C., Chen, P., Robinson, P. J., & Lavin, M. F. (2006). Involvement of novel autophosphorylation sites in ATM activation. *Embo j, 25*(15), 3504-3514.
Kraemer, K. H., Lee, M. M., & Scotto, J. (1987). Xeroderma pigmentosum. Cutaneous, ocular, and neurologic abnormalities in 830 published cases. *Arch Dermatol, 123*(2), 241-250.
Kurimasa, A., Kumano, S., Boubnov, N. V., Story, M. D., Tung, C. S., Peterson, S. R., & Chen, D. J. (1999). Requirement for the kinase activity of human DNA-dependent protein kinase catalytic subunit in DNA strand break rejoining. *Mol Cell Biol, 19*(5), 3877-3884.
Kwon, I., Xiang, S., Kato, M., Wu, L., Theodoropoulos, P., Wang, T., . . . McKnight, S. L. (2014). Poly-dipeptides encoded by the C9orf72 repeats bind nucleoli, impede RNA biogenesis, and kill cells. *Science, 345*(6201), 1139-1145.
Kwong, L. K., Neumann, M., Sampathu, D. M., Lee, V. M., & Trojanowski, J. Q. (2007). TDP-43 proteinopathy: the neuropathology underlying major forms of sporadic and familial frontotemporal lobar degeneration and motor neuron disease. *Acta Neuropathol, 114*(1), 63-70.
Lagier-Tourenne, C., Baughn, M., Rigo, F., Sun, S., Liu, P., Li, H. R., . . . Ravits, J. (2013). Targeted degradation of sense and antisense C9orf72 RNA foci as therapy for ALS and frontotemporal degeneration. *Proc Natl Acad Sci U S A, 110*(47), E4530-4539.
Lakin, N. D., Weber, P., Stankovic, T., Rottinghaus, S. T., Taylor, A. M., & Jackson, S. P. (1996). Analysis of the ATM protein in wild-type and ataxia telangiectasia cells. *Oncogene, 13*(12), 2707-2716.
Lavin, M. F., & Shiloh, Y. (1997). The genetic defect in ataxia-telangiectasia. *Annu Rev Immunol, 15*, 177-202.
Lee, J. H., Goodarzi, A. A., Jeggo, P. A., & Paull, T. T. (2010). 53BP1 promotes ATM activity through direct interactions with the MRN complex. *Embo j, 29*(3), 574-585.
Lee, J. H., & Paull, T. T. (2005). ATM activation by DNA double-strand breaks through the Mre11-Rad50-Nbs1 complex. *Science, 308*(5721), 551-554.
Lee, J. K., Shin, J. H., Lee, J. E., & Choi, E.-J. (2015). Role of autophagy in the pathogenesis of amyotrophic lateral sclerosis. *Biochimica et Biophysica Acta (BBA) - Molecular Basis of Disease, 1852*(11), 2517-2524.
Lee, K. H., Zhang, P., Kim, H. J., Mitrea, D. M., Sarkar, M., Freibaum, B. D., . . . Taylor, J. P. (2016). C9orf72 Dipeptide Repeats Impair the Assembly, Dynamics, and Function of Membrane-Less Organelles. *Cell, 167*(3), 774-788.e717.
Lee, Y. B., Chen, H. J., Peres, J. N., Gomez-Deza, J., Attig, J., Stalekar, M., . . . Shaw, C. E. (2013). Hexanucleotide repeats in ALS/FTD form length-dependent RNA foci, sequester RNA binding proteins, and are neurotoxic. *Cell Rep, 5*(5), 1178-1186.

Levine, T. P., Daniels, R. D., Gatta, A. T., Wong, L. H., & Hayes, M. J. (2013). The product of C9orf72, a gene strongly implicated in neurodegeneration, is structurally related to DENN Rab-GEFs. *Bioinformatics, 29*(4), 499-503.

Lewis, P. D., Corr, J. B., Arlett, C. F., & Harcourt, S. A. (1979). Increased sensitivity to gamma irradiation of skin fibroblasts in Friedreich's ataxia. *Lancet, 2*(8140), 474-475.

Li, J., Chen, J., Ricupero, C. L., Hart, R. P., Schwartz, M. S., Kusnecov, A., & Herrup, K. (2012). Nuclear accumulation of HDAC4 in ATM deficiency promotes neurodegeneration in ataxia telangiectasia. *Nat Med, 18*(5), 783-790.

Li, J., Hart, R. P., Mallimo, E. M., Swerdel, M. R., Kusnecov, A. W., & Herrup, K. (2013). EZH2-mediated H3K27 trimethylation mediates neurodegeneration in ataxia-telangiectasia. *Nat Neurosci, 16*(12), 1745-1753.

Li, X., & Manley, J. L. (2005). Inactivation of the SR protein splicing factor ASF/SF2 results in genomic instability. *Cell, 122*(3), 365-378.

Lim, D. S., Kim, S. T., Xu, B., Maser, R. S., Lin, J., Petrini, J. H., & Kastan, M. B. (2000). ATM phosphorylates p95/nbs1 in an S-phase checkpoint pathway. *Nature, 404*(6778), 613-617.

Lindahl, T., & Barnes, D. E. (2000). Repair of endogenous DNA damage. *Cold Spring Harb Symp Quant Biol, 65*, 127-133.

Lindquist, S. G., Duno, M., Batbayli, M., Puschmann, A., Braendgaard, H., Mardosiene, S., . . . Nielsen, J. E. (2013). Corticobasal and ataxia syndromes widen the spectrum of C9ORF72 hexanucleotide expansion disease. *Clin Genet, 83*(3), 279-283.

Ling, S. C., Polymenidou, M., & Cleveland, D. W. (2013). Converging mechanisms in ALS and FTD: disrupted RNA and protein homeostasis. *Neuron, 79*(3), 416-438.

Liu, Y., Pattamatta, A., Zu, T., Reid, T., Bardhi, O., Borchelt, D. R., . . . Ranum, L. P. (2016). C9orf72 BAC Mouse Model with Motor Deficits and Neurodegenerative Features of ALS/FTD. *Neuron, 90*(3), 521-534.

Longhese, M. P., Bonetti, D., Manfrini, N., & Clerici, M. (2010). Mechanisms and regulation of DNA end resection. *The EMBO Journal, 29*(17), 2864-2874.

Lopez-Gonzalez, R., Lu, Y., Gendron, T. F., Karydas, A., Tran, H., Yang, D., . . . Gao, F. B. (2016). Poly(GR) in C9ORF72-Related ALS/FTD Compromises Mitochondrial Function and Increases Oxidative Stress and DNA Damage in iPSC-Derived Motor Neurons. *Neuron, 92*(2), 383-391.

Lou, Z., Minter-Dykhouse, K., Franco, S., Gostissa, M., Rivera, M. A., Celeste, A., . . . Chen, J. (2006). MDC1 maintains genomic stability by participating in the amplification of ATM-dependent DNA damage signals. *Mol Cell, 21*(2), 187-200.

Lukas, C., Falck, J., Bartkova, J., Bartek, J., & Lukas, J. (2003). Distinct spatiotemporal dynamics of mammalian checkpoint regulators induced by DNA damage. *Nat Cell Biol, 5*(3), 255-260.

Ma, Y., Pannicke, U., Schwarz, K., & Lieber, M. R. (2002). Hairpin opening and overhang processing by an Artemis/DNA-dependent protein kinase complex in nonhomologous end joining and V(D)J recombination. *Cell, 108*(6), 781-794.

Mackenzie, I. R., Arzberger, T., Kremmer, E., Troost, D., Lorenzl, S., Mori, K., . . . Neumann, M. (2013). Dipeptide repeat protein pathology in C9ORF72 mutation cases: clinico-pathological correlations. *Acta Neuropathol, 126*(6), 859-879.

Mackenzie, I. R., Frick, P., Grasser, F. A., Gendron, T. F., Petrucelli, L., Cashman, N. R., . . . Neumann, M. (2015). Quantitative analysis and clinico-pathological correlations of different dipeptide repeat protein pathologies in C9ORF72 mutation carriers. *Acta Neuropathol, 130*(6), 845-861.

Madabhushi, R., Pan, L., & Tsai, L. H. (2014). DNA damage and its links to neurodegeneration. *Neuron, 83*(2), 266-282.

Magistretti, P. J., & Pellerin, L. (1996). Cellular mechanisms of brain energy metabolism. Relevance to functional brain imaging and to neurodegenerative disorders. *Ann N Y Acad Sci, 777*, 380-387.

Mailand, N., Bekker-Jensen, S., Faustrup, H., Melander, F., Bartek, J., Lukas, C., & Lukas, J. (2007). RNF8 ubiquitylates histones at DNA double-strand breaks and promotes assembly of repair proteins. *Cell, 131*(5), 887-900.

Mann, D. M. A., Rollinson, S., Robinson, A., Bennion Callister, J., Thompson, J. C., Snowden, J. S., . . . Pickering-Brown, S. (2013). Dipeptide repeat proteins are present in the p62 positive inclusions in patients with frontotemporal lobar degeneration and motor neurone disease associated with expansions in C9ORF72. *Acta Neuropathologica Communications, 1*, 68-68.

Mari, P. O., Florea, B. I., Persengiev, S. P., Verkaik, N. S., Bruggenwirth, H. T., Modesti, M., . . . van Gent, D. C. (2006). Dynamic assembly of end-joining complexes requires interaction between Ku70/80 and XRCC4. *Proc Natl Acad Sci U S A, 103*(49), 18597-18602.

Masukata, H., & Tomizawa, J. (1984). Effects of point mutations on formation and structure of the RNA primer for ColE1 DNA replication. *Cell, 36*(2), 513-522.

Matsumoto, G., Wada, K., Okuno, M., Kurosawa, M., & Nukina, N. (2011). Serine 403 Phosphorylation of p62/SQSTM1 Regulates Selective Autophagic Clearance of Ubiquitinated Proteins. *Molecular Cell, 44*(2), 279-289.

Matsuoka, S., Ballif, B. A., Smogorzewska, A., McDonald, E. R., Hurov, K. E., Luo, J., . . . Elledge, S. J. (2007). ATM and ATR Substrate Analysis Reveals Extensive Protein Networks Responsive to DNA Damage. *Science, 316*(5828), 1160-1166.

May, S., Hornburg, D., Schludi, M. H., Arzberger, T., Rentzsch, K., Schwenk, B. M., . . . Edbauer, D. (2014). C9orf72 FTLD/ALS-associated Gly-Ala dipeptide repeat proteins cause neuronal toxicity and Unc119 sequestration. *Acta Neuropathol, 128*(4), 485-503.

McCloy, R. A., Rogers, S., Caldon, C. E., Lorca, T., Castro, A., & Burgess, A. (2014). Partial inhibition of Cdk1 in G 2 phase overrides the SAC and decouples mitotic events. *Cell Cycle, 13*(9), 1400-1412.

Meek, K., Dang, V., & Lees-Miller, S. P. (2008). DNA-PK: the means to justify the ends? *Adv Immunol, 99*, 33-58.

Meisenberg, C., Ashour, M. E., El-Shafie, L., Liao, C., Hodgson, A., Pilborough, A., . . . El-Khamisy, S. F. (2017). Epigenetic changes in histone acetylation underpin resistance to the topoisomerase I inhibitor irinotecan. *Nucleic Acids Research, 45*(3), 1159-1176.

Mimaki, T., Itoh, N., Abe, J., Tagawa, T., Sato, K., Yabuuchi, H., & Takebe, H. (1986). Neurological manifestations in xeroderma pigmentosum. *Ann Neurol, 20*(1), 70-75.

Mischo, H. E., Gomez-Gonzalez, B., Grzechnik, P., Rondon, A. G., Wei, W., Steinmetz, L., . . . Proudfoot, N. J. (2011). Yeast Sen1 helicase protects the genome from transcription-associated instability. *Mol Cell, 41*(1), 21-32.

Mizielinska, S., Gronke, S., Niccoli, T., Ridler, C. E., Clayton, E. L., Devoy, A., . . . Isaacs, A. M. (2014). C9orf72 repeat expansions cause neurodegeneration in Drosophila through arginine-rich proteins. *Science, 345*(6201), 1192-1194.

Mizielinska, S., & Isaacs, A. M. (2014). C9orf72 amyotrophic lateral sclerosis and frontotemporal dementia: gain or loss of function? *Curr Opin Neurol, 27*(5), 515-523.

Mizuno, Y., Amari, M., Takatama, M., Aizawa, H., Mihara, B., & Okamoto, K. (2006). Immunoreactivities of p62, an ubiqutin-binding protein, in the spinal anterior horn cells of patients with amyotrophic lateral sclerosis. *J Neurol Sci, 249*(1), 13-18.

Mizushima, N., & Komatsu, M. (2011). Autophagy: renovation of cells and tissues. *Cell, 147*(4), 728-741.

Mizushima, N., Yoshimori, T., & Ohsumi, Y. (2011). The role of Atg proteins in autophagosome formation. *Annu Rev Cell Dev Biol, 27*, 107-132.

Moreira, M. C., Barbot, C., Tachi, N., Kozuka, N., Uchida, E., Gibson, T., . . . Koenig, M. (2001). The gene mutated in ataxia-ocular apraxia 1 encodes the new HIT/Zn-finger protein aprataxin. *Nat Genet, 29*(2), 189-193.

Mori, K., Weng, S. M., Arzberger, T., May, S., Rentzsch, K., Kremmer, E., . . . Edbauer, D. (2013). The C9orf72 GGGGCC repeat is translated into aggregating dipeptide-repeat proteins in FTLD/ALS. *Science, 339*(6125), 1335-1338.

Morris, J. R., Boutell, C., Keppler, M., Densham, R., Weekes, D., Alamshah, A., . . . Solomon, E. (2009). The SUMO modification pathway is involved in the BRCA1 response to genotoxic stress. *Nature, 462*(7275), 886-890.

Moshous, D., Pannetier, C., Chasseval Rd, R., Deist Fl, F., Cavazzana-Calvo, M., Romana, S., . . . Villartay, J. P. (2003). Partial T and B lymphocyte immunodeficiency and predisposition to lymphoma in patients with hypomorphic mutations in Artemis. *J Clin Invest, 111*(3), 381-387.

Mu, J. J., Wang, Y., Luo, H., Leng, M., Zhang, J., Yang, T., . . . Qin, J. (2007). A proteomic analysis of ataxia telangiectasia-mutated (ATM)/ATM-Rad3-related (ATR) substrates identifies the ubiquitin-proteasome system as a regulator for DNA damage checkpoints. *J Biol Chem, 282*(24), 17330-17334.

Murante, R. S., Henricksen, L. A., & Bambara, R. A. (1998). Junction ribonuclease: an activity in Okazaki fragment processing. *Proc Natl Acad Sci U S A, 95*(5), 2244-2249.

Murata, T., Ohtsuka, C., & Terayama, Y. (2008). Increased mitochondrial oxidative damage and oxidative DNA damage contributes to the neurodegenerative process in sporadic amyotrophic lateral sclerosis. *Free Radic Res, 42*(3), 221-225.

Nagaoka, U., Kim, K., Jana, N. R., Doi, H., Maruyama, M., Mitsui, K., . . . Nukina, N. (2004). Increased expression of p62 in expanded polyglutamine-expressing cells and its association with polyglutamine inclusions. *J Neurochem, 91*(1), 57-68.

Neumann, M., Sampathu, D. M., Kwong, L. K., Truax, A. C., Micsenyi, M. C., Chou, T. T., . . . Lee, V. M. (2006). Ubiquitinated TDP-43 in frontotemporal lobar degeneration and amyotrophic lateral sclerosis. *Science, 314*(5796), 130-133.

New, J. H., Sugiyama, T., Zaitseva, E., & Kowalczykowski, S. C. (1998). Rad52 protein stimulates DNA strand exchange by Rad51 and replication protein A. *Nature, 391*(6665), 407-410.

Nezis, I. P., Simonsen, A., Sagona, A. P., Finley, K., Gaumer, S., Contamine, D., . . . Brech, A. (2008). Ref(2)P, the Drosophila melanogaster homologue of mammalian p62, is required for the formation of protein aggregates in adult brain. *J Cell Biol, 180*(6), 1065-1071.

Noon, A. T., Shibata, A., Rief, N., Lobrich, M., Stewart, G. S., Jeggo, P. A., & Goodarzi, A. A. (2010). 53BP1-dependent robust localized KAP-1 phosphorylation is essential for heterochromatic DNA double-strand break repair. *Nat Cell Biol, 12*(2), 177-184.

O'Neill, T., Dwyer, A. J., Ziv, Y., Chan, D. W., Lees-Miller, S. P., Abraham, R. H., . . . Rathbun, G. A. (2000). Utilization of oriented peptide libraries to identify substrate motifs selected by ATM. *J Biol Chem, 275*(30), 22719-22727.

O'Rourke, J. G., Bogdanik, L., Muhammad, A. K., Gendron, T. F., Kim, K. J., Austin, A., . . . Baloh, R. H. (2015). C9orf72 BAC Transgenic Mice Display Typical Pathologic Features of ALS/FTD. *Neuron, 88*(5), 892-901.

O'Rourke, J. G., Bogdanik, L., Yanez, A., Lall, D., Wolf, A. J., Muhammad, A. K., . . . Baloh, R. H. (2016). C9orf72 is required for proper macrophage and microglial function in mice. *Science, 351*(6279), 1324-1329.

Palau, F., & Espinos, C. (2006). Autosomal recessive cerebellar ataxias. *Orphanet J Rare Dis, 1*, 47.

Pankiv, S., Clausen, T. H., Lamark, T., Brech, A., Bruun, J. A., Outzen, H., . . . Johansen, T. (2007). p62/SQSTM1 binds directly to Atg8/LC3 to facilitate degradation of ubiquitinated protein aggregates by autophagy. *J Biol Chem, 282*(33), 24131-24145.

Paull, T. T. (2015). Mechanisms of ATM Activation. *Annu Rev Biochem, 84*, 711-738.

Perry, J., & Kleckner, N. (2003). The ATRs, ATMs, and TORs are giant HEAT repeat proteins. *Cell, 112*(2), 151-155.

Peters, O. M., Cabrera, G. T., Tran, H., Gendron, T. F., McKeon, J. E., Metterville, J., . . . Brown, R. H., Jr. (2015). Human C9ORF72 Hexanucleotide Expansion Reproduces RNA Foci and Dipeptide

Repeat Proteins but Not Neurodegeneration in BAC Transgenic Mice. *Neuron, 88*(5), 902-909.
Polymenidou, M., Lagier-Tourenne, C., Hutt, K. R., Huelga, S. C., Moran, J., Liang, T. Y., . . . Cleveland, D. W. (2011). Long pre-mRNA depletion and RNA missplicing contribute to neuronal vulnerability from loss of TDP-43. *Nat Neurosci, 14*(4), 459-468.
Pouliot, J. J., Yao, K. C., Robertson, C. A., & Nash, H. A. (1999). Yeast gene for a Tyr-DNA phosphodiesterase that repairs topoisomerase I complexes. *Science, 286*(5439), 552-555.
Prudencio, M., Belzil, V. V., Batra, R., Ross, C. A., Gendron, T. F., Pregent, L. J., . . . Petrucelli, L. (2015). Distinct brain transcriptome profiles in C9orf72-associated and sporadic ALS. *Nat Neurosci, 18*(8), 1175-1182.
Reddy, K., Zamiri, B., Stanley, S. Y., Macgregor, R. B., Jr., & Pearson, C. E. (2013). The disease-associated r(GGGGCC)n repeat from the C9orf72 gene forms tract length-dependent uni- and multimolecular RNA G-quadruplex structures. *J Biol Chem, 288*(14), 9860-9866.
Renton, A. E., Majounie, E., Waite, A., Simon-Sanchez, J., Rollinson, S., Gibbs, J. R., . . . Traynor, B. J. (2011). A hexanucleotide repeat expansion in C9ORF72 is the cause of chromosome 9p21-linked ALS-FTD. *Neuron, 72*(2), 257-268.
Roberts, S. A., Strande, N., Burkhalter, M. D., Strom, C., Havener, J. M., Hasty, P., & Ramsden, D. A. (2010). Ku is a 5'-dRP/AP lyase that excises nucleotide damage near broken ends. *Nature, 464*(7292), 1214-1217.
Rogakou, E. P., Pilch, D. R., Orr, A. H., Ivanova, V. S., & Bonner, W. M. (1998). DNA double-stranded breaks induce histone H2AX phosphorylation on serine 139. *J Biol Chem, 273*(10), 5858-5868.
Rosen, D. R., Siddique, T., Patterson, D., Figlewicz, D. A., Sapp, P., Hentati, A., . . . *et al.* (1993). Mutations in Cu/Zn superoxide dismutase gene are associated with familial amyotrophic lateral sclerosis. *Nature, 362*(6415), 59-62.
Rossi, S., Serrano, A., Gerbino, V., Giorgi, A., Di Francesco, L., Nencini, M., . . . Cozzolino, M. (2015). Nuclear accumulation of mRNAs underlies G4C2-repeat-induced translational repression in a cellular model of C9orf72 ALS. *J Cell Sci, 128*(9), 1787-1799.
Roy, D., & Lieber, M. R. (2009). G clustering is important for the initiation of transcription-induced R-loops in vitro, whereas high G density without clustering is sufficient thereafter. *Mol Cell Biol, 29*(11), 3124-3133.
Rulten, S. L., & Caldecott, K. W. (2013). DNA strand break repair and neurodegeneration. *DNA Repair (Amst), 12*(8), 558-567.
Rulten, S. L., Fisher, A. E., Robert, I., Zuma, M. C., Rouleau, M., Ju, L., . . . Caldecott, K. W. (2011). PARP-3 and APLF function together to accelerate nonhomologous end-joining. *Mol Cell, 41*(1), 33-45.
Rulten, S. L., Rotheray, A., Green, R. L., Grundy, G. J., Moore, D. A. Q., Gómez-Herreros, F., . . . Caldecott, K. W. (2014). PARP-1 dependent recruitment of the amyotrophic lateral sclerosis-associated protein FUS/TLS to sites of oxidative DNA damage. *Nucleic Acids Research, 42*(1), 307-314.
Rusten, T. E., & Stenmark, H. (2010). p62, an autophagy hero or culprit? *Nat Cell Biol, 12*(3), 207-209.
Santos-Pereira, J. M., & Aguilera, A. (2015). R loops: new modulators of genome dynamics and function. *Nat Rev Genet, 16*(10), 583-597.
Santos-Pereira, J. M., Herrero, A. B., Garcia-Rubio, M. L., Marin, A., Moreno, S., & Aguilera, A. (2013). The Npl3 hnRNP prevents R-loop-mediated transcription-replication conflicts and genome instability. *Genes Dev, 27*(22), 2445-2458.
Sareen, D., O'Rourke, J. G., Meera, P., Muhammad, A., Grant, S., Simpkinson, M., . . . Baloh, R. H. (2013). Targeting RNA foci in iPSC-derived motor neurons from ALS patients with C9ORF72 repeat expansion. *Science translational medicine, 5*(208), 208ra149-208ra149.
Sasaki, S. (2011). Autophagy in Spinal Cord Motor Neurons in Sporadic Amyotrophic Lateral Sclerosis. *Journal of Neuropathology & Experimental Neurology, 70*(5), 349-359.

Schludi, M. H., May, S., Grasser, F. A., Rentzsch, K., Kremmer, E., Kupper, C., . . . Edbauer, D. (2015). Distribution of dipeptide repeat proteins in cellular models and C9orf72 mutation cases suggests link to transcriptional silencing. *Acta Neuropathol, 130*(4), 537-555.

Schrader, M., & Fahimi, H. D. (2006). Peroxisomes and oxidative stress. *Biochim Biophys Acta, 1763*(12), 1755-1766.

Sellier, C., Campanari, M. L., Julie Corbier, C., Gaucherot, A., Kolb-Cheynel, I., Oulad-Abdelghani, M., . . . Charlet-Berguerand, N. (2016). Loss of C9ORF72 impairs autophagy and synergizes with polyQ Ataxin-2 to induce motor neuron dysfunction and cell death. *Embo j, 35*(12), 1276-1297.

Seshacharyulu, P., Pandey, P., Datta, K., & Batra, S. K. (2013). Phosphatase: PP2A structural importance, regulation and its aberrant expression in cancer. *Cancer Lett, 335*(1), 9-18.

Shiloh, Y. (2003). ATM and related protein kinases: safeguarding genome integrity. *Nat Rev Cancer, 3*(3), 155-168.

Shiloh, Y., & Ziv, Y. (2013). The ATM protein kinase: regulating the cellular response to genotoxic stress, and more. *Nat Rev Mol Cell Biol, 14*(4), 197-210.

Sivadasan, R., Hornburg, D., Drepper, C., Frank, N., Jablonka, S., Hansel, A., . . . Sendtner, M. (2016). C9ORF72 interaction with cofilin modulates actin dynamics in motor neurons. *Nat Neurosci, 19*(12), 1610-1618.

Sket, P., Pohleven, J., Kovanda, A., Stalekar, M., Zupunski, V., Zalar, M., . . . Rogelj, B. (2015). Characterization of DNA G-quadruplex species forming from C9ORF72 G4C2-expanded repeats associated with amyotrophic lateral sclerosis and frontotemporal lobar degeneration. *Neurobiol Aging, 36*(2), 1091-1096.

Skourti-Stathaki, K., Kamieniarz-Gdula, K., & Proudfoot, N. J. (2014). R-loops induce repressive chromatin marks over mammalian gene terminators. *Nature, 516*(7531), 436-439.

Skourti-Stathaki, K., & Proudfoot, N. J. (2014). A double-edged sword: R loops as threats to genome integrity and powerful regulators of gene expression. *Genes Dev, 28*(13), 1384-1396.

Skourti-Stathaki, K., Proudfoot, N. J., & Gromak, N. (2011). Human senataxin resolves RNA/DNA hybrids formed at transcriptional pause sites to promote Xrn2-dependent termination. *Mol Cell, 42*(6), 794-805.

Smith, G. C., Cary, R. B., Lakin, N. D., Hann, B. C., Teo, S. H., Chen, D. J., & Jackson, S. P. (1999). Purification and DNA binding properties of the ataxia-telangiectasia gene product ATM. *Proc Natl Acad Sci U S A, 96*(20), 11134-11139.

Sollier, J., Stork, C. T., Garcia-Rubio, M. L., Paulsen, R. D., Aguilera, A., & Cimprich, K. A. (2014). Transcription-coupled nucleotide excision repair factors promote R-loop-induced genome instability. *Mol Cell, 56*(6), 777-785.

Song, C., Hotz-Wagenblatt, A., Voit, R., & Grummt, I. (2017). SIRT7 and the DEAD-box helicase DDX21 cooperate to resolve genomic R loops and safeguard genome stability. *Genes Dev*.

Spescha, R. D., Shi, Y., Wegener, S., Keller, S., Weber, B., Wyss, M. M., . . . Camici, G. G. (2013). Deletion of the ageing gene p66(Shc) reduces early stroke size following ischaemia/reperfusion brain injury. *Eur Heart J, 34*(2), 96-103.

Staker, B. L., Hjerrild, K., Feese, M. D., Behnke, C. A., Burgin, A. B., & Stewart, L. (2002). The mechanism of topoisomerase I poisoning by a camptothecin analog. *Proceedings of the National Academy of Sciences of the United States of America, 99*(24), 15387-15392.

Stewart, G. S., Panier, S., Townsend, K., Al-Hakim, A. K., Kolas, N. K., Miller, E. S., . . . Durocher, D. (2009). The RIDDLE syndrome protein mediates a ubiquitin-dependent signaling cascade at sites of DNA damage. *Cell, 136*(3), 420-434.

Stewart, G. S., Stankovic, T., Byrd, P. J., Wechsler, T., Miller, E. S., Huissoon, A., . . . Taylor, A. M. (2007). RIDDLE immunodeficiency syndrome is linked to defects in 53BP1-mediated DNA damage signaling. *Proc Natl Acad Sci U S A, 104*(43), 16910-16915.

Stolz, A., Ernst, A., & Dikic, I. (2014). Cargo recognition and trafficking in selective autophagy. *Nat Cell Biol, 16*(6), 495-501.

Su, Z., Zhang, Y., Gendron, T. F., Bauer, P. O., Chew, J., Yang, W. Y., . . . Disney, M. D. (2014). Discovery of a biomarker and lead small molecules to target r(GGGGCC)-associated defects in c9FTD/ALS. *Neuron, 83*(5), 1043-1050.

Sudria-Lopez, E., Koppers, M., de Wit, M., van der Meer, C., Westeneng, H. J., Zundel, C. A., . . . Pasterkamp, R. J. (2016). Full ablation of C9orf72 in mice causes immune system-related pathology and neoplastic events but no motor neuron defects. *Acta Neuropathol, 132*(1), 145-147.

Sutovsky, S., Smolek, T., Alafuzoff, I., Blaho, A., Parrak, V., Turcani, P., . . . Zilka, N. (2016). Atypical Huntington's disease with the clinical presentation of behavioural variant of frontotemporal dementia. *J Neural Transm (Vienna), 123*(12), 1423-1433.

Suzuki, K., Kodama, S., & Watanabe, M. (1999). Recruitment of ATM protein to double strand DNA irradiated with ionizing radiation. *J Biol Chem, 274*(36), 25571-25575.

Tan, S. L. W., Chadha, S., Liu, Y., Gabasova, E., Perera, D., Ahmed, K., . . . Venkitaraman, A. R. (2017). A Class of Environmental and Endogenous Toxins Induces BRCA2 Haploinsufficiency and Genome Instability. *Cell, 169*(6), 1105-1118.e1115.

Tao, Z., Wang, H., Xia, Q., Li, K., Li, K., Jiang, X., . . . Ying, Z. (2015). Nucleolar stress and impaired stress granule formation contribute to C9orf72 RAN translation-induced cytotoxicity. *Hum Mol Genet, 24*(9), 2426-2441.

Taylor, A. M., Groom, A., & Byrd, P. J. (2004). Ataxia-telangiectasia-like disorder (ATLD)-its clinical presentation and molecular basis. *DNA Repair (Amst), 3*(8-9), 1219-1225.

Therrien, M., Rouleau, G. A., Dion, P. A., & Parker, J. A. (2013). Deletion of C9ORF72 results in motor neuron degeneration and stress sensitivity in C. elegans. *PLoS One, 8*(12), e83450.

Tresini, M., Warmerdam, D. O., Kolovos, P., Snijder, L., Vrouwe, M. G., Demmers, J. A., . . . Marteijn, J. A. (2015). The core spliceosome as target and effector of non-canonical ATM signalling. *Nature, 523*(7558), 53-58.

Troakes, C., Maekawa, S., Wijesekera, L., Rogelj, B., Siklos, L., Bell, C., . . . Al-Sarraj, S. (2012). An MND/ALS phenotype associated with C9orf72 repeat expansion: abundant p62-positive, TDP-43-negative inclusions in cerebral cortex, hippocampus and cerebellum but without associated cognitive decline. *Neuropathology, 32*(5), 505-514.

Tuduri, S., Crabbe, L., Conti, C., Tourriere, H., Holtgreve-Grez, H., Jauch, A., . . . Pasero, P. (2009). Topoisomerase I suppresses genomic instability by preventing interference between replication and transcription. *Nat Cell Biol, 11*(11), 1315-1324.

Uematsu, N., Weterings, E., Yano, K., Morotomi-Yano, K., Jakob, B., Taucher-Scholz, G., . . . Chen, D. J. (2007). Autophosphorylation of DNA-PKCS regulates its dynamics at DNA double-strand breaks. *J Cell Biol, 177*(2), 219-229.

Uziel, T., Lerenthal, Y., Moyal, L., Andegeko, Y., Mittelman, L., & Shiloh, Y. (2003). Requirement of the MRN complex for ATM activation by DNA damage. *Embo j, 22*(20), 5612-5621.

Valdmanis, P. N., & Rouleau, G. A. (2008). Genetics of familial amyotrophic lateral sclerosis. *Neurology, 70*(2), 144-152.

Valko, M., Rhodes, C. J., Moncol, J., Izakovic, M., & Mazur, M. (2006). Free radicals, metals and antioxidants in oxidative stress-induced cancer. *Chem Biol Interact, 160*(1), 1-40.

van den Bosch, M., Bree, R. T., & Lowndes, N. F. (2003). The MRN complex: coordinating and mediating the response to broken chromosomes. *EMBO Rep, 4*(9), 844-849. doi:10.1038/sj.embor.embor925

Vaz, B., Popovic, M., Newman, Joseph A., Fielden, J., Aitkenhead, H., Halder, S., . . . Ramadan, K. (2016). Metalloprotease SPRTN/DVC1 Orchestrates Replication-Coupled DNA-Protein Crosslink Repair. *Molecular Cell, 64*(4), 704-719.

Wahba, L., Amon, J. D., Koshland, D., & Vuica-Ross, M. (2011). RNase H and multiple RNA biogenesis factors cooperate to prevent RNA:DNA hybrids from generating genome instability. *Mol Cell, 44*(6), 978-988.

Waite, A. J., Baumer, D., East, S., Neal, J., Morris, H. R., Ansorge, O., & Blake, D. J. (2014). Reduced C9orf72 protein levels in frontal cortex of amyotrophic lateral sclerosis and frontotemporal degeneration brain with the C9ORF72 hexanucleotide repeat expansion. *Neurobiol Aging, 35*(7), 1779.e1775-1779.e1713.

Walker, C., Herranz-Martin, S., Karyka, E., Liao, C., Lewis, K., Elsayed, W., . . . El-Khamisy, S. F. (2017). C9orf72 expansion disrupts ATM-mediated chromosomal break repair. *Nat Neurosci, 20*(9), 1225-1235.

Walker, J. R., Corpina, R. A., & Goldberg, J. (2001). Structure of the Ku heterodimer bound to DNA and its implications for double-strand break repair. *Nature, 412*(6847), 607-614.

Wang, B., & Elledge, S. J. (2007). Ubc13/Rnf8 ubiquitin ligases control foci formation of the Rap80/Abraxas/Brca1/Brcc36 complex in response to DNA damage. *Proc Natl Acad Sci U S A, 104*(52), 20759-20763.

Wang, B., Matsuoka, S., Carpenter, P. B., & Elledge, S. J. (2002). 53BP1, a mediator of the DNA damage checkpoint. *Science, 298*(5597), 1435-1438.

Wang, J. C. (2002). Cellular roles of DNA topoisomerases: a molecular perspective. *Nat Rev Mol Cell Biol, 3*(6), 430-440.

Wang, W. Y., Pan, L., Su, S. C., Quinn, E. J., Sasaki, M., Jimenez, J. C., . . . Tsai, L. H. (2013). Interaction of FUS and HDAC1 regulates DNA damage response and repair in neurons. *Nat Neurosci, 16*(10), 1383-1391.

Wang, X., Blanchard, J., Grundke-Iqbal, I., Wegiel, J., Deng, H. X., Siddique, T., & Iqbal, K. (2014). Alzheimer disease and amyotrophic lateral sclerosis: an etiopathogenic connection. *Acta Neuropathol, 127*(2), 243-256.

Wang, Y., Zhang, N., Zhang, L., Li, R., Fu, W., Ma, K., . . . Zhao, Y. (2016). Autophagy Regulates Chromatin Ubiquitination in DNA Damage Response through Elimination of SQSTM1/p62. *Molecular Cell, 63*(1), 34-48.

Watts, F. Z. (2016). Repair of DNA Double-Strand Breaks in Heterochromatin. *Biomolecules, 6*(4), 47.

Webster, C. P., Smith, E. F., Bauer, C. S., Moller, A., Hautbergue, G. M., Ferraiuolo, L., . . . De Vos, K. J. (2016). The C9orf72 protein interacts with Rab1a and the ULK1 complex to regulate initiation of autophagy. *Embo j, 35*(15), 1656-1676.

Weinfeld, M., Mani, R. S., Abdou, I., Acetuno, R. D., & Glover, J. N. M. (2011). Tidying up loose ends: the role of polynucleotide kinase/phosphatase in DNA strand break repair. *Trends in biochemical sciences, 36*(5), 262-271.

Weissman, L., de Souza-Pinto, N. C., Stevnsner, T., & Bohr, V. A. (2007). DNA repair, mitochondria, and neurodegeneration. *Neuroscience, 145*(4), 1318-1329.

Wen, X., Tan, W., Westergard, T., Krishnamurthy, K., Markandaiah, S. S., Shi, Y., . . . Trotti, D. (2014). Antisense proline-arginine RAN dipeptides linked to C9ORF72-ALS/FTD form toxic nuclear aggregates that initiate in vitro and in vivo neuronal death. *Neuron, 84*(6), 1213-1225.

West, S. C. (2003). Molecular views of recombination proteins and their control. *Nat Rev Mol Cell Biol, 4*(6), 435-445. doi:10.1038/nrm1127

Williams, R. S., & Tainer, J. A. (2007). Learning our ABCs: Rad50 directs MRN repair functions via adenylate kinase activity from the conserved ATP binding cassette. *Mol Cell, 25*(6), 789-791.

Williams, R. S., Williams, J. S., & Tainer, J. A. (2007). Mre11-Rad50-Nbs1 is a keystone complex connecting DNA repair machinery, double-strand break signaling, and the chromatin template. *Biochem Cell Biol, 85*(4), 509-520.

Woodbine, L., Gennery, A. R., & Jeggo, P. A. (2014). The clinical impact of deficiency in DNA non-homologous end-joining. *DNA Repair (Amst), 16*, 84-96.

Wu, Y., Hou, F., Wang, X., Kong, Q., Han, X., & Bai, B. (2016). Aberrant Expression of Histone Deacetylases 4 in Cognitive Disorders: Molecular Mechanisms and a Potential Target. *Frontiers in Molecular Neuroscience, 9*, 114.

Xiao, S., MacNair, L., McGoldrick, P., McKeever, P. M., McLean, J. R., Zhang, M., . . . Robertson, J. (2015). Isoform-specific antibodies reveal distinct subcellular localizations of C9orf72 in amyotrophic lateral sclerosis. *Ann Neurol, 78*(4), 568-583.

Xu, B., & Clayton, D. A. (1996). RNA-DNA hybrid formation at the human mitochondrial heavy-strand origin ceases at replication start sites: an implication for RNA-DNA hybrids serving as primers. *Embo j, 15*(12), 3135-3143.

Xu, Z., Poidevin, M., Li, X., Li, Y., Shu, L., Nelson, D. L., . . . Jin, P. (2013). Expanded GGGGCC repeat RNA associated with amyotrophic lateral sclerosis and frontotemporal dementia causes neurodegeneration. *Proc Natl Acad Sci U S A, 110*(19), 7778-7783.

Yang, C., Wang, H., Qiao, T., Yang, B., Aliaga, L., Qiu, L., . . . Xu, Z. (2014). Partial loss of TDP-43 function causes phenotypes of amyotrophic lateral sclerosis. *Proc Natl Acad Sci U S A, 111*(12), E1121-1129.

Yang, D., Abdallah, A., Li, Z., Lu, Y., Almeida, S., & Gao, F. B. (2015). FTD/ALS-associated poly(GR) protein impairs the Notch pathway and is recruited by poly(GA) into cytoplasmic inclusions. *Acta Neuropathol, 130*(4), 525-535.

Yang, D. Q., Halaby, M. J., Li, Y., Hibma, J. C., & Burn, P. (2011). Cytoplasmic ATM protein kinase: an emerging therapeutic target for diabetes, cancer and neuronal degeneration. *Drug Discov Today, 16*(7-8), 332-338.

Yang, M., Liang, C., Swaminathan, K., Herrlinger, S., Lai, F., Shiekhattar, R., & Chen, J. F. (2016). A C9ORF72/SMCR8-containing complex regulates ULK1 and plays a dual role in autophagy. *Sci Adv, 2*(9), e1601167.

Yang, S. W., Burgin, A. B., Jr., Huizenga, B. N., Robertson, C. A., Yao, K. C., & Nash, H. A. (1996). A eukaryotic enzyme that can disjoin dead-end covalent complexes between DNA and type I topoisomerases. *Proc Natl Acad Sci U S A, 93*(21), 11534-11539.

Yazdi, P. T., Wang, Y., Zhao, S., Patel, N., Lee, E. Y., & Qin, J. (2002). SMC1 is a downstream effector in the ATM/NBS1 branch of the human S-phase checkpoint. *Genes Dev, 16*(5), 571-582.

Yu, K., Chedin, F., Hsieh, C. L., Wilson, T. E., & Lieber, M. R. (2003). R-loops at immunoglobulin class switch regions in the chromosomes of stimulated B cells. *Nat Immunol, 4*(5), 442-451.

Yuce, O., & West, S. C. (2013). Senataxin, defective in the neurodegenerative disorder ataxia with oculomotor apraxia 2, lies at the interface of transcription and the DNA damage response. *Mol Cell Biol, 33*(2), 406-417.

Zamiri, B., Reddy, K., Macgregor, R. B., Jr., & Pearson, C. E. (2014). TMPyP4 porphyrin distorts RNA G-quadruplex structures of the disease-associated r(GGGGCC)n repeat of the C9orf72 gene and blocks interaction of RNA-binding proteins. *J Biol Chem, 289*(8), 4653-4659.

Zeller, P., Padeken, J., van Schendel, R., Kalck, V., Tijsterman, M., & Gasser, S. M. (2016). Histone H3K9 methylation is dispensable for Caenorhabditis elegans development but suppresses RNA:DNA hybrid-associated repeat instability. *Nat Genet, 48*(11), 1385-1395. doi:10.1038/ng.3672

Zhang, J., Tripathi, D. N., Jing, J., Alexander, A., Kim, J., Powell, R. T., . . . Walker, C. L. (2015b). ATM functions at the peroxisome to induce pexophagy in response to ROS. *Nat Cell Biol, 17*(100).

Zhang, K., Donnelly, C. J., Haeusler, A. R., Grima, J. C., Machamer, J. B., Steinwald, P., . . . Rothstein, J. D. (2015a). The C9orf72 repeat expansion disrupts nucleocytoplasmic transport. *Nature, 525*(7567), 56-61.

Zhang, Y. J., Gendron, T. F., Grima, J. C., Sasaguri, H., Jansen-West, K., Xu, Y. F., . . . Petrucelli, L. (2016). C9ORF72 poly(GA) aggregates sequester and impair HR23 and nucleocytoplasmic transport proteins. *Nat Neurosci, 19*(5), 668-677.

Zhang, Y. J., Jansen-West, K., Xu, Y. F., Gendron, T. F., Bieniek, K. F., Lin, W. L., . . . Petrucelli, L. (2014). Aggregation-prone c9FTD/ALS poly(GA) RAN-translated proteins cause neurotoxicity by inducing ER stress. *Acta Neuropathol, 128*(4), 505-524.

Zhao, D. Y., Gish, G., Braunschweig, U., Li, Y., Ni, Z., Schmitges, F. W., . . . Greenblatt, J. F. (2016). SMN and symmetric arginine dimethylation of RNA polymerase II C-terminal domain control termination. *Nature, 529*(7584), 48-53.

Zu, T., Liu, Y., Banez-Coronel, M., Reid, T., Pletnikova, O., Lewis, J., . . . Ranum, L. P. (2013). RAN proteins and RNA foci from antisense transcripts in C9ORF72 ALS and frontotemporal dementia. *Proc Natl Acad Sci U S A, 110*(51), E4968-4977.